PHYSICAL LAYER DESIGN AND PERFORMANCE ANALYSIS FOR COOPERATIVE COMMUNICATION IN WIRELESS MULTI-HOP NETWORKS

A Dissertation
Presented to
The Academic Faculty

by

Feng Wang

In Partial Fulfillment
of the Requirements for the Degree
Doctor of Philosophy in the
School of Electrical and Computer Engineering

Georgia Institute of Technology
May 2018

PHYSICAL LAYER DESIGN AND PERFORMANCE ANALYSIS FOR COOPERATIVE COMMUNICATION IN WIRELESS MULTI-HOP NETWORKS

Approved by:

Dr. Mary Ann Weitnauer, Advisor
Professor, School of ECE
Georgia Institute of Technology

Dr. Geoffery Ye Li
Professor, School of ECE
Georgia Institute of Technology

Dr. Matthieu Bloch
Associate Professor, School of ECE
Georgia Institute of Technology

Dr. Alenka Zajic
Associate Professor, School of ECE
Georgia Institute of Technology

Dr. Luca Dieci
Professor, School of Mathematics
Georgia Institute of Technology

Date Approved: November 12, 2017

To my parents, my wife and my daughter.

ACKNOWLEDGEMENTS

It is my pleasure to thank a great number of individuals who have given me support and encouragement over the past eight years. I wish to express my special gratitude to my Ph. D adviser, Dr. Mary Ann Weitnauer, who has been a mentor, colleague, and friend to me. Her guidance and encouragement have support have excited me through the transition from an engineer to a scholar, and made this a rewarding journey.

I would like to give my special thanks to my dissertation committee of Dr. Geoffery Ye Li, Dr. Matthieu Bloch, Dr. Alenka Zajic, and Dr. Luca Dieci for their support. Their suggestions have greatly helped me to improve my dissertation.

I would like to thank my colleagues at the Smart Antenna Research Lab, Qiongjie Lin, Dr. Jian Lin, Dr. Jin Woo Jung, Dr. Haejoon Jung, Dr. Yong Jun Chang and Dr. Ali Hassan, for what I have learned through our discussions and conversations.

Finally, I give thanks to my family. Without my wife Hua Ye and my parents' support for the past several years, I could never have finished this dissertation.

TABLE OF CONTENTS

LIST OF TABLES

LIST OF FIGURES

SUMMARY

Cooperative communication is a technique which can improve the reliability and throughput of a wireless network through the cooperation between distributed wireless nodes. The contributions of this thesis include the design and analysis of some novel approaches for different cooperative communication schemes for the physical layer in wireless multi-hop networks.

The first contribution is a new approach that combines random delay and phase dithering for single carrier cooperative transmission (CT); its benefit is that it lowers the coordination overheads in cooperative communication schemes. Simulation results, under different channel models, are compared with the results of the state-of-the-art practical phase dithering approach. The results show significant signal to noise ratio (SNR) gain, or equivalently, that higher data rates can be achieved. The approach is also robust to different channel models and can lower the overhead in channel estimation significantly, while the constant envelope characteristic of the transmitted signal is kept.

The second contribution is a novel equalization algorithm in the frequency domain for the multiple carrier frequency offsets (CFOs) problem of cooperation communication. Using a permutation-based approach that employs the pseudo-banded matrix characterization, a recursive and computationally efficient equalization algorithm is proposed. This linear minimum mean-square error (MMSE) equalization algorithm works for both the virtual multiple-input-multiple-output (MIMO) or distributed spatial multiplexing (DSM) MIMO scheme and the distributed space time block coding (STBC)

scheme, for both orthogonal frequency division multiplexing (OFDM) and single-carrier frequency-domain equalization (SC-FDE). To the author's knowledge, this is the first time a generalized approach has been proposed for such problems. Simulation results show that large frequency offsets can be compensated with high computational efficiency.

The third contribution is a new set-based bounding approach to analyze diversity for SC-FDE over inter-symbol interference (ISI) channels, including linear equalizers such as zero forcing (ZF) and minimum mean-square error (MMSE). The diversity order of both the error probability and the outage diversity gain are analyzed. In previous works, the channel was constrained to have identical and independent distributed paths, whereas in this work we have relaxed the constraint to be a more practical channel with just independent paths. For finite length data blocks, the diversity order of the error probability and the outage diversity gain of ZF SC-FDE are proved to be one; the outage diversity gain of MMSE SC-FDE and its relationship to the channel memory length and data rate are proved rigorously, and the diversity order of the error probability of MMSE SC-FDE is shown to be one.

The fourth contribution is a new method to calculate the joint probability density distribution (PDF) of the non-zero eigenvalues of the equivalent cascaded MIMO channel of the multi-hop amplify-and-forward (A&F) relay network. The closed form expression has the form of a product of determinants of matrices, while the entries of these matrices are expressed as multi-dimensional integrals, where the maximum integration dimension is the number of relay clusters (the number of hops minus one). While previously the

distribution could be found practically only by Monte Carlo simulation, now it can be evaluated by computationally efficient numerical methods. The contribution can be further employed to analyze the performance of the multi-hop network. To the authors' knowledge, it is the first time a practical numerical method and an explicit closed form expression are presented for this problem.

CHAPTER 1. INTRODUCTION

1.1 Motivation for Cooperative Communication

Wireless communication has attracted enormous interest of researchers and experienced a huge boost in use in the last two decades, for it provides a feasible way of ubiquitous communication. While single-hop networks, such as cellular networks and wireless local area networks (WLANs), are commercially successful, other kinds of networks, such as wireless ad hoc networks (WANETs) and wireless sensor network (WSNs), are still not widely deployed. Because of the detrimental effects of the terrestrial wireless channel, such as path loss, shadowing, fading, and interference, one aim of the recent wireless communication research has been to improve the reliability and throughput of a multi-hop network by cooperative communication [4, 5, 8, 9, 10-16].

Multiple antennas at the transmitter or the receiver or both can be used to overcome the detrimental effects of the terrestrial wireless channel, by providing array gain and diversity gain, for improved reliability, and spatial multiplexing, for higher data rates. The classic multiple-input-multiple-output (MIMO) system [10] can provide all of these gains in various combinations. Two typical MIMO configurations, point-to-point MIMO and multi-user MIMO (MU-MIMO), are shown in Fig. 1.

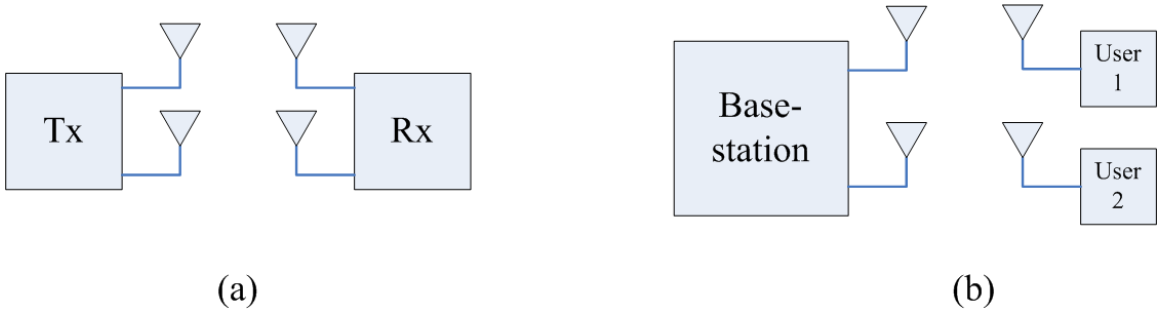

Figure 1 Topologies of typical MIMO systems: (a) point-to-point MIMO (b) MU-MIMO

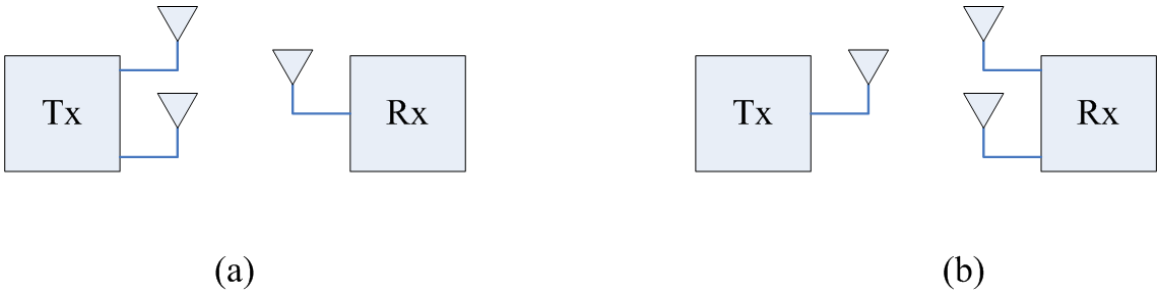

Figure 2 Topologies of typical MIMO systems: (a) MISO (b) SIMO

A MIMO system can be operated a variety of ways, the extremes ways being full transmit diversity, which maximizes the reliability, and full spatial multiplexing, which maximizes the transmission rate. When only the transmitter or only the receiver has multiple antennas, only array and diversity gains are possible. These configurations, called multi-input-single- output (MISO) and single-input-multi-output (SIMO), respectively, are shown in Fig. 2.

Most of the contributions of this dissertation treat distributed and multihop versions of MIMO and MISO configurations. Different cooperative communication schemes have specific purposes: distributed MISO, as known as cooperative diversity (CD) or

cooperative transmission (CT) [4, 5], is intended to improve the reliability or loss rate of data transmission over fading channels, while distributed MIMO, as known as virtual multiple-input-multiple-output (MIMO) [11-14] or distributed spatial multiplexing (DSM) [15, 16] are intended to improve the throughput of data transmission. CD and DSM networks generally consist of one or more source nodes, one or more stages or clusters of single-antenna relay nodes, and one destination node; the source and destination nodes could have a single antenna or be multi-antenna terminals. When these single-antenna nodes cooperate with each other to mimic a virtual antenna array, performance gains similar to those of traditional multi-antenna terminals can be achieved.

This dissertation addresses some practical and theoretical issues in physical layer signal processing and performance analysis of different cooperative communication schemes in wireless multi-hop networks.

1.2 Coordination Overhead for Cooperative Diversity

One practical issue for CD is the coordination overhead, which involves control packets or signaling to determine the transmission parameters of each node in CD. While it was generally not mentioned in the CD proposals [4, 5, 7, 8], this overhead makes the efficiency of CD doubtful. A new approach that combines random delay and phase dithering, proposed for single carrier CD to lower the coordination overhead, is proposed in Chapter 3 in this dissertation.

1.3 Multiple CFOs Problem for Cooperative Communication

Another issue is the multiple carrier frequency offsets (CFOs) problem, which originates from the distributed manner of the transmission [47]. The multiple CFOs problem can be compensated on the receiver side [49-58], however, performance and computational efficiency is an issue. A novel equalization algorithm in the frequency domain is proposed for the multiple carrier frequency offsets (CFOs) problem in Chapter 4 in this dissertation. This generalized approach compensates large frequency offsets and has high computational efficiency.

1.4 Diversity of Linear Equalizers for SC-FDE

While single-carrier frequency-domain equalization (SC-FDE) [29] is widely used in wideband wireless and MIMO systems [31-35], and surely finds its place in cooperative communication, the diversity analysis for the point-to-point SC-FDE linear equalizer is still controversial [69, 73, 75-77]. A new set-based bounding approach is proposed in Chapter 5 to perform rigorous diversity analysis for SC-FDE linear equalizers, such as zero forcing (ZF) and minimum mean-square error (MMSE), and new conclusions are presented.

1.5 Joint PDF of the Nonzero Eigenvalues of the Equivalent Channel Matrix for Multi-hop DSM MIMO with A&F Relays

In the multi-hop virtual MIMO or DSM schemes, we are especially interested in amplify-and-forward (AF) relaying [15], for its simplicity and low overhead cost in application. However, nowadays, the analysis or evaluation of the network is based on Monte-Carlo simulation only [15, 16]. As in point-to-point MIMO, the joint distribution

of the eigenvalues of the scheme's equivalent MIMO channel is important for analysis of the system, but such a distribution was previously unavailable. A novel approach in Chapter 6 provides the closed form expression for the joint PDF of the nonzero eigenvalues.

CHAPTER 2. ORIGIN AND HISTORY OF THE PROBLEM

2.1 Background

How to improve the throughput and connectivity of the wireless networks is one of the most important topics in the research of wireless communication, and significant progress has been made. In recent years, research in wireless networks suggests that cooperation between the nodes can improve the throughput and connectivity of the network dramatically [4, 5, 8, 9, 10-16].

The idea behind cooperative communication dates back to the information theoretic aspects of the classic 3-node relay channel [1, 2], where a single relay node helps the source node send information to the destination node, as shown in Fig. 3. The 3-node relay channel may be the simplest cooperative multi-hop network, yet its capacity is generally unknown, except for some specific cases [2]. However, some useful results on the bounds of the relay channel capacity exist; among these, are the cut-set upper bound based on the max-flow min-cut theorem [3] and some achievable lower bounds with specific relaying protocols, such as decode-and-forward (DF), compress-and-forward (CF) and amplify-and-forward (AF), assuming full or global channel state information (CSI). Global CSI means both CSI on the receiver side (CSIR) and CSI on the transmitter side (CSIT), which needs some kind of feedback from the receiver to the transmitter.

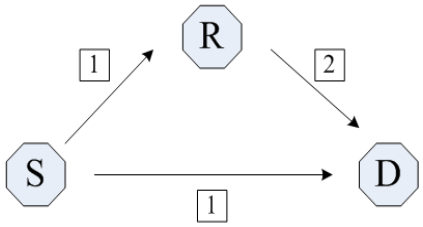

Figure 3 Classic 3-node relay network

Recent works on cooperative communication are different from this classic relay channel in many aspects. Physical layer cooperative communication happens when multiple single-antenna radios (not connected by wire) transmit and receive in a way that mimics a terminal with an antenna array; hence the cooperating radios are often referred to as virtual arrays. [4] proposed the concept of user CD (CT in [5]), a new form of spatial diversity which is realized by user cooperation in a mobile network. The relaying protocols suggested in [2], such as DF and AF, were employed in [4, 5], while coded cooperation, which can be viewed as an implementation of CF, was employed in [6]. These works on cooperative communication inspired many efforts in this area. The CD schemes generally assume CSIR only and consider the reliability characteristics, such as diversity order, symbol error rate (SER) and outage probability of the relay channel under the wireless fading effect [7]. The information theoretic results in [2] were extended in [8] to multi-hop cooperative transmission with multiple relays, as the cooperative diversity scheme was also extended from the model of single relay channel to multiple relay channel [9]. An example of multiple relay based two-hop CD network is shown in Fig. 4, which can be easily extended to multi-hop case.

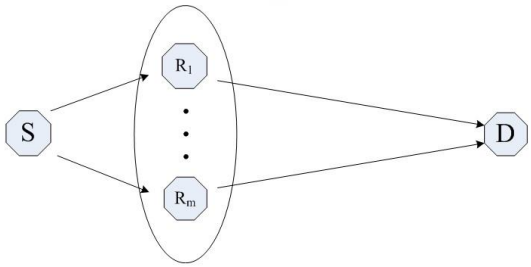

Figure 4 multiple relay based cooperative diversity

CD is not the only scheme proposed for cooperative communication. To obtain the spatial multiplexing gain of classic multiple-input-multiple-output (MIMO) system [9], cooperative MIMO schemes were proposed in [11, 12], where cooperative transmission and/or cooperative reception for single-antenna nodes were explored. Similar ideas were proposed for multi-hop distributed networks as Virtual MIMO [13, 14], or distributed spatial multiplexing (DSM) [15] (cooperative spatial multiplexing in [16]) to achieve high throughput and spectral efficiency in a distributed multi-hop network with single-antenna nodes.

Despite the variety and complexity of the cooperative communication schemes, the tremendous results on classic point-to-point MIMO can be applied directly; meanwhile, due to the distributive manner of cooperative communication, there are still a lot of key practical issues that need to be solved in application, especially, the coordination overhead and the multiple carrier frequency offsets (CFOs) problem.

In the following paragraphs in this chapter, we first discuss the state of the art CD schemes, and then the practical issues such as coordination overhead and the multiple CFOs problem, and last the performance analysis for DSM.

It is well known that multiple co-located transmit antennas can achieve micro spatial diversity gain [17, 18] and are very effective to tackle the multipath fading effect in wireless communication. Spatial diversity gain is realized by transmitting redundant signals in space through independently fading channels to the receiver; however, this method is difficult to implement on a user terminal. To ensure independent fading between the paths from different transmit antennas to the receiver, the transmit antennas should be located apart by a distance which is generally larger than several carrier's wavelengths, especially when the multipath has a narrow angular spread, while the user terminals are limited in size to provide enough space which is necessary to de-correlate the antennas. Cooperative diversity has been studied as a way for one or more single-antenna radios to help another single-antenna radio to transmit a single message more reliably, through combining in the physical layer, to combat multipath fading in terrestrial wireless communication. A "virtual" antenna array is composed by these single-antenna radios in cooperation. Another benefit of CD is that it also provides the macro diversity [19, 20] to counteract the large-scale shadow fading effect, where the co-located transmit antennas will fail. While there are vast varieties of the existing solutions for CD, we will divide the schemes into two large categories, according to with or without coordination.

2.2 Cooperative Diversity with Coordination

In this case, each transmitter needs to know its waveform assignment or the index of its transmitted waveform, so distributed or centralized coordination is necessary between these transmitter nodes. Another requirement for coordination may come from the channel estimation at the receiver side because generally transmitters should access

orthogonal channels to transmit training sequences independently, such as time-division multiple access (TDMA) or frequency-division multiple access (FDMA), which requires coordination. The existing schemes can be further divided into different sub-categories.

The first sub-category is cooperative diversity with orthogonal relay channels, either by code division multiple access (CDMA), TDMA, or FDMA. The scheme in [4] is a coherent demodulation case where the CSI is known on the receiver side. The schemes of [21] and [22] assume a flat fading channel and non-coherent demodulation and differential demodulation, respectively; these types of demodulation have the advantages that channel estimation is not necessary, a simple receiver implementation, and less overhead in time varying channels. Orthogonal relay channels provide full diversity and are easy to implement, but they have low spectrum efficiency. In these papers, exact time synchronization is necessary.

The second sub-category is non-orthogonal relay channels, which generally uses multiple-antenna space time coding (STC) or space frequency coding (SFC) [23] techniques. These techniques improve the spectrum efficiency compared to the orthogonal relay channels. Due to the similarity between the classic point-to-point MIMO and distributed MIMO, classic STC and SFC techniques can be introduced directly to the cooperative transmission if the DF mode is adopted for the relays. For example, the Alamouti scheme [24], can be used for cooperative diversity under flat fading channels. There are also non-coherent STC schemes [25] and differential STC schemes [26, 27, 28], which simplify the channel estimation requirement for the flat fading channel. For frequency selective fading channels, space time block coding (STBC) or space frequency

block coding (SFBC) [23], which combines spatial diversity with SC-FDE [29] or OFDM [30] transmission, can also be implemented. These works include (1) time reversal STBC (TR-STBC) [31], which extends the Alamouti scheme to the frequency selective channel, (2) STBC SC-FDE [32], which extends the transit sequences of TR-STBC to have a circular cyclic form, and thus the equalization can be implemented with SC-FDE in frequency domain, like OFDM, (3) the SFBC SC-FDE [33], and (4) STBC OFDM [34]. The equalization techniques for these STBC SC-FDE schemes are described in [35]. Most of these works are extended from the Alamouti scheme, and focus on the 2-transmitter (Tx) and 1-receiver (Rx) antennas case. Orthogonal STBC can be employed for the 2-transmitter case, and there is a rate loss when there are more transmitters. One issue about the STBC SC-FDE schemes is that rigorous diversity analysis is unavailable; even for point-to-point SC-FDE transmission, the conclusions of diversity order from different works [69, 73, 75, 76, 77] contradict each other and make this topic controversial. This dissertation offers in Chapter 5 the first rigorous derivation of diversity order for SC-FDE.

A distributed STC scheme that assumes flat fading and AF relaying was proposed in [36], and the idea was further developed into a differential scheme in [37] and generalized in [38].

Other approaches include the coded cooperation and turbo-coded cooperation [39, 40], which combine cooperative transmission with channel coding, wherein the users can transmit redundant information of their cooperative partners. Protocols for the two-user scenario were designed in [39, 40].

2.3 Cooperative Diversity without Coordination

As we mentioned in the introduction, the need for coordination introduces large overhead in the network and limits the scalability of cooperative transmission. While coordination is a MAC layer function, most of the work on cooperative transmission focuses on the physical layer and makes the simple assumption that the nodes are already well coordinated, without concern about how much is the overhead and how the coordination is realized. However, an ideal cooperative transmission is like the concept as Opportunistic large array (OLA) [41] where its most important property is that all the nodes transmit the same signal concurrently to cooperate without any coordination. OLA networks seems to be ideal for message broadcasting or flooding in a wireless network, however, in practice, the node density of a network is seldom high enough to maintain the OLA transmission [42]. Generally, there are only a limited number of relay nodes in the next hop who can decode the broadcast message, and the assumption that the received power can sum up [41, 42] does not hold unless orthogonal relay channels are employed, as those practical OLA networks which are studied in [99, 100].

Instead of transmitting the same signal concurrently from all the relay nodes as in OLA transmission, cooperative diversity schemes can provide transmit diversity to improve the reliability of data transmission. It is of great significance for the physical layer design to operate without coordination, and tolerate synchronization error which is inevitable in the network. To remove the requirement for coordination in cooperative transmission, a randomization technique is necessary. The scheme of time-variant phase rotations with AF protocol was suggested in [43] to transform the space diversity into

time diversity by creating a time-selective fading channel, and the diversity can be recovered by channel coding technique. This scheme was extended to a randomized DF version in [44]. A disadvantage of [44] is, under some channel models, it needs a very long phase dithering sequence to keep its performance, which introduces extra overhead. A distributed random delay diversity version was proposed in [45], which can transform the space diversity into frequency diversity by creating a frequency-selective fading channel, and the diversity can be recovered by channel equalization technique. A randomized STC scheme was proposed in [46], where each relay node transmits an independent random linear combination of the codewords that would have been transmitted by all the elements of a multi-antenna system, with a disadvantage that the peak to average ratio (PAR) of the transmitted signal is high; on the other hand, the scheme could be viewed as a deterministic space time code transmitted over a randomized channel. This dissertation offers in Chapter 3 a new approach that combines random delay and phase dithering for single carrier cooperative transmission (CT) which lowers the coordination overheads in cooperative communication.

2.4 Cooperative Communication with Asynchronism

Asynchronism is an important problem in cooperative transmission [47]. While most of the cooperative communication approaches assume the channel is quasi-static, such an assumption cannot be maintained under multiple CFOs and Doppler frequency shifts, as it is hard for a distributive synchronization mechanism [48] in a wireless network to provide high accuracy. The timing estimation error and frequency estimation offset will accumulate hop by hop, while some other factors, such as propagation delay, processing

delay, and frequency drift, will make the problem even worse. While the timing asynchronism is similar to the dispersion in a multipath channel and can be compensated by equalization techniques [7], some authors have addressed the problem of multiple CFOs with compensation or equalization algorithms.

For the multiple CFOs problem of cooperative diversity with delay diversity for the flat fading channel, a symbol-rate MMSE-DFE was developed in [49], and its enhanced version was presented in [50], to improve computation efficiency, a MLSE equalizer based on the Viterbi algorithm was developed in [51]. Multiple CFOs compensation algorithms for OFDM transmission were also developed in [52, 53, 54, 55]. In [95], a compensation algorithm for distributed TR-STBC transmission is suggested, wherein the matrix inversion problem in equalization was transformed into a banded matrix LDL^H factorization [95] to simplify computation.

The multiple CFOs problem also exists for virtual MIMO and DSM schemes [56]. While [57] focused on preamble design and CFO estimation, [58] presented a compensation algorithm for multiple CFOs for this scheme. One issue about these compensation algorithms is that they only work for small CFOs [54, 58] and the high computation load. This dissertation offers in Chapter 4 a novel recursive equalization algorithm in frequency domain which is computationally efficient.

2.5 Performance Analysis of DSM and Virtual MIMO and DSM

Among the different proposals for virtual MIMO [11, 12, 13, 14] and DSM [15, 16, 60], the DSM scheme with AF mode relaying [15] is of particular interest for its simplicity

and low coordination overhead. However, closed form analyses for this scheme are generally unavailable, and the performance evaluation generally depends on Monte-Carlo simulation. This is because we have little knowledge about the statistical characteristics of the equivalent cascaded MIMO channel of this scheme. To the author's knowledge, there are few exact closed form expressions and they only exist for the 2-hop case, including the SER analysis in [59], and the marginal probability density function (PDF) of the eigenvalues for ergodic capacity analysis in [61, 62]. A closed form expression of the distribution of the eigenvalues of the equivalent channel matrix is needed. This dissertation offers in Chapter 6 a novel approach to get the closed form expression for this joint distribution.

CHAPTER 3. COOPERATIVE TRANSMISSION WITH RANDOMIZED DELAY AND PHASE DITHERING

Most of the present methods, either the cooperative transmission with orthogonal relay channels [4], or the distributed space time coding approach [9, 36, 37], make the simple assumption that the nodes are already well coordinated by the MAC layer function. The transmitters need to know the index of the waveform, so distributed or centralized coordination is necessary between these transmitter nodes. The need for coordination introduces large overhead in the network and limits the scalability of the transmission, and is difficult to accomplish in practice.

To avoid the overhead, each node involved in CD can autonomously and randomly select its waveform index. The problem with this approach is that the nodes might choose the same index and this could cause link failure if the two copies destructively combine at the receiver. This is especially of concern in line-of-sight (LOS) channels where the cooperating nodes are approximately the same distance from the receiver. Several randomization approaches have been developed. In [46], the randomized space-time coding approach was proposed, in which each relay will transmit an independent, random linear combination of the STC waveform choices. One disadvantage of this approach is that, the peak to average ratio (PAR) of the transmitted signal increases because the linear combination of the space-time codewords destroys the constant envelope characteristic. The higher PAR leads to low power efficiency in the transmitter. In [44], by translating the slow or constant channel into a time-selective channel with a random phase dithering approach, the temporal diversity can be harvested by error correction decoding at the receiver and the transmitted signal maintains a constant envelope. However, a

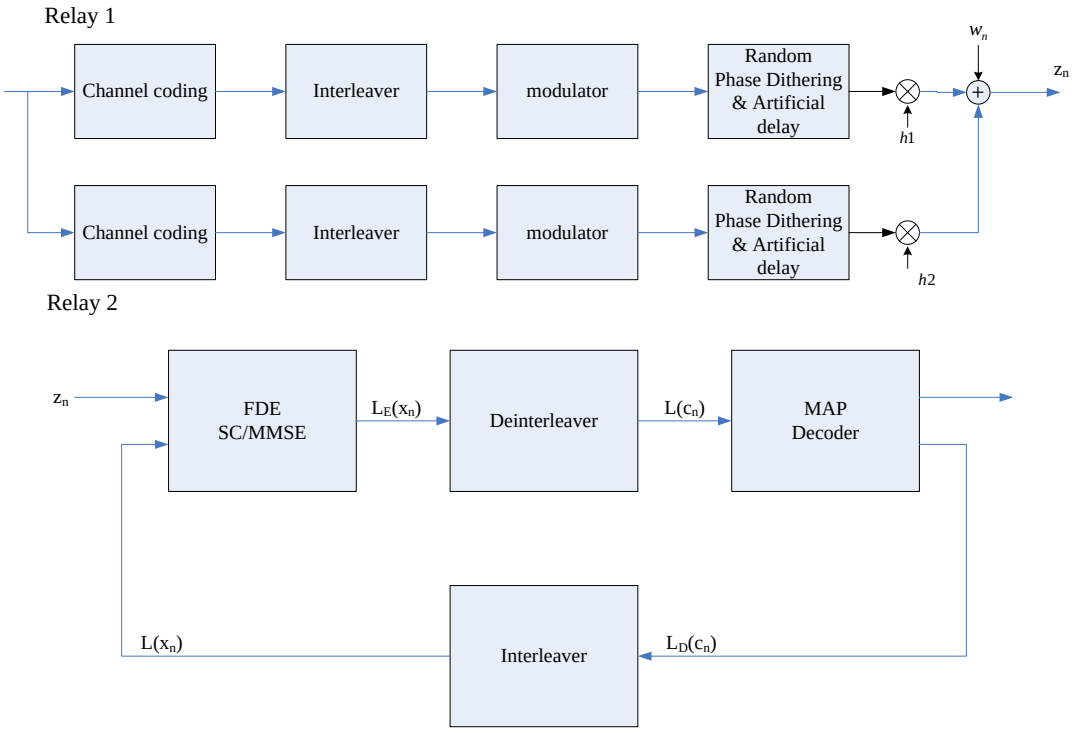

Figure 5 System Model for Tx and Rx

disadvantage of [44] is, under some channel models, phase dithering needs a very long dithering sequence to keep its performance, which means extra overhead in channel estimation.

We propose a new approach which combines random delay and phase dithering for single carrier cooperative transmission, which preserves the constant envelope characteristic. Combining the delay and dithering creates more randomness in the effective channel gain, or equivalently, mitigates the problem with randomized approaches (i.e., that the nodes might choose the same waveform), which shortens the frame length, and decreases training overhead. As in [44], both the multi-user AWGN channel scenario and the multi-user Rayleigh channel scenario are considered.

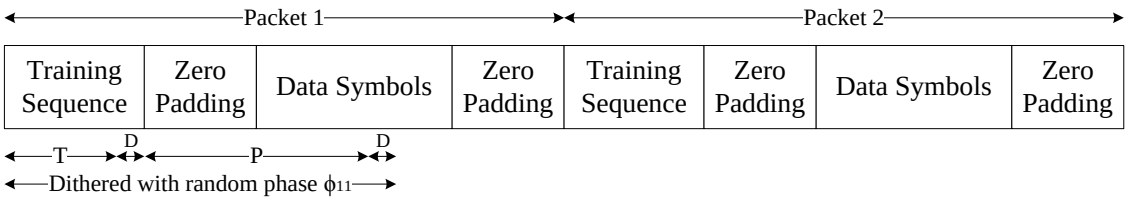

Figure 6 Frame Structure

In the following sections, we first describe the system model, then analysis using information theory and then show simulation results. We compare the new method and the phase-dithering-only approach via simulation, for both types of channels, assuming frequency domain turbo equalization (FDTE) [63]. Significant gains in both channel scenarios are shown.

3.1 System Model

3.1.1 System Model

Figure 5 shows the system model for both the transmitter side and the receiver side, where two relays are employed. Frequency domain turbo equalization (FDTE) was utilized on the receiver side.

3.1.2 Frame Structure Design

As shown in Figure 6, the whole encoded block of data was divided into N packets, each packet is a subset of the block comprised of consecutive coded bits. A training sequence is inserted ahead of each packet. All the relays transmit the same data and same training sequence, but random delay and phase dithering is applied on a packet basis. The relay will introduce an additional artificial delay which is chosen randomly for each packet.

Different packet will be modulated by a different random carrier phase. All the symbols within on packet will be modulated by the same random carrier phase. Different relay nodes will use different random phase sequences to modulate the packets in the block. So the composite equivalent channel could be frequency-selective and time-selective.

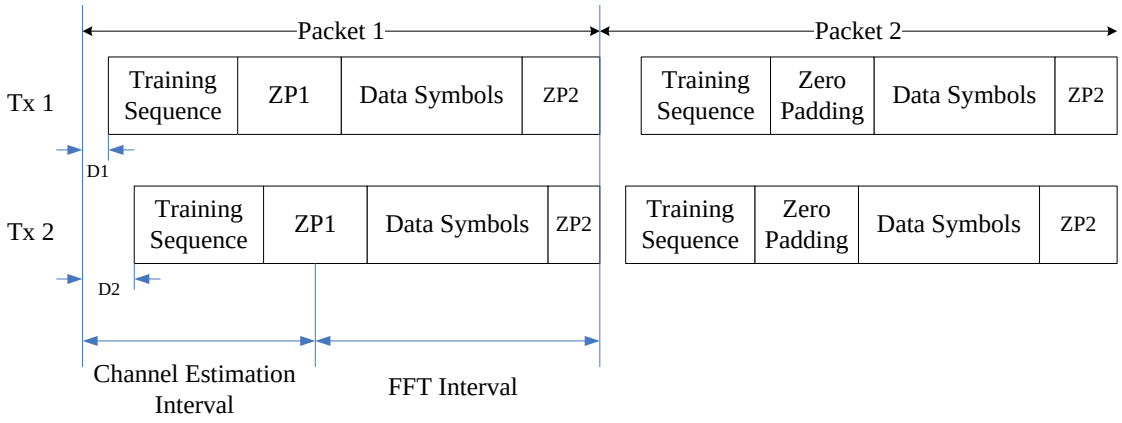

Figure 7 Channel Estimation

The training sequence at the head of a packet is introduced the same delay and phase as the data symbols in the packet. The training sequence is utilized to estimate the composite channel which is shown in Figure 7.

3.2 Comparison of Phase Dithering Approach and Our Approach using Information Theory

The random phase dithering approach was suggested in [44] for cooperative transmission without coordination. Our approach which combines random delay [45] and phase dithering was proposed. In this section, the information rate with modulation constrained input (BPSK, QPSK, etc.) for these two different approaches are analyzed from the view point of information theory.

3.2.1 Channel Model and Information Rate for the Phase Dithering Approach

We consider the modulation-constrained discrete time AWGN channel. The input-output relationship is given by

$$y = \sqrt{E_s} hx + n$$

Where x is the input information-bearing symbol which is selected from a symbol set $S = \{s_m\}_{m=0}^{M-1}$ with probability $p_m = \Pr\{x = s_m\}$, y is the channel output, and n is the additive white Gaussian noise term. The noise is modeled as a complex Gaussian random variable with zero mean and variance $N_o/2$ per dimension. E_s represents the average signal energy.

The information rate for a deterministic channel discrete-input continuous-output memoryless channel is the mutual information given by [7]

$$I(y;x) = \sum_{m=0}^{M-1} p_m \iint_{\mathrm{C}} p(y \mid s_m) \log_2 \left(\frac{p(y \mid s_m)}{\sum_{n=0}^{M-1} p(y \mid s_n) p_n} \right) dy \, .$$

With random phase dithering, the equivalent channel is a time fading channel. Under the assumption that the data block is long and the number for phase dithering is large enough, we consider that the equivalent channel is randomized sufficiently and ergodic. The information rate for the phase dithering approach is the ergodic information rate of the

equivalent channel $C_{PD} = \int I(y(\frac{E_s}{N_o}, \alpha); x) f_{|h|}(\alpha) d\alpha$ where the probability density function for $|h|$ is $f_{|h|}(\alpha)$.

For the two relay scenario with uniform distributed continuous phase dithering, and assume the amplitude of the channel gains from the relays are all equal to 1, then $f_{|h|}(\alpha) = \frac{2}{\pi\sqrt{4-\alpha^2}}$, where $0 \le \alpha \le 2$.

3.2.2 Channel Model and Information Rate for Our Approach

Our approach combines random delay and phase dithering. We analyze the information rate for the memory channel, which is introduced by delay, and show that it is larger than the information rate for the phase dithering approach.

The input-output relationship for a channel with memory is given by

$$y_k = \sqrt{E_s} \sum_{l=0}^{L-1} h_k(l) x_{k-l} + n_k ,$$

where x_k is the input information-bearing symbol at time k, y_k is the channel output at time k, and n_k is the additive white Gaussian noise term. $h_k(l)$ is the channel coefficient for the l th path of the channel impulse response at time k. We analyze the case for an ergodic channel with memory.

The information rate for this memory channel model is defined by

$I = \lim_{N \to \infty} \frac{1}{N} I(X^N; Y^N)$, where X^N and Y^N are the input and output sequences, respectively. Let $X^N = (x_1, x_2, \ldots, x_N)$ and $Y^N = (y_1, y_2, \ldots, y_N)$.

The calculation of the information rate for memory channel model involves multidimensional integrations, and it is generally difficult to compute even for moderately large N. A statistical estimation method was suggested in [64] to get the information rate for memory channel, where the Shannon-McMillan-Breiman theorem and the BCJR algorithm were applied.

We rewrite the expression for information rate as

$I = \lim_{N \to \infty} \left(\frac{1}{N} H(Y^N) - \frac{1}{N} H(N^N) \right)$, where $N^N = (n_1, n_2, \ldots, n_N)$.

Because $\frac{1}{N} H(N^N)$ is the entropy of the noise and can be calculated easily, what we need to do is to find $\frac{1}{N} H(Y^N) = -\frac{1}{N} E\left[\log(p(Y^N)) \right]$.

The expected value can be estimated by the Monte Carlo method. However, with identical uniformly identically distributed (u.i.d.) input, the output is stationary and ergodic when the channel is ergodic or deterministic. Then Shannon-McMillan-Breiman theorem can be applied and the averaging can be performed on a single long run of a realization of the channel output sequence to estimate the expectation, and the BCJR algorithm can be employed to calculate $p(Y^N)$.

Suppose the memory channel can be described by a trellis diagram with n_s states, and we denote the state of the trellis at time k by $S_k = (x_{k-1}, x_{k-2}, \ldots, x_{k-L+1})$.

We define

$$\alpha_k(m) = p(Y^N, S_k = m)$$

and

$$\gamma_k(m', m) = p(Y^N \mid S_k = m, S_{k-1} = m') \bullet p(S_k = m \mid S_{k-1} = m'),$$

where $0 \le m, m' \le n_s - 1$.

The forward recursion of the BCJR algorithm can be used to calculate

$$\alpha_k(m) = \sum_{m'=0}^{n_s-1} \gamma_k(m', m)\alpha_{k-1}(m').$$

Finally, the desired probability $p(Y^N)$ can be obtained by

$$p(Y^N) = \sum_{m=0}^{n_s-1} \alpha_N(m).$$

3.2.3 Information Rate Simulation Results

Both the multi-user AWGN channel scenario and the multi-user Rayleigh channel scenario are simulated, and we analyze the results for the information rate and the actual packet error rate for our cooperative transmission scheme.

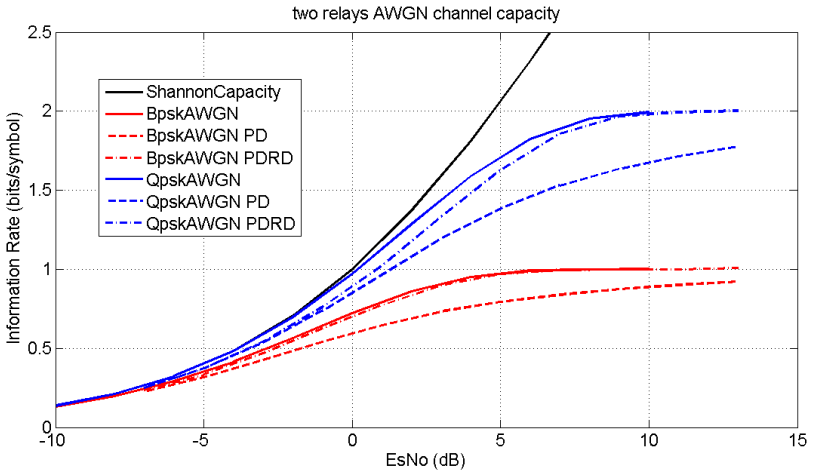

Figure 8 Information Rate of Phase Dithering and our proposal under AWGN channel Information

We analyze the two relay case, and assume a quasi-static channel and perfect channel estimation on the receiver side. The modulation schemes are BPSK and QPSK modulation with Gray Mapping. Figure 8 shows the information rate under two relays AWGN channel scenario for both BPSK and QPSK modulation. Figure 9 shows the information rate under two relays dynamic or block fading Rayleigh channel scenario for QPSK modulation. Here the relay AWGN channel means the two relay to destination channels all have amplitude one but uniformly distributed phase. The squares of the Rayleigh channels' magnitudes have mean 1. The legend "PD" represents the phase dithering approach, and the legend "PDRD" represents our approach, which combines phase dithering and random delay. The Shannon capacity and the information rate for a real single AWGN channel with BPSK or QPSK modulation is also plotted out as a reference. It is shown that when the signal-to-noise ratio (SNR) EsNo is low, the

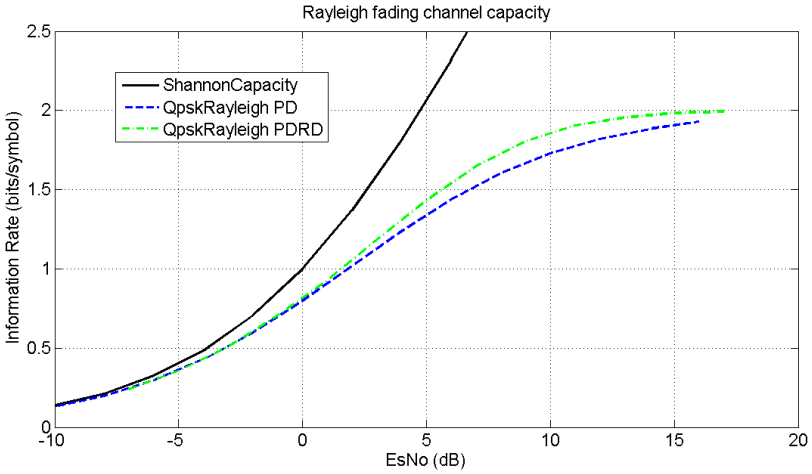

Figure 9 Rate of Phase Dithering and our proposal under dynamic Rayleigh channel

information rates of different approaches are all close to the Shannon capacity. But when EsNo increases, our approach has a higher information rate than the phase dithering approach, or say, our approach needs smaller EsNo than the phase dithering approach to get the same information rate. For example, in Figure 8 and for BPSK modulation, the gain in EsNo is about 1dB when information rate is 0.5, about 3dB when information rate is 0.75; and the gain in EsNo is about 2.5dB when information rate is 1.5 for QPSK modulation; in Figure 9, the gain in EsNo is about 1dB when information rate is 1.5 for QPSK modulation.

3.3 Packet Error Rate Analysis

The information rate analysis in last section shows that our approach has higher capacity than phase dithering only approach. However, in a real world system, the performance is also influenced by other factors such as the code, frame length, interleaver, demodulation

algorithms, etc. in this section, we analyze the Packet Error Rate (PER) by simulation. The FDTE receiver was utilized to get the PER. Both the two-relay AWGN channel scenario and the two-relay Rayleigh channel scenario are simulated, and the results are compared with the results by phase dithering approach only. We assume perfect channel estimation on the receiver side, and QPSK modulation with Gray mapping. Figure 10 shows the packet error rate (PER) under AWGN channel, Figure 11 shows the PER under dynamic or block fading Rayleigh channel, and Figure 12 shows the PER under quasi-static Rayleigh channel. An (2, 1, 7) convolution code is utilized; the frame length is 2560 bits. We can see the improvement of our proposal over the phase-dithering-only approach. In Figure 10 for AWGN channel, when the number of packets in each block, N=20, the improvement in EbNo is about 5.5dB when PER=0.01, and about 7.5dB when PER=0.001, after two iterations between the decoder and equalizer. In Figure 11 for dynamic Rayleigh channel, when N=20, the improvement in EbNo is about 1.0dB when PER=0.01, after two iterations between the decoder and equalizer. In Figure 12 for static Rayleigh channel, when N=20, the improvement in EbNo is about 2.0dB when PER=0.1. From Figure 10, we find that our proposal has good performance when N=20, which is much better than phase dithering only method with N>20, this means less overhead for channel estimation and a higher efficiency.

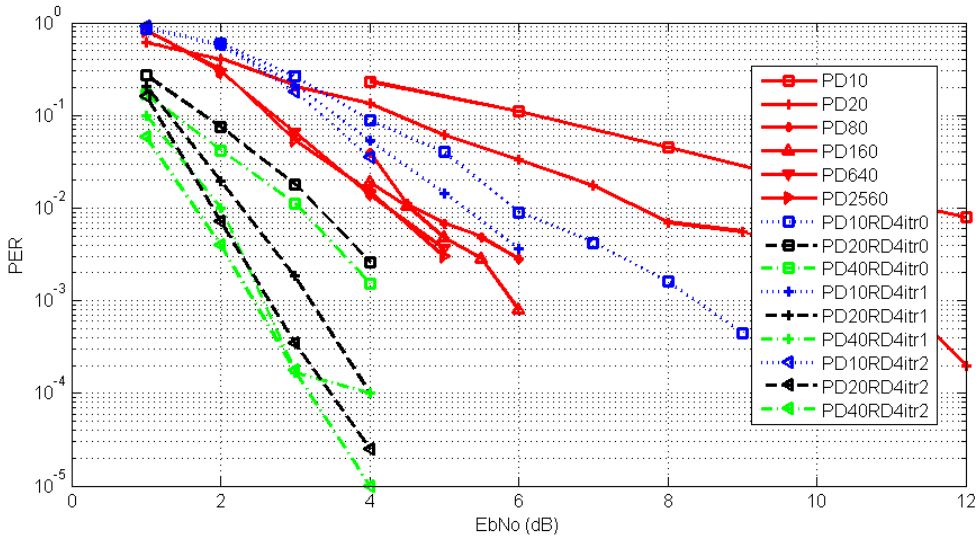

Figure 10 PER of Phase Dithering and our proposal under AWGN channel

3.4 Conclusion

A new approach which combines random delay and phase dithering is proposed for cooperative transmission while the constant envelop characteristic of the transmitted signal was kept. The simulated results of information rate and error rate are compared with the results by phase-dithering-only approach. It shows that our approach is more robust to different channel models, with less channel estimation overhead, and can achieve better performance with a higher information rate or a gain in SNR.

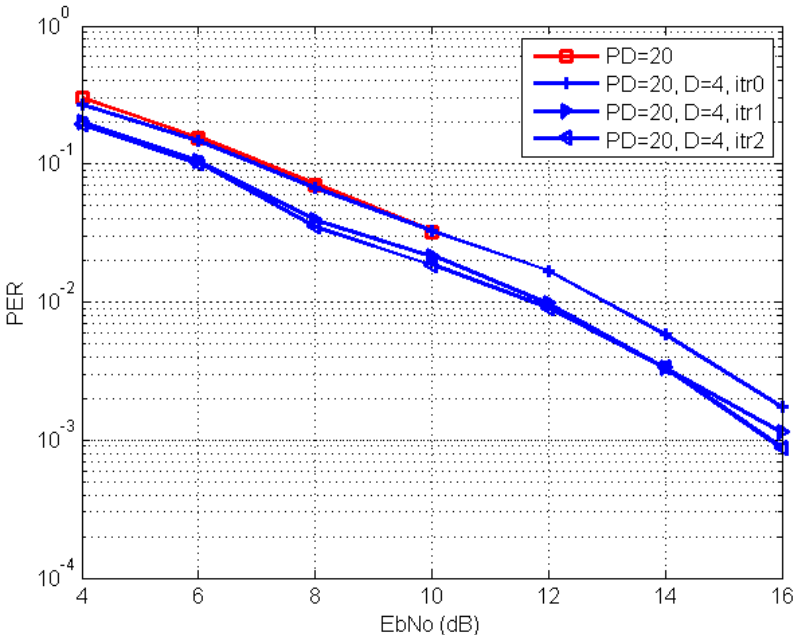

Figure 11 PER of Phase Dithering and our proposal under dynamic Rayleigh channel

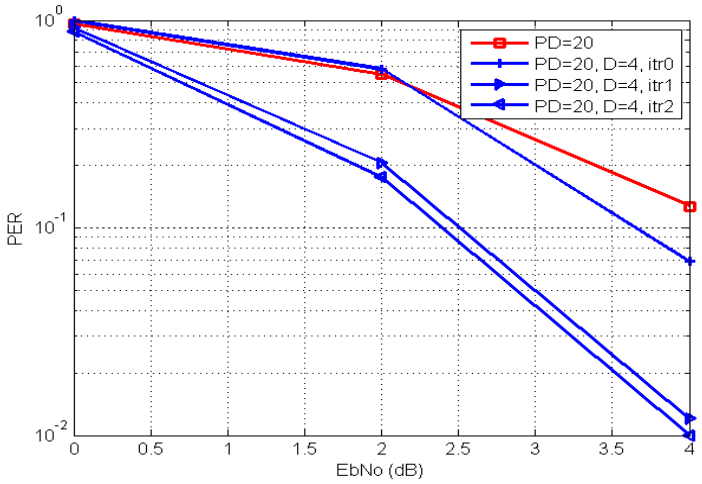

Figure 12 PER of Phase Dithering and our proposal under quasi-static Rayleigh channel

CHAPTER 4. MULTIPLE CFOS EQUALIZATION IN DSM MIMO OFDM AND STBC SC-FDE

One of the most critical issues in cooperation communication is the multiple carrier frequency offsets (CFOs) problem as an asynchronism [47], which originates from the distributed manner of the transmission and the difficulty in global synchronization [48] for a distributed wireless network.

For CT, multiple CFOs compensation algorithms for OFDM transmission are also developed in [52, 53, 54, 55], where the compensation algorithm for distributed TR-STBC transmission is suggested [94]. The multiple CFOs problem also exists for virtual MIMO and DSM schemes [56, 58. The major drawbacks of these compensation algorithms are that they only work for small CFOs [54, 58] and the high computation load.

Here we develop a Linear MMSE equalization [65] algorithm in the frequency domain to compensate the CFOs, assuming the CFOs are known at the destination. By using the permutation based approach which employs the pseudo banded matrix characterization, a computationally efficient equalization algorithm is proposed. This permutation-based approach can be generalized for the problem of frequency domain equalization with multiple CFOs problems, for both OFDM and SC-FDE, and for both distributed MIMO and STBC scenarios. To the author's knowledge, this is the first time a generalized approach has been proposed for such problems. Also, the algorithm is evaluated by

simulation to show that it can compensate large frequency offsets and have high computational efficiency.

In the remainder of this chapter, we use the following notations: for a matrix $\mathbf{A}$, $\{\mathbf{A}\}_{\substack{a\le m\le b\\ c\le n\le d}}$ denotes a corresponding submatrix, and $[\mathbf{A}]_{mn}$ denotes an element; $\overline{(\bullet)}$ and $(\bullet)_N$ denote the complex conjugate and modulo-N operations; $\lfloor x \rfloor$ is the closest integer which is smaller than or equal to x, i.e., the floor operation.

4.1 Multiple CFOs Equalization in DSM MIMO OFDM

We first develop the algorithm within a DSM MIMO OFDM system with distributed transmit antennas. The performance of any OFDM system is highly sensitive to CFO because of the loss of orthogonality among subcarriers and the inter-carrier interference thus introduced. Therefore, accurate CFO estimation and tracking is important in OFDM systems. However, in the DSM scenario, because the different sources have different CFOs, the destination cannot track just one carrier frequency, and this causes the multiple CFOs problem in DSM. The compensation algorithm [58] fails if the channel becomes frequency selective.

4.1.1 System Model

Consider the DSM MIMO OFDM scheme with M_T transmit antennas and M_R receive antennas. The receive antennas belong to a multi-antenna receiver, but the transmit

antennas belong to different transmitters geographically scattered, and thus multiple CFOs happen. Suppose N is the number of subcarriers in OFDM modulation.

After removing the cyclic prefix (CP), the time domain received signal samples at the j-th receive antenna can be expressed as the $N \times 1$ vector $\mathbf{y}_j$, where

$$\mathbf{y}_j = \sum_{i=1}^{M_T} \mathbf{\Lambda}_i \mathbf{H}_{ji} \mathbf{x}_i + \mathbf{z}_i , \qquad (1)$$

where $\mathbf{x}_i$ is an $N \times 1$ vector of the time domain transmitted signal samples at the i-th transmit antenna, $\mathbf{z}_i$ is a vector of the additive white Gaussian noise (AWGN) samples with zero mean and covariance σ_n^2 at the i-th transmit antenna, $\mathbf{H}_{ji}$ is the circulant channel impulse response (CIR) matrix from the i-th transmit antenna to the j-th receive antenna, $\mathbf{\Lambda}_i$ is the phase error matrix for the i-th transmit antenna relative to the receiver, where $\mathbf{\Lambda}_i = diag(\xi_i^{(1)}, \xi_i^{(2)}, \cdots, \xi_i^{(N)})$ and $\xi_i^{(k)} = \exp(\frac{j2\pi k\varepsilon_i}{N})$ for k=1, 2, $\cdots$, N , and ε_i denotes the i-th transmit antenna's relative CFO normalized by the subcarrier frequency spacing.

From (1), the frequency domain received signal for the j-th receive antenna is an $N \times 1$ vector as

$$\tilde{\mathbf{y}}_j = \mathbf{F}\mathbf{y}_j = \sum_{i=1}^{M_T} \mathbf{F}\mathbf{\Lambda}_i \mathbf{F}^H \tilde{\mathbf{H}}_{ji} \tilde{\mathbf{x}}_i + \tilde{\mathbf{z}}_i ,$$

where $\tilde{\mathbf{H}}_{ji} = \mathbf{F}\mathbf{H}_{ji}\mathbf{F}^H$, $\tilde{\mathbf{x}}_i = \mathbf{F}\mathbf{x}_i$, $\tilde{\mathbf{z}}_i = \mathbf{F}\mathbf{z}_i$, $\mathbf{F}$ is the $N \times N$ discrete Fourier transform (DFT) matrix, and $\mathbf{F}^H$ is its Hermitian.

Define $\tilde{\mathbf{y}} = [\tilde{\mathbf{y}}_1^T, \tilde{\mathbf{y}}_2^T, \cdots, \tilde{\mathbf{y}}_{M_R}^T]^T$, $\tilde{\mathbf{z}} = [\tilde{\mathbf{z}}_1^T, \tilde{\mathbf{z}}_2^T, \cdots, \tilde{\mathbf{z}}_{M_R}^T]^T$, and $\tilde{\mathbf{x}} = [\tilde{\mathbf{x}}_1^T, \tilde{\mathbf{x}}_2^T, \cdots, \tilde{\mathbf{x}}_{M_T}^T]^T$, we get

$$\tilde{\mathbf{y}} = \tilde{\mathbf{H}}\tilde{\mathbf{x}} + \tilde{\mathbf{z}}, \qquad (2)$$

where the corresponding submatrix of $\tilde{\mathbf{H}}$ is $\left\{\tilde{\mathbf{H}}\right\}_{\substack{(i-1)N+1 \le m \le iN \\ (j-1)N+1 \le n \le jN}} = \mathbf{F}\mathbf{\Lambda}_i\mathbf{F}^H\tilde{\mathbf{H}}_{ji}$, which is approximately band-limited if ε_i is small, i.e., only the elements close to the diagonal axis are big in value, others are close to 0. Note that $\tilde{\mathbf{H}}_{ji}$ is diagonal, and $\mathbf{F}\mathbf{\Lambda}_i\mathbf{F}^H$ is circulant.

The traditional LMMSE estimate of $\tilde{\mathbf{x}}$ from (12) is $\hat{\tilde{\mathbf{x}}} = \tilde{\mathbf{H}}^H\left(\tilde{\mathbf{H}}\tilde{\mathbf{H}}^H + \mathbf{I}\sigma_n^2/\sigma_s^2\right)^{-1}\tilde{\mathbf{y}}$, where the matrix inversion computation load is $O\left(M_R N\right)^3$, which is huge when $M_R N$ is big. [54] proposed a linear equalization approach to compensate the multiple CFOs for the STBC OFDM case, which can be modified for the spatial multiplexing case. However, the approach needs a matrix inversion per subcarrier per antenna, so the computation load is $O\left(NM_T M_R^3\left(2L+1\right)^3\right)$, where $M_T \ll L \ll M_R N$; and the approach fails under large CFOs.

4.1.2 The Proposed Permutation Based Multiple CFOs Equalization Algorithm

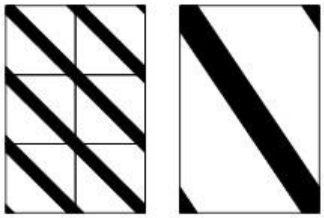

(a) Pattern of $\tilde{\mathbf{H}}$ (b) Pattern of $\hat{\mathbf{H}}$

Figure 13 The patterns of the banded matrix approximation for $\tilde{\mathbf{H}}$ and $\hat{\mathbf{H}}$

We propose an equalization algorithm in this section which can dramatically reduce this computational load by employing a recursive manner and the pseudo banded characteristic of the permutated matrix.

Define the permutation matrices as $\left[\mathbf{P}_L\right]_{i,j} = \begin{cases} 1 & \text{for } j = \mu_i \\ 0, & \text{otherwise} \end{cases}$ and $\left[\mathbf{P}_R\right]_{i,j} = \begin{cases} 1 & \text{for } j = \pi_i \\ 0, & \text{otherwise} \end{cases}$,

where $\mu_i = \left(\left(i-1\right)_N\right) \times M_R + \left\lfloor \left(i-1\right)/N \right\rfloor + 1$ and $\pi_i = \left(\left(i-1\right)_N\right) \times M_T + \left\lfloor \left(i-1\right)/N \right\rfloor + 1$.

Then from (2) we get

$$\hat{\mathbf{y}} = \hat{\mathbf{H}}\hat{\mathbf{x}} + \hat{\mathbf{z}}, \tag{3}$$

where $\hat{\mathbf{y}} = \mathbf{P}_L\tilde{\mathbf{y}}$, $\hat{\mathbf{x}} = \mathbf{P}_R\tilde{\mathbf{x}}$, $\hat{\mathbf{z}} = \mathbf{P}_R\tilde{\mathbf{z}}$ and $\hat{\mathbf{H}} = \mathbf{P}_L\tilde{\mathbf{H}}\mathbf{P}_R^T$. Note that $\hat{\mathbf{H}}$ is pseudo banded as the result of permutation and the pseudo banded characteristic of the submatrices of $\tilde{\mathbf{H}}$, as shown in Fig. 13.

Define $c(k) \triangleq \left((i-1+NM_R)_{NM_R} \right)+1$ and $c'(k) \triangleq \left((k-1+NM_T)_{NM_T} \right)+1$; these functions make the circular index operation. Let $\bar{\mathbf{y}}_k = [\tilde{y}_{c((k-L-1)M_R+1)}, \tilde{y}_{c((k-L-1)M_R+2)}, \cdots, \tilde{y}_{c((k+L)M_R)}]^T$ and define the $(2L+1)M_R \times NM_T$ submatrix $\widehat{\mathbf{H}}_k$ as $\left[\widehat{\mathbf{H}}_k\right]_{mn} = \left[\widehat{\mathbf{H}}\right]_{c((k-L-1)M_R+m),n}$ for $k = 1, \cdots, N$, where L is a parameter we choose for equalization, $M_T \ll L \ll M_R N$. Then from (3) we get

$$\bar{\mathbf{y}}_k = \widehat{\mathbf{H}}_k \tilde{\mathbf{x}} + \bar{\mathbf{z}}_k \text{ for } k = 1, \cdots, N . \quad (4)$$

Let $\bar{\mathbf{x}}_k = [\tilde{x}_{c'((k-1)M_T+1)}, \tilde{x}_{c'((k-1)M_T+2)}, \cdots, \tilde{x}_{c'(kM_T)}]^T$. From the discussion of $\widehat{\mathbf{H}}$, we conclude that the information of $\bar{\mathbf{x}}_k$ is mainly concentrated in $\bar{\mathbf{y}}_k$, and from (4) we get the LMMSE estimate of $\bar{\mathbf{x}}_k$ as

$$\hat{\bar{\mathbf{x}}}_k = \mathbf{A}_k \mathbf{\Phi}_k^{-1} \bar{\mathbf{y}}_k \text{ for } k = 1, \cdots, N , \quad (5)$$

where $\mathbf{A}_k = \left\{ \widehat{\mathbf{H}}_k \right\}_{\substack{1 \le m \le (2L+1)M_R \\ (k-1)M_T+1 \le n \le (k+1)M_T}}^{H}$ and $\mathbf{\Phi}_k = \widehat{\mathbf{H}}_k \widehat{\mathbf{H}}_k^H + \mathbf{I}\sigma_n^2 / \sigma_s^2$. The inversion of $\mathbf{\Phi}_k$ needs computational load $O\left(M_R(2L+1)\right)^3$ per subcarrier, but next we will find a recursive manner to reduce this load dramatically.

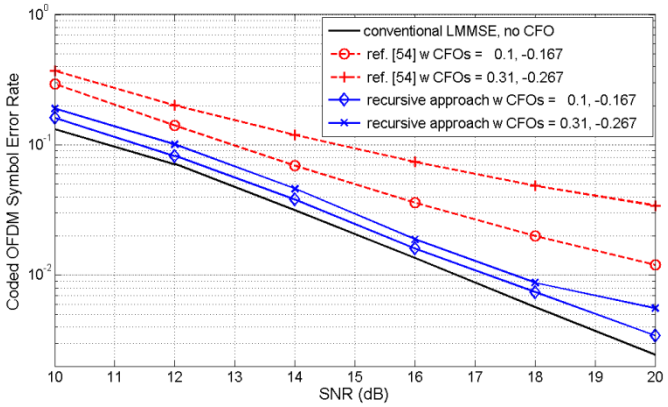

Figure 14 Coded OFDM SER of the multiple CFOs equalization for 2x2 DSM

Because $\widehat{\mathbf{H}}_k$ shares most of the elements of $\widehat{\mathbf{H}}_{k+1}$, it is not hard to find that we can write in the block partition manner as $\mathbf{\Phi}_{k+1} = \begin{bmatrix} \mathbf{\Xi} & \mathbf{r}_{k+1} \\ \mathbf{r}_{k+1}^H & \mathbf{v}_{k+1} \end{bmatrix}$ and $\mathbf{\Phi}_k = \begin{bmatrix} \mathbf{v}_k & \mathbf{r}_k^H \\ \mathbf{r}_k & \mathbf{\Xi} \end{bmatrix}$, where $\mathbf{\Xi}$ is a $2LM_R \times 2LM_R$ square matrix. As an extension derived from [50], if we have obtained $\mathbf{\Phi}_{k+1}^{-1} = \begin{bmatrix} \mathbf{\Theta} & \mathbf{w}_{k+1} \\ \mathbf{w}_{k+1}^H & \mathbf{s}_{k+1} \end{bmatrix}$, where $\mathbf{\Theta}$ is a $2LM_R \times 2LM_R$ square matrix, then we get

$$\mathbf{\Phi}_k^{-1} = \begin{bmatrix} \mathbf{v}_k^{-1} + \mathbf{v}_k^{-1}\mathbf{r}_k^H \mathbf{\Psi} \mathbf{r}_k \mathbf{v}_k^{-1} & -\mathbf{v}_k^{-1}\mathbf{r}_k^H \mathbf{\Psi} \\ -\mathbf{\Psi}\mathbf{r}_k \mathbf{v}_k^{-1} & \mathbf{\Psi} \end{bmatrix}, \tag{6}$$

where $\mathbf{\Psi} = \mathbf{\Xi}^{-1} + \mathbf{\Xi}^{-1}\mathbf{r}_k \left(\mathbf{v}_k - \mathbf{r}_k^H \mathbf{\Xi}^{-1}\mathbf{r}_k\right)^{-1} \mathbf{r}_k^H \mathbf{\Xi}^{-1}$ and $\mathbf{\Xi}^{-1} = \mathbf{\Theta} + \mathbf{\Theta}\mathbf{r}_{k+1}\left(\mathbf{v}_{k+1} - \mathbf{r}_{k+1}^H \mathbf{\Theta}\mathbf{r}_{k+1}\right)^{-1} \mathbf{r}_{k+1}^H \mathbf{\Theta}$.

The matrix inversion computational load per subcarrier here is only $O\left(M_R\right)^3$, and the main load is $O\left(M_T{}^2 N\right)$ for matrix multiplication. We further reduce this computational load by approximate $\widehat{\mathbf{H}}$ with $\widehat{\mathbf{H}}_b$ in (5) and (6), where

$$\left[\widehat{\mathbf{H}}_b\right]_{ij}=\begin{cases}\left[\widehat{\mathbf{H}}\right]_{c(i),c'(j)} \text{ for } (m-L-1)M_R+1\le i\le (m+L)M_R,\\ \qquad\qquad (m-L-1)M_T+1\le j\le (m+L)M_T,\ 1\le m\le N\ .\\ 0, \qquad \text{otherwise}\end{cases}$$

With (6) and this band matrix approximation, (5) can be solved recursively by starting from $k=N$ and ending with $k=1$, and only one inversion for a $(2L+1)\times(2L+1)$ matrix $\mathbf{\Phi}_N$ is needed. The total computation load is $O\left(NM_T{}^2(2L+1)\right)$, compared with $O\left(NM_TM_R^3(2L+1)^3\right)$ in [54].

4.1.3 Simulation Results

Fig. 14 depicts the simulation results for the coded OFDM Symbol Error Rate (SER) vs. SNR of the equalizer for 2x2 DSM OFDM case with multiple CFOs. In Monte Carlo simulation, we use the coded OFDM scheme with QPSK modulation, 128 subcarriers OFDM, $1/2$ rate convolutional code with generator [133, 171] and constraint length 7, hard decoding; the channel is 2x2 i.i.d. Rayleigh with 2 i.i.d. taps, and we set $L=10$ in this simulation for our recursive approach combined with band matrix approximation. We also plot out the result of the modified approach from [54] for comparison.

The black curve is the SER of a LMMSE detector with no CFOs, which plays as a benchmark for comparison. We plot two sets of curves with different CFOs, one with the CFOs 0.1 and -0.167, the other with the CFOs 0.31 and -0.267. We found that our recursive equalization algorithm works under both small CFOs and large CFOs, which

outperforms the approach of [54] quite well under large CFOs, and with much smaller computation load.

4.2 Multiple CFOs Equalization in STBC SC-FDE

Here we consider the STBC SC-FDE system with distributed transmit antennas. Similar to the DSM OFDM case, which was introduced in the last section, the performance of the STBC SC-FDE system is also highly sensitive to multiple CFOs as a block data transmission and frequency domain equalization scheme. We will show in this section that our approach also works for SC-FDE and STBC to compensate large frequency offsets and have high computational efficiency.

4.2.1 System Model

We consider the 2x1 SC-FDE STBC scheme supposed by [32] with two transmit and one receive antenna. Denote the nth symbol of the kth transmitted block from antenna i by $\mathbf{x}_i^{(k)}(n)$, where $\mathbf{x}_i$ is an $N \times 1$ vector for $i = 1,2$. After removing the cyclic prefix (CP), the time domain received signal samples at the j-th slot can be expressed as the $N \times 1$ vector $\mathbf{y}_j$, then received blocks at the k-th and $k+1$-th time slots are given by

$$\mathbf{y}^{(j)} = \sum_{i=1}^{2} \varphi_i^{(j)} \mathbf{\Lambda}_i \mathbf{H}_i \mathbf{x}_i^{(j)} + \mathbf{z}^{(j)} \quad \text{for} \quad j = k, k+1, \tag{7}$$

where $\mathbf{z}^{(j)}$ is a vector of the additive white Gaussian noise (AWGN) samples with zero mean and covariance σ_n^2 at the j-th slot, $\mathbf{H}_i$ is the circulant channel impulse response

(CIR) matrix from the i-th transmit antenna to the receive antenna, $\mathbf{\Lambda}_i$ is the phase error matrix for the i-th transmit antenna relative to the receiver, where $\mathbf{\Lambda}_i = diag(\xi_i^{(1)}, \xi_i^{(2)}, \cdots, \xi_i^{(N)})$ and $\xi_i^{(k)} = \exp(\frac{j2\pi k\varepsilon_i}{N})$ for k=1, 2, ⋯, N , here ε_i denotes the i-th transmit antenna's relative CFO normalized by the subcarrier frequency spacing. $\varphi_i^{(j)}$ are some known constants introduced by carrier offsets in the period of CP [32].

As in [32], for an odd integer number k we define

$\mathbf{x}_1^{(k+1)}(n) = -\overline{\mathbf{x}}_2^{(k)}\left((-n)_N\right)$ and $\mathbf{x}_2^{(k+1)}(n) = \overline{\mathbf{x}}_1^{(k)}\left((-n)_N\right)$.

From (7), the frequency domain received signal for the k-th and $k+1$-th time slots time slots are $N \times 1$ vectors as

$$\tilde{\mathbf{y}}_j = \mathbf{F}\mathbf{y}^{(j)} = \sum_{i=1}^{2} \varphi_i^{(j)} \mathbf{F}\mathbf{\Lambda}_i \mathbf{F}^H \tilde{\mathbf{H}}_i \tilde{\mathbf{x}}_i^{(j)} + \tilde{\mathbf{z}}_j \quad \text{for } j = k, k+1, \tag{8}$$

where $\tilde{\mathbf{H}}_i = \mathbf{F}\mathbf{H}_i\mathbf{F}^H$, $\tilde{\mathbf{x}}_i^{(j)} = \mathbf{F}\mathbf{x}_i^{(j)}$, $\tilde{\mathbf{z}}_j = \mathbf{F}\mathbf{z}^{(j)}$.

From the properties of the DFT, we have [32]

$\tilde{\mathbf{x}}_1^{(k+1)} = -\overline{\tilde{\mathbf{x}}}_2^{(k)}$ and $\tilde{\mathbf{x}}_2^{(k+1)} = -\overline{\tilde{\mathbf{x}}}_1^{(k)}$.

Without loss of generality, let $k = 1$, and define $\tilde{\mathbf{y}} = [\tilde{\mathbf{y}}_1^T, \overline{\tilde{\mathbf{y}}}_2^T]^T$, $\tilde{\mathbf{z}} = [\tilde{\mathbf{z}}_1^T, \tilde{\mathbf{z}}_2^T]^T$, and $\tilde{\mathbf{x}} = [\tilde{\mathbf{x}}_1^{(1)T}, \tilde{\mathbf{x}}_2^{(1)T}]^T$, from (8) we get

$$\tilde{\mathbf{y}} = \tilde{\mathbf{H}}\tilde{\mathbf{x}} + \tilde{\mathbf{z}}, \tag{9}$$

where $\tilde{\mathbf{H}} = \begin{bmatrix} \varphi_1^{(k)}\tilde{\mathbf{\Lambda}}_1\tilde{\mathbf{H}}_1 & \varphi_2^{(k)}\tilde{\mathbf{\Lambda}}_2\tilde{\mathbf{H}}_2 \\ \overline{\varphi}_1^{(k+1)}\overline{\tilde{\mathbf{\Lambda}}}_1\overline{\tilde{\mathbf{H}}}_1 & -\overline{\varphi}_2^{(k+1)}\overline{\tilde{\mathbf{\Lambda}}}_2\overline{\tilde{\mathbf{H}}}_2 \end{bmatrix}$ and $\tilde{\mathbf{\Lambda}}_i = \mathbf{F}\mathbf{\Lambda}_i\mathbf{F}^H$ which is approximately band-limited if ε_i is small. Note that $\tilde{\mathbf{H}}_i$ is diagonal, and $\mathbf{F}\mathbf{\Lambda}_i\mathbf{F}^H$ is circulant.

The traditional LMMSE estimate of $\tilde{\mathbf{x}}$ from (9) is $\hat{\tilde{\mathbf{x}}} = \tilde{\mathbf{H}}^H\left(\tilde{\mathbf{H}}\tilde{\mathbf{H}}^H + \mathbf{I}\sigma_n^2/\sigma_s^2\right)^{-1}\tilde{\mathbf{y}}$, where the matrix inversion computational load is high.

4.2.2 Permutation Based Multiple CFOs Equalization Algorithm

Now we adopt the same steps as Eq. (1)-(6) which are introduced in last section to get $\hat{\tilde{\mathbf{x}}}$, and thus $\hat{\tilde{\mathbf{x}}}_1^{(1)}$ and $\hat{\tilde{\mathbf{x}}}_2^{(1)}$.

Then we get the estimation for the transmitted data as

$$\hat{\mathbf{x}}_i^{(1)} = \mathbf{F}^H\hat{\tilde{\mathbf{x}}}_i^{(1)} \text{ for } i = 1,2. \qquad (10)$$

4.2.3 Simulation Results

Fig. 15 depicts the simulation results for the uncoded SC-FDE Symbol Error Rate (SER) vs. SNR of the equalizer for 2x1 uncoded STBC SC-FDE case [32] with multiple CFOs. In Monte Carlo simulation, we use an uncoded SC-FDE scheme with QPSK modulation and block data length $N = 64$, the channels from the transmit antennas to the receive antanna are i.i.d. Rayleigh with 2 i.i.d. taps, and we set $L = 10$ in this simulation for our recursive approach combined with band matrix approximation. An error is counted when there is decision error in the whole STBC codeword.

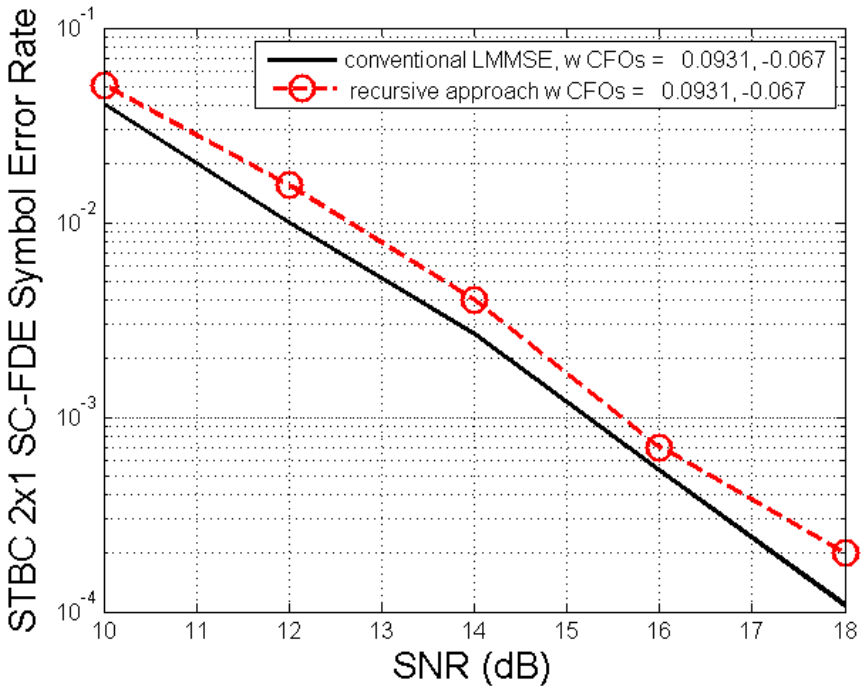

Figure 15 SC-FDE SER for 2x1 STBC under multiple CFOs

The black curve is the SER of a LMMSE detector with no CFOs, which plays as a benchmark for comparison. We plot the performance curve of the proposed approach under the normalized CFOs 0.0931 and -0.067. We found that our recursive equalization algorithm has the performance very close to that of the conventional LMMSE.

The corresponding simulation results for Bit Error Rate (BER) vs. SNR are plotted out in Fig. 16. One interesting phenomenon is that the proposed approach has lower BER than the conventional LMMSE as shown in Fig. 16, though the SER is still higher as shown in Fig. 15. Further analysis shows that the proposed approach has lower conditional BER in a decided SC-FDE symbol with decision error, as shown in Fig. 17.

4.3 Conclusion

A Linear MMSE equalization algorithm in the frequency domain is developed to compensate the multiple CFOs. By using the permutation based approach which employs the pseudo banded matrix characterization, a recursive and computationally efficient equalization algorithm is proposed. This approach can be generalized for the problem of frequency domain equalization with multiple CFOs problems, for both OFDM and SC-FDE, and for both distributed MIMO and STBC scenarios. The algorithm is evaluated by simulation to show that it can compensate large frequency offsets and have high computational efficiency.

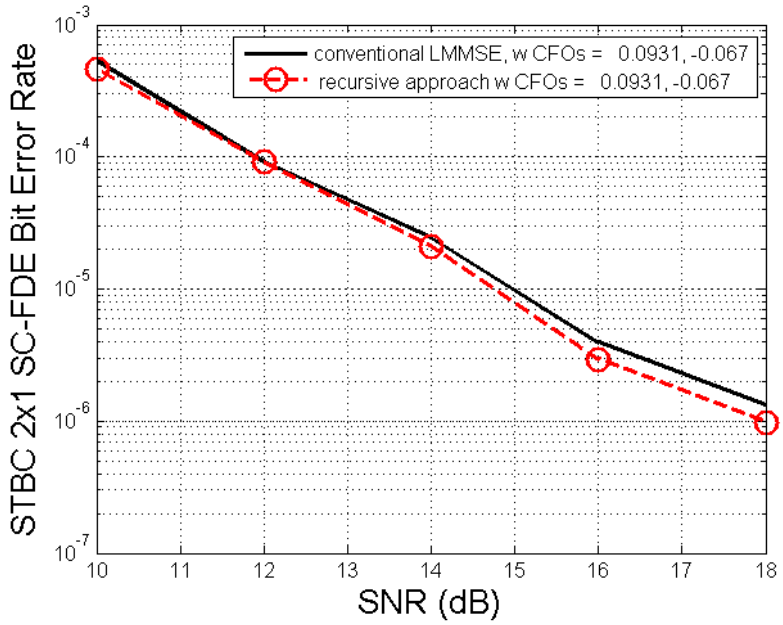

Figure 16 BER for SC-FDE 2x1 STBC under multiple CFOs

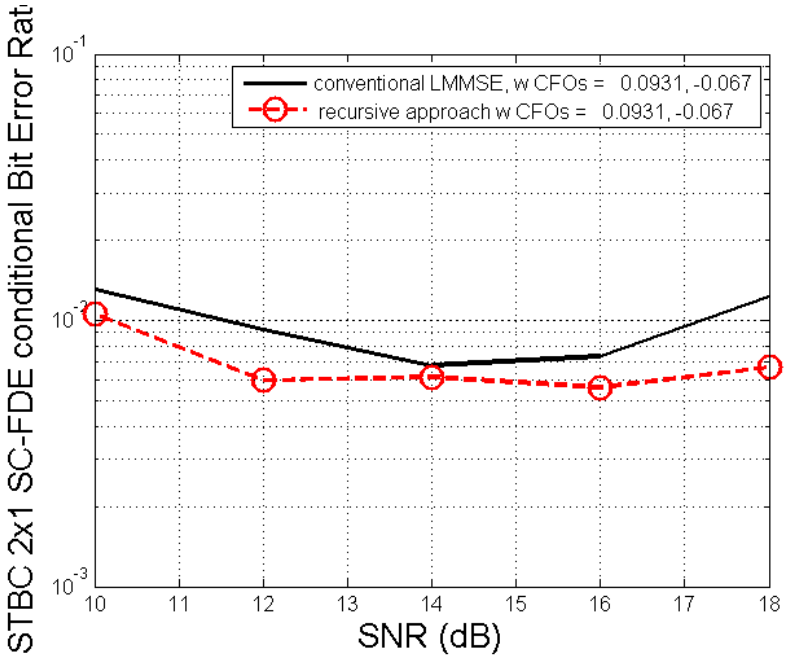

Figure 17 conditional BER for SC-FDE 2x1 STBC under multiple CFOs

CHAPTER 5. DIVERSITY ORDER ANALYSIS OF LINEAR SC-FDE

The single-carrier frequency-domain equalizer (SC-FDE) is a block data processing technique for frequency selective channels, first suggested in [66]. Similar to orthogonal frequency-division multiplexing (OFDM), its frequency domain counterpart, SC-FDE is preferred over the time domain equalizer for the broadband channel with a long channel impulse response (CIR) because of its lower complexity. Also, when compared to coded OFDM, SC-FDE has a much lower peak-to-average power ratio in transmitting, but similar error performance [67]. The above advantages make SC-FDE desirable for wireless broadband transmission. Single Carrier-FDMA, which is a modified version of SC-FDE for multiple accessing, is the uplink transmission technique for 3GPP LTE [68]. A good survey about SC-FDE is found in [67].

Outage probability is an appropriate metric for systems with powerful channel codes, however, for a system without such channel coding and where the data is decided at the output of the equalizer, the average symbol error probability (SEP) is popular. The diversity orders of these two metrics can be different and are important for fading channels. If the channel has only two taps, the most straightforward approach involves finding the probability density function (PDF) of the signal to interference noise ratio (SINR) by variable transformation [92, section 3-6]; for more taps, this generally involves multi-dimensional integration, which is extremely involved and generally leads to no explicit conclusion, so a new mathematical approach is desired. As we explain in

the next section and summarize in Table 1, several authors have analyzed diversity order of outage and SEP, however their results contradict each other and make this topic controversial.

In this dissertation, we present a novel bounding technique to analyze diversity. It is a unified approach to derive the diversity order of the outage probability and SEP for both the minimum mean-square error (MMSE) and the zero forcing (ZF) SC-FDE. It is the first time these diversity orders have been derived strictly. The study shows that the diversity orders of SEP for both the MMSE and ZF SC-FDE are one. We have also relaxed the constraint for the channel model from channels with identical and independent distributed (i.i.d.) paths [69, 70] to channels with just independent paths in our analysis; this is a useful contribution because the average tap powers of most real channels decay exponentially [71]. The results proven in this dissertation are summarized in the bottom of Table 1.

Analysis of the outage probability and diversity order for linear SC-FDE was first attempted in [72]; the study revealed that full diversity can be achieved for very low rate and diversity one for high rate, for MMSE SC-FDE. Limitations of this study include approximation of outage regions, only considers very high or very low data rates, and that the transmission block length must be equal to the number of channel taps.

The study in [73] finds the outage diversity order of MMSE SC-FDE for the channel with i.i.d. paths. For the channel with memory length ν, block data length n and data rate R, the outage diversity gain is $d_{out}^{MMSE} = \min\left(\lfloor 2^{-R} n \rfloor + 1, \nu + 1\right)$. Explaining further in [69], the

authors follow the techniques used in diversity-multiplexing tradeoff (DMT) analysis in [78], which were originally proposed for the analysis of the diversity order of multiple-in

Table 1 the asymptotic analysis of diversity order for SC-FDE

Reference	Channel model	Type of equalization	Type of metric	Diversity order	Notes
[73]	i.i.d. channel paths	MMSE	Outage	$\min\left(\lfloor 2^{-R}n \rfloor+1, \nu+1\right)$	Problematic proof
[69]		MMSE	Outage	$\min\left(\lfloor 2^{-R}n \rfloor+1, \nu+1\right)$	
[69]		MMSE	SEP	$\min\left(\lfloor 2^{-R}n \rfloor+1, \nu+1\right)$	Wrong conclusion
[70]		ZF	Outage	1	Problematic proof
[74]		ML	SEP	full	
[75, 76]		ML	SEP	1	
[77]	i.i.d. channel paths	ML	SEP	≥ 1	The conclusion contradicts [75, 76]
[77]		MMSE DFE	SEP	full	
This work	inde-pendent channel paths	ZF	SEP	1	
		ZF	Outage	1	
		MMSE	SEP	1	
		MMSE	Outage	$\min\left(\lfloor 2^{-R}n \rfloor+1, \nu+1\right)$	

multiple-output (MIMO) transmission. In the proof of [69, Lemma 1], the authors implicitly assert that if two functions are exponentially equal, i.e., if $f(\boldsymbol{\beta}, \bar{\gamma}) \doteq g(\boldsymbol{\beta}, \bar{\gamma})$, then $P(f(\boldsymbol{\beta}, \bar{\gamma}) > c) \doteq P(g(\boldsymbol{\beta}, \bar{\gamma}) > c)$, where $\bar{\gamma}$ is the average signal to noise ratio (SNR), $\boldsymbol{\beta}$ represents a vector of random variables, $P(\cdot)$ is the probability measure, and c

is a positive constant. Exponential equality will be defined in the next paragraph. However, this assertion can be verified not to be always correct and we give a counter-example and the details in Appendix A.1.

The study in [70, Theorem 1] showed that the outage diversity order for the zero forcing (ZF) SC-FDE is one. The proof is given in [70, Appendix B]. However, in deriving the lower bound of the diversity, a property is simply assumed that the distribution of the SINR when SINR is close to 0 will be similar to that of a chi-squared random variable and the first order derivative of its cumulative distribution function (CDF) at zero is bounded and nonzero. Such an assertion is lack of proof. In this dissertation, we use upper and lower bounds to avoid this assumption.

In summary, with regard to the outage diversity of the linear SC-FDE, rigorous analysis is needed to support the claimed results in [69, 70, 73].

For SEP diversity, [74] claimed uncoded SC-FDE achieves full diversity gain with maximum-likelihood (ML) detection. However, [75] points out an error in [74] and claims the diversity order is 1 for optimal ML detection, thus 1 is the upper bound for any detection algorithm, while [76] makes the same claim. [77] argued that [75] only derived the lower bound for diversity order of ML detection, and claimed that the MMSE SC-DFE with decision feedback can achieve full diversity. However, such analyses for linear equalizers, i.e., both ZF and MMSE SC-FDE, are still absent. Our work shows that the diversity orders of SEP of ZF and MMSE SC-FDE are both 1, and thus achieves the upper bound of diversity order for SC-FDE. We should point out that the analysis in [77]

assumes an equalizer with infinite data block length, and the diversity order is analyzed only for outage. Table 1 summarizes the issues with these previous works and shows what is proved in this dissertation.

5.1 System Model

In this section, we first define the model for the SC-FDE. Next, we give our notation for diversity order for SEP and outage probability.

5.1.1 SC-FDE

We consider the block data transmission scheme over a static frequency selective channel with independent paths and memory length ν , the channel vector $\mathbf{h} = [h_0, h_1, \cdots, h_\nu]^T \sim \mathcal{CN}(0, \mathbf{D})$, where $\mathbf{D}$ is a diagonal matrix with positive diagonal elements, i.e., the elements of $\mathbf{h}$ are independently complex Gaussian distributed. The information symbol block $\mathbf{x}$ is a column vector with length $n \geq \nu + 1$, with uncorrelated, zero mean components, $E\left[\mathbf{x}\mathbf{x}^H\right] = \sigma_s^2 \mathbf{I}$. In the SC-FDE scheme, a cyclic prefix (CP) is inserted before $\mathbf{x}$ on the transmitter side and removed on the receiver side, to avoid inter-block interference. Suppose $\mathbf{y}$ is the received signal after CP removal, and then the input-output model is $\mathbf{y} = \mathbf{H}\mathbf{x} + \mathbf{n}$, where $\mathbf{H}$ is the circulant matrix generated with $\mathbf{h}$ and the noise vector is $\mathbf{n} \sim \mathcal{CN}(0, \sigma_n^2 \mathbf{I})$. The output of equalization is

$$\hat{\mathbf{y}} = \mathbf{W}\mathbf{y} = \mathbf{W}(\mathbf{H}\mathbf{x} + \mathbf{n}), \tag{11}$$

where $\mathbf{W}$ is the equalization matrix [29, 67]. The computationally efficient algorithm

uses the fast Fourier transform (FFT) and inverse FFT, and leads to the SC-FDE. The channel frequency response (CFR) $\boldsymbol{\lambda} = (\lambda_1, \lambda_2, \cdots, \lambda_n)^T$ is the n-point discrete Fourier transform (DFT) of $\mathbf{h}$

$$\boldsymbol{\lambda} = \mathbf{F}\mathbf{h}, \tag{12}$$

where $\mathbf{F}$ is a $n \times (\nu + 1)$ matrix with element $[\mathbf{F}]_{kl} = e^{-j2\pi(k-1)(l-1)/n}$, i.e., $\mathbf{F}$ is a submatrix formed by the first $\nu + 1$ columns of the DFT matrix. Note that the λ_k's are eigenvalues of $\mathbf{H}$ and complex Gaussian.

We define the transmission SNR $\bar{\gamma} = \sigma_s^2 / \sigma_n^2$ and

$$\gamma_k = \bar{\gamma} |\lambda_k|^2 . \tag{13}$$

5.1.2 Diversity analysis

Let $\mathrm{P}_e(\gamma)$ be the SEP with channel-dependent SNR γ, which is depicted in [7, Eq. (4.1-15)]. While γ is parameterized by $\bar{\gamma}$, the average SEP is defined as

$$\bar{P}_{e,\gamma}(\bar{\gamma}) = \int_0^\infty P_e(\gamma) p_\gamma(\gamma) d\gamma , \tag{14}$$

where $p_\gamma(\gamma)$ is the PDF of γ. The diversity order of error probability is defined as [18]

$$d_e = -\lim_{\bar{\gamma} \to \infty} \log \bar{P}_{e,\gamma}(\bar{\gamma}) / \log \bar{\gamma} . \tag{15}$$

The channel capacity is $C(\gamma)=\log(1+\gamma)$ and the outage probability is defined as $P_{out,\gamma}(R)=P\left[C(\gamma)<R\right]$, where R is the transmission rate. The outage diversity order is defined as $d_{out}=-\lim_{\bar{\gamma}\to\infty}\log P_{out,\gamma}(R,\nu,n,\bar{\gamma})/\log\bar{\gamma}$. Outage event $C(\gamma)<R$ is equivalent to $\gamma<2^R-1$. Note d_{out} is modulation-independent whereas d_e is modulation-dependent.

As in [78], we denote *exponential equality* by $f(\bar{\gamma})\doteq\bar{\gamma}^d$ if $d=\lim_{\bar{\gamma}\to\infty}\frac{\log f(\bar{\gamma})}{\log\bar{\gamma}}$, d is called the *exponential order* of $f(\bar{\gamma})$; we define as $f(\bar{\gamma})\dot{\leq}\bar{\gamma}^d$ if $f(\bar{\gamma})\leq\hat{f}(\bar{\gamma})$ for any function $\hat{f}(\bar{\gamma})$ such that $\hat{f}(\bar{\gamma})\doteq\bar{\gamma}^d$, and we define as $f(\bar{\gamma})\dot{\geq}\bar{\gamma}^d$ if $f(\bar{\gamma})\geq\breve{f}(\bar{\gamma})$ for any $\breve{f}(\bar{\gamma})$ such that $\breve{f}(\bar{\gamma})\doteq\bar{\gamma}^d$.

5.2 General Approach and Simple Example

In this section, we first describe our general approach to find diversity order, which uses upper and lower bounds, and then we show a simple example to illustrate our set-based approach to find the bounds.

5.2.1 General approach

We first state Proposition 1, which is the basis for our novel approach in this dissertation.

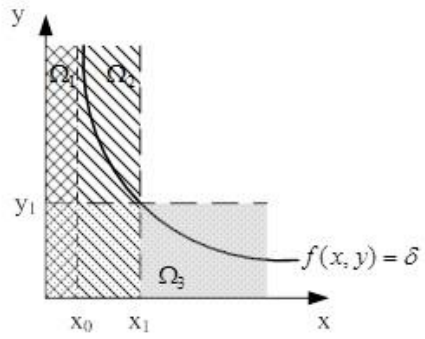

Figure 18 Integration region for diversity analysis of MMSE SC-FDE, $0 < \delta < 1$

Proposition 1: If $f(\bar{\gamma}) \dot{\geq} \bar{\gamma}^d$ and $f(\bar{\gamma}) \dot{\leq} \bar{\gamma}^d$, then $f(\bar{\gamma}) \doteq \bar{\gamma}^d$. This is clear from $\lim_{\bar{\gamma}\to\infty} \frac{\log f(\bar{\gamma})}{\log \bar{\gamma}} \geq d$ and $\lim_{\bar{\gamma}\to\infty} \frac{\log f(\bar{\gamma})}{\log \bar{\gamma}} \leq d$, then $\lim_{\bar{\gamma}\to\infty} \frac{\log f(\bar{\gamma})}{\log \bar{\gamma}} = d$. Similarly, if $\overline{f}(\bar{\gamma}) \geq f(\bar{\gamma}) \geq \underline{f}(\bar{\gamma})$ when $\bar{\gamma}$ is big enough, and $\overline{f}(\bar{\gamma}) \doteq \underline{f}(\bar{\gamma}) \doteq \bar{\gamma}^d$, then $f(\bar{\gamma}) \doteq \bar{\gamma}^d$.

Thus, our approach for each type of equalizer is as follows: we find upper and lower bounds for each of the error probability and the outage probability, and we show the upper and lower bounds are of the same exponential order; thus the bounds are tight in the sense of diversity order and we can claim that the equalizer has a certain diversity order. While trivial upper and lower bounds are easy to find, the challenging aspect of this work is to find bounds that have the same diversity order.

5.2.2 Simple example of finding bounds

As an illustration of how we find bounds, we consider the simplest case for the outage of MMSE SC-FDE. We show that the diversity order depends on the outage threshold of instantaneous SINR at the output of the equalizer.

The simplest case is $n=\nu+1=2$ when the elements of **h** are i.i.d. complex Gaussian distributed, for which the unbiased decision point SINR [72] is $\gamma_{MMSE}=\frac{2}{f(x,y)}-1$, where $f(x,y)=\frac{1}{1+x}+\frac{1}{1+y}$, $x=\bar{\gamma}\left|\lambda_1\right|^2$, $y=\bar{\gamma}\left|\lambda_2\right|^2$, and λ_1, λ_2 are i.i.d. complex Gaussian according to (12). Suppose outage happens when $f(x,y)>\delta$, which is equivalent to a threshold on γ_{MMSE}. Then the outage probability is $P_{out}=P(\Omega)=\iint_{\Omega}p(x)p(y)dxdy$, where the integration region $\Omega=\{(x,\,y):\,f(x,y)>\delta\}$, which is below the curve in Fig. 18. Note $x>0,\,y>0$.

The case for $0<\delta<1$ is shown in Fig. 18. Note that Ω_2 includes Ω_1. We define the following regions as: $\Omega_k=\{(x,\,y):\,x_{k-1}>x>0,\,y>0\}$ for $k=1,2$, and $\Omega_3=\{(x,\,y):\,x>0,\,y_1>y>0\}$. It is clear that $\Omega_1\subset\Omega\subset(\Omega_2\cup\Omega_3)$, so we can get the upper bound as

$P(\Omega_2)+P(\Omega_3)>P(\Omega_2\cup\Omega_3)>P(\Omega)$. We can find $P(\Omega_2)$ by integration, specifically, $P(\Omega_2)=\int_0^{x_1}p_x(x)dx$, where $x=\bar{\gamma}\left|\lambda_1\right|^2$ is exponentially distributed. It is easy to find that $-\lim_{\bar{\gamma}\to\infty}\frac{\log P(\Omega_2)}{\log\bar{\gamma}}=1$, which means the diversity order of $P(\Omega_2)$ is 1, or $P(\Omega_2)\doteq\bar{\gamma}^{-1}$. Similarly, $P(\Omega_3)\doteq\bar{\gamma}^{-1}$. It is trivial to prove that $P(\Omega_2)+P(\Omega_3)\doteq\bar{\gamma}^{-1}$.

The lower bound is $P(\Omega_1) < P(\Omega)$; using the same technique, we have $P(\Omega_1) \doteq \bar{\gamma}^{-1}$. Since the upper and lower bounds have the same diversity order, we conclude that MMSE SC-FDE has diversity order of one, for $n = \nu + 1 = 2$, $0 < \delta < 1$, and i.i.d. complex Gaussian elements in $\mathbf{h}$.

This simple case is clear for explanation. But generally we have $n > \nu + 1$, the elements of $\mathbf{h}$ are not i.i.d. complex Gaussian, and the λ_k's in (12) are not independent, so there is no such straightforward relation between the integration region and the diversity order shown in this example. However, we will still rely on operations on sets and bounding techniques for diversity analysis.

5.3 Diversity Analysis of ZF SC-FDE

Following the general approach we just introduced, we will find the diversity order of ZF SC-FDE in this section. Some results from this will be used in the analysis of MMSE SC-FDE.

For the ZF SC-FDE, the equalizer in (11) is $\mathbf{W} = \mathbf{W}_{ZF} = (\mathbf{H}^H \mathbf{H})^{-1} \mathbf{H}^H$, and the unbiased decision point SNR is [72]

$$\gamma = \gamma_{ZF} = \frac{1}{\frac{1}{n}\sum_{i=1}^{n} \frac{1}{\bar{\gamma}|\lambda_i|^2}} = \frac{n}{\sum_{i=1}^{n} \frac{1}{\gamma_i}}. \tag{16}$$

If the analytical expression of the distribution of γ is known, the diversity order of error can be obtained by using the results of [93], and the diversity of outage can also be

derived. Although it is possible to find the distribution by variable transformation, the expression includes a multidimensional integral. In the simplest case where $n = \nu + 1 = 2$, the CDF of γ_{ZF} is only a two dimensional integral [70, Appendix C]. In other cases, the integral dimensions are higher and too complicated to be of any use in analysis.

We next develop Proposition 2 and Lemma 1 to facilitate the diversity analysis of SEP, which is an extension of [93, Proposition 1].

Proposition 2: For an instantaneous SNR γ_x, we can deduce from [7, Eq. (4.2-93)] that

$$M_4 Q(\sqrt{M_3 \gamma_x}) \le \mathrm{P}_e(\gamma_x) \le M_2 Q(\sqrt{M_1 \gamma_x}), \tag{17}$$

where $Q(\bullet)$ is the Gaussian tail function, M_1, M_2, M_3 and M_4 are modulation-dependent positive constants. From (14) we get $M_4 \int_0^\infty Q(\sqrt{M_3 \gamma}) p_{\gamma_x}(\gamma) d\gamma \le \bar{P}_{e,\gamma_x} \le M_2 \int_0^\infty Q(\sqrt{M_1 \gamma}) p_{\gamma_x}(\gamma) d\gamma$.

Lemma 1: If the following three assumptions are fulfilled:

AS1) The instantaneous SNR $\gamma_x = n\bar{\gamma}\beta + \gamma_{th}$, where $\bar{\gamma}$ is the average SNR, β is a channel dependent nonnegative random variable, γ_{th} is a nonnegative constant.

AS2) The SEP of the memoryless modulation follows (17).

AS3) The CDF $F_\beta(\beta) = a\beta^t + o(\beta^t)$ for $\beta < C$, where $C > 0$, $a > 0$, and $t \ge 0$. Here we denote a function $f(y)$ of y as $o(y^t)$ if $\lim_{y \to 0} f(y)/y^t = 0$.

Then $\overline{\mathrm{P}}_{e,\gamma_x} \doteq \overline{\gamma}^{-t}$, i.e., the error diversity order is $d_e = t$.

Proof: First we find a upper bound for the average SEP $\overline{\mathrm{P}}_{e,\gamma_x}$. Because $\gamma_x \geq n\gamma_i$, where $\gamma_i = \overline{\gamma}\beta$, it is straightforward to find $\overline{\mathrm{P}}_{e,n\gamma_i} \doteq \overline{\gamma}^{-t}$ from [93, Proposition 1] and $\overline{\mathrm{P}}_{e,\gamma_x} \dot{\leq} \overline{\gamma}^{-t}$.

Next we find a lower bound for $\overline{\mathrm{P}}_{e,\gamma_x}$ (thus the upper bound for d_e in (15)). For $\gamma_x < \gamma_{th}+1$, or $\beta < 1/(n\overline{\gamma})$, the instantaneous SEP satisfies $\mathrm{P}_e(\gamma_x) > \underline{C}$, where $\underline{C} = \mathrm{P}_e(\gamma_{th}+1)$ is a positive constant (note $\mathrm{P}_e(x)$ is monotone decreasing if $x > 0$). Let $p(\beta)$ be the PDF of β, then

$$\overline{\mathrm{P}}_{e,\gamma_x} = \int_0^{\infty} \mathrm{P}_e(\gamma_x)\, p(\gamma_x)\mathrm{d}\gamma_x > \int_0^{\gamma_{th}+1} \mathrm{P}_e(\gamma_x)\, p(\gamma_x)\mathrm{d}\gamma_x$$
$$> \int_0^{\gamma_{th}+1} \underline{C}\, p(\gamma_x)\mathrm{d}\gamma_x = \underline{C}\int_0^{\frac{1}{n\overline{\gamma}}} p(\beta)\mathrm{d}\beta = \underline{C}F_{\beta}(\frac{1}{n\overline{\gamma}}) \doteq \overline{\gamma}^{-t},$$

From (15) we get $d_e \leq t$. From Proposition 1 we conclude $\overline{\mathrm{P}}_{e,\gamma_x} \doteq \overline{\gamma}^{-t}$ or $d_e = t$. □

We note that Lemma 1 does not address a particular equalizer. It is a result of assuming a certain affine dependence of SNR on $\overline{\gamma}$.

Next, Proposition 3 and 4 constitute a special case of Lemma 1; we use this special case frequently in our work.

Proposition 3: If $\gamma_x = \bar{\gamma}\beta$ and β is exponentially distributed, then from Lemma 1, we get $\int_0^\infty Q(\sqrt{M\gamma}) p_{\gamma_x}(\gamma) d\gamma \doteq \bar{\gamma}^{-1}$ for any positive constant M, and we conclude $\bar{P}_{e,\gamma_x}(\bar{\gamma}) \doteq \bar{\gamma}^{-1}$.

Proposition 4: If $x_1, x_2, \cdots, x_d$ are independent exponential random variables, then $P\left(x_i \le t/\bar{\gamma} \text{ for } d \ge i \ge 1\right) \doteq \bar{\gamma}^{-d}$ for some positive real t. It is straightforward to prove this using integration. This simply extends the analysis in Section II to d variables.

Now we summarize the analysis for ZF SC-FDE, which is presented in the remainder of this section. The lower bounds for SEP and outage probability are derived in Lemma 2; the upper bounds are derived using Lemmas 3, 4 and Lemma 5; and the final result is Theorem 1.

Lemma 2: The outage probability of the ZF SC-FDE is lower bounded as $P_{out,\gamma_{ZF}}(R) \dot{\ge} \bar{\gamma}^{-1}$, and the average SEP of the ZF SC-FDE is lower bounded as $\bar{\mathrm{P}}_{e,\gamma_{ZF}} \dot{\ge} \bar{\gamma}^{-1}$.

Proof: From (16), $\gamma_{ZF} \le n\gamma_i = \widehat{\gamma}_i$ for any i. From Prop. 3, $\bar{P}_{e,n\gamma_i} \doteq \bar{\gamma}^{-1}$. We get $P_e(\gamma_{ZF}) \ge P_e(n\gamma_i)$ and $\bar{P}_{e,\gamma_{ZF}} \ge \bar{P}_{e,n\gamma_i}$, because $P_e(\gamma)$ is a decreasing function. From $C(\gamma_{ZF}) \le C(n\gamma_i)$, we get $P_{out,\gamma_{ZF}}(R) \ge P_{out,n\gamma_i}(R)$. □

Lemma 3: Define a new random variable γ_{LB} by its CDF $F_{\gamma_{LB}}(\varepsilon) = \min(1, \sum_{i=1}^{n} F_{\gamma_i}(\varepsilon)) = \min(1, \sum_{i=1}^{n} F_{|\lambda_i|^2}(\frac{\varepsilon}{\bar{\gamma}}))$; then $F_{\gamma_{LB}}(\varepsilon) \ge F_{\gamma_{ZF}}(\varepsilon)$ for any $\varepsilon \ge 0$.

Proof:

$$F_{\gamma_{ZF}}(\varepsilon)=\Pr(\gamma_{ZF}\le\varepsilon)\le 1-\Pr\left(\bigcap_{i=1}^{n}U_i\right)=\Pr\left(\overline{\bigcap_{i=1}^{n}U_i}\right)=\Pr\left(\bigcup_{i=1}^{n}\bar{U}_i\right)\le\sum_{i=1}^{n}\Pr(\bar{U}_i)=\sum_{i=1}^{n}F_{\gamma_i}(\varepsilon) \quad ,$$

where $U_i=\{U:\gamma_i>\varepsilon\}$. Therefore $F_{\gamma_{ZF}}(\varepsilon)\le\sum_{i=1}^{n}F_{\gamma_i}(\varepsilon)$. □

Lemma 4: If $F_{\gamma_{LB}}(\varepsilon)\ge F_{\gamma_{ZF}}(\varepsilon)$ for any $\varepsilon\ge 0$, then $\bar{\mathrm{P}}_{e,\gamma_{ZF}}\le\bar{\mathrm{P}}_{e,\gamma_{LB}}$ and $P_{out,\gamma_{ZF}}(R)\le P_{out,\gamma_{LB}}(R)$.

Proof: Because $P_e(\gamma)$ is a decreasing continuous function of γ, $P_e(\gamma)\ge 0$, and $P_e(\infty)=0$, we have $P_e(\gamma)=\int_{\gamma}^{\infty}-P_e'(x)dx$, where $P_e'(\gamma)=dP_e(\gamma)/d\gamma<0$. Then from (14) we get

$$\bar{P}_{e,\gamma}=\int_0^{\infty}\int_{\gamma}^{\infty}-P_e'(x)p_{\gamma}(\gamma)dxd\gamma=\int_0^{\infty}\int_0^{x}-P_e'(x)\,p_{\gamma}(\gamma)d\gamma dx=\int_0^{\infty}-P_e'(x)F_{\gamma}(x)dx\,.$$

The third equality follows by change of the order of integration. Then from $F_{\gamma_{LB}}(\varepsilon)\ge F_{\gamma_{ZF}}(\varepsilon)$ we conclude $\bar{\mathrm{P}}_{e,\gamma_{ZF}}\le\bar{\mathrm{P}}_{e,\gamma_{LB}}$ and $P_{out,\gamma_{ZF}}(R)\le P_{out,\gamma_{LB}}(R)$. □

Lemma 5: The outage probability of ZF SC-FDE is upper bounded as $P_{out,\gamma_{ZF}}(R)\dot{\le}\,\bar{\gamma}^{-1}$; the average SEP of ZF SC-FDE is upper bounded as $\bar{\mathrm{P}}_{e,\gamma_{ZF}}\dot{\le}\,\bar{\gamma}^{-1}$.

Proof: With γ_{LB} defined in Lemma 3, then $F_{\gamma_{LB}}(\varepsilon) = \sum_{i=1}^{n} F_{|\lambda_i|^2}(\varepsilon/\bar{\gamma})$ when $\varepsilon/\bar{\gamma}$ is small enough or $\bar{\gamma}$ is big enough, and it follows From Prop. 4 that $P_{out,\gamma_{LB}}(R) = F_{\gamma_{LB}}(2^R - 1) \doteq \bar{\gamma}^{-1}$.

From Lemma 4, we have $P_{out,\gamma_{ZF}}(R) \le P_{out,\gamma_{LB}}(R) \doteq \bar{\gamma}^{-1}$.

Let $\gamma_{LB} = \bar{\gamma}\left|\lambda_{LB}\right|^2$ where $F_{|\lambda_{LB}|^2}(x) = \min(1, \sum_{i=1}^{n} F_{|\lambda_i|^2}(x))$, so $p_{|\lambda_{LB}|^2}(x) = \sum_{i=1}^{n} p_{|\lambda_i|^2}(x)$ for small enough x. It can be derived from Lemma 1 that $\overline{\mathrm{P}}_{e,\gamma_{LB}} \doteq \bar{\gamma}^{-1}$.

From Lemma 3 and Lemma 4, we have $\overline{\mathrm{P}}_{e,\gamma_{ZF}} \le \overline{\mathrm{P}}_{e,\gamma_{LB}}$. □

Theorem 1: The diversity order of the error probability of the ZF SC-FDE is 1, i.e., $d_e^{ZF} = 1$; and the diversity order of the outage of the ZF SC-FDE is 1, i.e., $d_{out}^{ZF} = 1$.

Proof: From Lemma 2 and Lemma 5. □

5.4 Diversity Analysis of MMSE SC-FDE

We study the diversity order of MMSE SC-FDE in this section. For the MMSE SC-FDE, the equalizer in (11) is $\mathbf{W} = \mathbf{W}_{MMSE} = (\mathbf{H}^H\mathbf{H} + \bar{\gamma}^{-1}\mathbf{I})^{-1}\mathbf{H}^H$, and the unbiased decision point SINR is [72]

$$\gamma = \gamma_{MMSE} = \frac{1}{\frac{1}{n}\sum_{k=1}^{n}\frac{1}{1+\bar{\gamma}\left|\lambda_k\right|^2}} - 1 = \frac{1}{\frac{1}{n}\sum_{k=1}^{n}\frac{1}{1+\gamma_k}} - 1. \tag{18}$$

It is reasonable to assume that in SEP analysis for MMSE SC-FDE, the interference is also complex Gaussian. This enables us to apply Props. 2 and 3.

Generally we have no analytical expression for the distribution of γ_{MMSE}. Similarly to the last section, we use a bounding approach to find the diversity of MMSE SC-FDE.

The facts that we clarified in the analysis of ZF SC-FDE are still indispensable for this section.

5.4.1 SEP analysis of MMSE SC-FDE

For SEP analysis, the upper bound is derived with Lemmas 6 and 7, the lower bound is derived with Lemmas 1 and 8, and the conclusion for error diversity order is given in Theorem 2.

Lemma 6: $\gamma_{MMSE} \geq \gamma_{ZF}$ for the linear SC-FDE.

Proof: We get from (18) that $\gamma_{MMSE} = \frac{\sum_{i=1}^{n}(1-\frac{1}{1+\gamma_i})}{\sum_{i=1}^{n}\frac{1}{1+\gamma_i}} = \frac{\sum_{i=1}^{n}1/(1+1/\gamma_i)}{\sum_{i=1}^{n}(1/\gamma_i)/(1+1/\gamma_i)} = \frac{\frac{1}{n}\sum_{i=1}^{n}f(1/\gamma_i)}{\frac{1}{n}\sum_{i=1}^{n}g(1/\gamma_i)}$,

where $f(x) = \frac{1}{1+x}$ and $g(x) = \frac{x}{1+x}$. By concavity of $f(x)$ and $g(x)$,

$\frac{1}{n}\sum_{i=1}^{n} f(1/\gamma_i) \geq f(\frac{1}{n}\sum_{i=1}^{n} 1/\gamma_i)$, $\frac{1}{n}\sum_{i=1}^{n} g(1/\gamma_i) \leq g(\frac{1}{n}\sum_{i=1}^{n} 1/\gamma_i)$. So

$\gamma_{MMSE} \geq f(\frac{1}{n}\sum_{i=1}^{n}\frac{1}{\gamma_i}) \Big/ g(\frac{1}{n}\sum_{i=1}^{n}\frac{1}{\gamma_i}) = \frac{1}{\frac{1}{n}\sum_{i=1}^{n} 1/\gamma_i} = \gamma_{ZF}$. □

Lemma 7: The average SEP of MMSE SC-FDE is upper bounded as $\overline{\mathrm{P}}_{e,\gamma_{MMSE}} \dot{\leq} \bar{\gamma}^{-1}$.

Proof: from Lemma 6 and Theorem 1, $\overline{\mathrm{P}}_{e,\gamma_{MMSE}} \dot{\leq} \bar{\gamma}^{-1}$. □

Lemma 8: The average SEP of MMSE SC-FDE is lower bounded as $\overline{\mathrm{P}}_{e,\gamma_{MMSE}} \dot{\geq} \bar{\gamma}^{-1}$.

Proof: from (18), we get $\gamma_{MMSE} \leq \frac{n}{1/(1+\gamma_i)} - 1$ or $\gamma_{MMSE} \leq n\gamma_i + n - 1$. We get $\overline{\mathrm{P}}_{e,\gamma_{MMSE}} \dot{\geq} \bar{\gamma}^{-1}$ from Lemma 1. □

Theorem 2: The diversity order of SEP of MMSE SC-FDE is 1, i.e., $d_e^{MMSE} = 1$.

Proof: From Lemma 7 and Lemma 8. □

5.4.2 Outage probability analysis of MMSE SC-FDE

We get the capacity $C(\gamma_{MMSE}) = -\log(\frac{1}{n}\sum_{k=1}^{n} 1/(1+\gamma_k))$ from (18), so the outage event $C(\gamma_{MMSE}) < R$ is equivalent to $\gamma_{MMSE} < \varepsilon$ or $\sum_{k=1}^{n} 1/(1+\gamma_k) > \delta$. Here and in the remainder of this dissertation, we define $\varepsilon = 2^R - 1$ and $\delta = n/(1+\varepsilon) = n/2^R$.

For outage probability analysis, the lower bound is derived in Lemma 10, the upper bound is derived with Lemmas 12, 13 and 16, and the conclusion for outage diversity order is given in Theorem 3. We also develop Definition 1, Lemmas 9 and 11 to help the proof of Lemma 12, and develop Lemmas 14, 15 to help the proof of Lemma 16.

*Lemma 9***:** With $\boldsymbol{\lambda}$ defined in (12), if $\tilde{\boldsymbol{\lambda}}$ is a $m \times 1$ sub-vector of $\boldsymbol{\lambda}$, and $\tilde{\gamma}_i = \overline{\gamma}\left|\tilde{\lambda}_i\right|^2$, then $P\left(\tilde{\gamma}_i \le t \text{ for } m \ge i \ge 1\right) \doteq \overline{\gamma}^{-\min(m,\ \nu+1)}$ for a positive real t.

Proof: See Appendix A.2. □

The next lemmas, Lemmas 10 through 12, have the rather complicated set constructions that were alluded to in Section III B. These constructions enable treatment of the general case of $n > \nu + 1$ and when the elements of $\mathbf{h}$ are not i.i.d.

Lemma 10: Outage probability of MMSE SC-FDE is lower bounded as $P_{out,\,\gamma_{MMSE}}(R) \dot{\ge} \overline{\gamma}^{-\min(\lfloor \delta \rfloor + 1,\ \nu+1)}$.

Proof: Outage probability is

$$P_{out,\gamma_{MMSE}}(R) = \Pr(\sum_{i=1}^{n}\frac{1}{1+\gamma_i} > \delta) \geq \Pr(\bigcup_{k=1}^{|K^{'}|} U_k^{'}) \geq \Pr(U_k^{'}), \tag{19}$$

where we define $S_k^{'} \subset \{1,2,\cdots,n\}$ with $|S_k^{'}| = 1+\lfloor \delta \rfloor$, and $U_k^{'} = \{U : \gamma_i < t_1 \text{ for every } i \in S_k^{'}\}$ where $t_1 = (1+\lfloor \delta \rfloor)/\delta - 1$ and $k \in K^{'} = \left\{1,2,\cdots,\binom{n}{1+\lfloor \delta \rfloor}\right\}$. If $\gamma_i < t_1$ for all $i \in S_k^{'}$, then $\sum_{i=1}^{n} 1/(1+\gamma_i) > \delta$ and outage happens, so $\bigcup_{k=1}^{|K^{'}|} U_k^{'}$ is contained in the outage space, and $\Pr(\sum_{i=1}^{n}\frac{1}{1+\gamma_i} > \delta) \geq \Pr(\bigcup_{k=1}^{|K^{'}|} U_k^{'})$. From Lemma 9, we have $\Pr(U_k^{'}) \doteq \bar{\gamma}^{-\min(1+\lfloor \delta \rfloor,\ \nu+1)}$. Finally we have $\Pr(\sum_{i=1}^{n}\frac{1}{1+\gamma_i} > \delta) \geq \Pr(U_k^{'}) \doteq \bar{\gamma}^{-\min(1+\lfloor \delta \rfloor,\ \nu+1)}$. □

Definition 1: Let the set $S_k \subset S = \{1,2,\cdots,n\}$, with cardinality $|S_k| = n - \lfloor \delta \rfloor$, and $k \in K = \left\{1,2,\cdots,\binom{n}{n-\lfloor \delta \rfloor}\right\}$, be one of the $n-\lfloor \delta \rfloor$ combinations of set S. Let $t_0 = \frac{n-\lfloor \delta \rfloor}{\delta - \lfloor \delta \rfloor} - 1$. For a specific k, if $\gamma_i > t_0$ for every $i \in S_k$, then $\sum_{i \in S_k}\frac{1}{1+\gamma_i} + \lfloor \delta \rfloor < \delta$, and this will ensure $\sum_{i=1}^{n} 1/(1+\gamma_i) < \delta$; define $U_k^{'} = \bigcap_{i_k \in S_k} U_{i_k}$, $U_{i_k} = \{U : \gamma_{i_k} > t_0\}$ and then $\bigcup_{k \in K} U_k^{'}$ is contained in the non-outage space. Note that $\bar{U}_k^{'} = \bigcup_{i_k \in S_k} \bar{U}_{i_k}$, and we get $\bigcap_{k \in K} \bar{U}_k^{'} = \bigcap_{k \in K}(\bigcup_{i_k \in S_k} \bar{U}_{i_k}) = \bigcup_{\mathbf{i} \in \mathfrak{I}}(\bigcap_{k \in K} \bar{U}_{i_k})$, $\mathbf{i} = (i_1, i_2, \cdots, i_{|K|})$ where $i_k \in S_k$ for every $k \in K$, $\mathfrak{I}$ is

the set of all possible $\mathbf{i}$, with cardinality $|\Im| = (n - \lfloor \delta \rfloor)^{|K|}$. For a specific $\mathbf{i}$, the order of the set $\bigcap_{k=1}^{|K|} \bar{U}_{i_k}$ is defined as the number of different values of all the elements of this vector $\mathbf{i}$, or the number of different constraints in the definition of the set, and is denoted as $order(\bigcap_{k=1}^{|K|} \bar{U}_{i_k})$.

Lemma 11: With all the definitions and notations given in *Definition 1*, we have $\underline{d} = \min_{\mathbf{i} \in \Im} order(\bigcap_{k=1}^{|K|} \bar{U}_{i_k}) = \lfloor \delta \rfloor + 1$.

Proof: Without loss of generality, we assume one of the sets who has the minimum set order $\underline{d}$ is $\bigcap_{k=1}^{|K|} \bar{U}_{i_k} = \bigcap_{i=1}^{\underline{d}} \bar{U}_i = \bar{U}_1 \bigcap \bar{U}_2 \bigcap \cdots \bigcap \bar{U}_{\underline{d}}$, note that $\bar{U}_k^{'} = \bigcup_{i_k \in S_k} \bar{U}_{i_k}$, all the $\bar{U}_k^{'}$'s can be grouped into $\underline{d}$ groups, and all the k can be grouped into $\underline{d}$ groups correspondingly. We have $1 \in S_k$ for all the k in the first group, so the intersection of all the $\bar{U}_k^{'}$'s in the first group is $\bar{U}_1$; similarly, we have $t \in S_k$ for all the k in group t, so the intersection of all the $\bar{U}_k^{'}$'s in group t is $\bar{U}_t$, for all the $t \in T = \{1, 2, \cdots, \underline{d} - 1\}$. For $\underline{d}$ to be the minimum order, then for all the k in group $\underline{d}$, we have $t \notin S_k$ for all $t \in T$, then $\underline{d} - 1 + |S_k| = n$ or $\underline{d} = n - |S_k| + 1 = \lfloor \delta \rfloor + 1$. □

Lemma 12: If $\delta \notin \mathbb{Z}$, i.e., if δ is a positive non-integer, then the outage probability of MMSE SC-FDE is upper bounded as $P_{out, \gamma_{MMSE}}(R) \dot{\leq} \bar{\gamma}^{-\min(\lfloor \delta \rfloor + 1, \nu + 1)}$.

Proof: using (19) and *Definition 1*, we get $\Pr(\sum_{i=1}^{n}\frac{1}{1+\gamma_i}>\delta)\le 1-\Pr(\bigcup_{k}U_k^{'})=\Pr(\overline{\bigcup_{k}U_k^{'}})$

$=\Pr(\bigcap_{k\in K}\overline{U_k^{'}})=\Pr(\bigcup_{\mathbf{i}\in\mathfrak{I}}(\bigcap_{k\in K}\bar{U}_{i_k}))\le\sum_{\mathbf{i}\in\mathfrak{I}}\Pr(\bigcap_{k\in K}\bar{U}_{i_k})=\sum_{\mathbf{i}\in\mathfrak{I}}\Pr(\bigcap_{k=1}^{|K|}\bar{U}_{i_k})$. From Lemma 9 and Lemma 11, we get $\Pr(\bigcap_{k\in K}\bar{U}_{i_k})\doteq\bar{\gamma}^{-\min(1+\lfloor\delta\rfloor,\,\nu+1)}$ for a set $\bigcap_{k=1}^{|K|}\bar{U}_{i_k}$ which has the minimum set order $\underline{d}=\lfloor\delta\rfloor+1$. So $\sum_{\mathbf{i}\in\mathfrak{I}}\Pr(\bigcap_{k\in K}\bar{U}_{i_k})\doteq\bar{\gamma}^{-\min(1+\lfloor\delta\rfloor,\,\nu+1)}$ because the diversity order is dominated by the minimum order, and we conclude $d_{out}^{MMSE}\ge d_{out}^{LB}=\min\left(\lfloor\delta\rfloor+1,\nu+1\right)$. □

Example: We give an example to illustrate Definition 1, Lemmas 11 and 12. Let $n=3$ and $\delta=1.5$, then as in Definition 1, $n-\lfloor\delta\rfloor=2$, $K=\{1,2,3\}$, the sets $S_1=\{1,2\}$, $S_2=\{1,3\}$, $S_3=\{2,3\}$. Then $\bar{U}_1^{'}=\bar{U}_1\cup\bar{U}_2$, $\bar{U}_2^{'}=\bar{U}_1\cup\bar{U}_3$, and we get $\overline{\bigcup_{k\in K}U_k^{'}}=\bigcap_{k\in K}\bar{U}_k^{'}=\bigcup_{\mathbf{i}\in\mathfrak{I}}(\bigcap_{k\in K}\bar{U}_{i_k})$, where $\mathfrak{I}=\{(1,1,2),(1,1,3),(1,3,2),(1,3,3),(2,1,2),(2,1,3),(2,3,2),(2,3,3)\}$, and $\mathbf{i}=(i_1,i_2,i_3)\in\mathfrak{I}$. According to Lemma 11, $\underline{d}=2$, this could be illustrated as following: for a specific $\mathbf{i}=(1,1,2)$, $order(\bigcap_{k=1}^{|K|}\bar{U}_{i_k})=2=\underline{d}$; and according to Lemma 9, the diversity order of the probability $P(\bigcap_{k=1}^{|K|}\bar{U}_{i_k})$ is also $\underline{d}$. Because the outage space is contained in $\overline{\bigcup_{k\in K}U_k^{'}}$, this leads to the result in Lemma 12, i.e., $d_{out}^{MMSE}\ge\min\left(\lfloor\delta\rfloor+1,\nu+1\right)$.

While *Lemma 12* is for the $\delta \notin \mathbb{Z}$ case, we derive the upper bound for the $\delta \in \mathbb{Z}$ case in *Lemmas 13* and *16.*

Lemma 13: If $\delta \in \mathbb{Z}$, i.e., δ is a positive integer, and $\delta \geq \nu + 1$, then outage probability of MMSE SC-FDE is upper bounded as $P_{out,\gamma_{MMSE}}(R) \dot{\leq} \bar{\gamma}^{-(\nu+1)}$.

Proof: From $\Pr(\sum_{i=1}^{n} \frac{1}{1+\gamma_i} > \delta) \leq \Pr(\sum_{i=1}^{n} \frac{1}{1+\gamma_i} > \delta - 0.5)$, from Lemma 12, we have $\Pr(\sum_{i=1}^{n} \frac{1}{1+\gamma_i} > \delta - 0.5) \dot{\leq} \bar{\gamma}^{-(\nu+1)}$, so we conclude $P_{out,\gamma_{MMSE}}(R) \dot{\leq} \bar{\gamma}^{-(\nu+1)}$. □

Lemma 14: $P(c < w_2 < a + b/w_1, \quad w_1 < d\ ) \dot{\leq} \bar{\gamma}^{-2}$, where $w_i = \sqrt{\bar{\gamma}}|h_i|$, $|h_1|$ and $|h_2|$ are independently Rayleigh distributed, a, b, c and d are some positive real constants.

Proof: First, we assume $|h_1|$ and $|h_2|$ are identically distributed with PDF $p_x(x) = 2xe^{-x^2}$.

Let $t_1 = d/\sqrt{\bar{r}}$, $t_2 = c/\sqrt{\bar{r}}$, $t_3 = d/\bar{r}$, $f(x) = \left(a + \frac{b}{x\sqrt{\bar{r}}}\right)\frac{1}{\sqrt{\bar{r}}}$ and $g(x) = \left(a + \frac{b}{x\sqrt{\bar{r}}}\right)^2 \frac{1}{\bar{r}}$.

We do the following integration for large enough $\bar{r}$:

$$P(c < w_2 < a + \frac{b}{w_1}, \quad w_1 < d\ ) = \int_0^{t_1} 2y_1 e^{-y_1^2} dy_1 \int_{t_2}^{f(y_1)} 2y_2 e^{-y_2^2} dy_2$$
$$\leq \int_0^{t_1} 2xe^{-x^2}(1 - e^{-g(x)})dx = \int_0^{t_3} 2xe^{-x^2}(1 - e^{-g(x)})dx + \int_{t_3}^{t_1} 2xe^{-x^2}(1 - e^{-g(x)})dx$$
$$\leq \int_0^{t_3} 2xdx + \int_{t_3}^{t_1} 2xg(x)dx = d^2\bar{\gamma}^{-2} + a^2\bar{\gamma}^{-1}\int_{t_3}^{t_1} 2xdx + 4ab\bar{\gamma}^{-1.5}\int_{t_3}^{t_1} 1dx + 2b^2\bar{\gamma}^{-2}\int_{t_3}^{t_1} x^{-1}dx$$
$$= d'\bar{\gamma}^{-2} + a'\bar{\gamma}^{-3} + c'\bar{\gamma}^{-2.5} + b'\bar{\gamma}^{-2}\ln\bar{\gamma} \doteq \bar{\gamma}^{-2}$$

Next, we consider the case when $|h_1|$ and $|h_2|$ have different variances. We can find that, by scaling, the events $c < w_2 < a + b/w_1$ and $w_1 < d$ are equivalent to $\tilde{c} < \tilde{w}_2 < \tilde{a} + \tilde{b}/\tilde{w}_1$ and $\tilde{w}_1 < \tilde{d}$, respectively, where $\tilde{w}_i = \sqrt{\bar{\gamma}}|\tilde{h}_i|$, $|\tilde{h}_1|$ and $|\tilde{h}_2|$ are i.i.d., and $\tilde{a}, \tilde{b}, \tilde{c}, \tilde{d}$ are some positive real constants.

We conclude $P(c < w_2 < a + b/w_1, \quad w_1 < d\ ) \dot{\leq} \bar{\gamma}^{-2}$. □

Lemma 15: Suppose $m < \nu + 1$. With $\boldsymbol{\lambda}$ defined in (12), if $\tilde{\boldsymbol{\lambda}}$ is a $(m+1)\times 1$ sub-vector of $\boldsymbol{\lambda}$ and $\tilde{\gamma}_i = \bar{\gamma}|\tilde{\lambda}_i|^2$, then $P\left(a < \tilde{\gamma}_{m+1} < b + c/\tilde{\gamma}_1, \tilde{\gamma}_i < d \text{ for } m \geq i \geq 1\right) \dot{\leq} \bar{\gamma}^{-(m+1)}$, where a, b, c and d are positive real.

Proof: Similar to the proof in Lemma 9, we have $\tilde{\boldsymbol{\lambda}} = \tilde{\mathbf{F}}\mathbf{h} = \tilde{\mathbf{F}}\mathbf{D}^{-1/2}\bar{\mathbf{h}} = \mathbf{U}\boldsymbol{\Sigma}\mathbf{V}\bar{\mathbf{h}} = \mathbf{U}\boldsymbol{\Sigma}'\breve{\mathbf{h}}$, where $\boldsymbol{\Sigma}'$ is $(m+1)\times(m+1)$ diagonal matrix with nonzero diagonal elements, $\boldsymbol{\Sigma} = \left[\boldsymbol{\Sigma}' \ \mathbf{0}\right]$ and $\mathbf{V}\bar{\mathbf{h}} = \left[\breve{\mathbf{h}}^t, \hat{\mathbf{h}}^t\right]^T$, $\breve{\mathbf{h}}$ is a $(m+1)\times 1$ vector, the $\breve{h}_i$'s are i.i.d. complex Gaussian. By LQ decomposition, we have $\tilde{\boldsymbol{\lambda}} = \mathbf{U}\boldsymbol{\Sigma}'\breve{\mathbf{h}} = \mathbf{L}\mathbf{Q}\breve{\mathbf{h}}$ and let $\tilde{\mathbf{h}} = \mathbf{Q}\breve{\mathbf{h}} = \mathbf{L}^{-1}\tilde{\boldsymbol{\lambda}} = \mathbf{L}_0\tilde{\boldsymbol{\lambda}}$, where the $\tilde{h}_i$'s are independent to each other, $\mathbf{L}_0 = \mathbf{L}^{-1}$ is a lower triangular matrix. Let $z_i = \sqrt{\tilde{\gamma}_i}$, $t = b + c/\tilde{\gamma}_1$. From $a < \tilde{\gamma}_{m+1} < t$, we get $\sqrt{a} < \sqrt{\tilde{\gamma}_{m+1}} < \sqrt{t} < \sqrt{b} + \sqrt{c/\tilde{\gamma}_1}$, or $a' < z_{m+1} < b' + c'/z_1$; Similarly, from $\tilde{\gamma}_i < d$, we get $z_i < d'$. Let $w_i = \sqrt{\bar{\gamma}}|\tilde{h}_i|$, from $\tilde{\mathbf{h}} = \mathbf{L}_0\tilde{\boldsymbol{\lambda}}$, we get $\mathbf{w} = \mathbf{L}_0\mathbf{z}$. So if $a' < z_{m+1} < b' + c'/z_1$ and $z_i < d'$ for $m \geq i \geq 1$, then we can find $\bar{a} < w_{m+1} < \bar{b} + \bar{c}/w_1$ and $w_i < \bar{d}$ for $m \geq i \geq 1$, and we conclude

$$P\left(a<\tilde{\gamma}_{m+1}<b+c/\tilde{\gamma}_1,\tilde{\gamma}_i<d \text{ for } m\geq i\geq 1\right)<P\left(a'<z_{m+1}<b'+c'/z_1,z_i<d' \text{ for } m\geq i\geq 1\right)$$
$$<P\left(\bar{a}<w_{m+1}<\bar{b}+\bar{c}/z_1,z_i<\bar{d} \text{ for } m\geq i\geq 1\right)\dot{\leq}\,\bar{\gamma}^{-(m+1)}.$$

The last exponential inequality is obtained from extension of Lemma 14. □

Lemma 16: If $\delta\in\mathbb{Z}$, i.e., δ is a positive integer, and $\delta<\nu+1$, then outage probability of MMSE SC-FDE is upper bounded as $P_{out,\gamma_{MMSE}}(R)\dot{\leq}\,\bar{\gamma}^{-(\delta+1)}$.

Proof: See Appendix A.3. □

Theorem 3: The outage diversity order of MMSE SC-FDE is $d_{out}^{MMSE}=\min\left(\left\lfloor 2^{-R}n\right\rfloor+1,\nu+1\right)$, where outage happens if $C(\gamma_{MMSE})<R$.

Proof: From Prop. 4 and Lemmas 11, 14, 15. □

From Theorem 3, we get $d_{out}^{MMSE}=\nu+1$ when $n\to\infty$, i.e., MMSE SC-FDE with infinite data block length achieves full outage diversity order. We should point out that although [77] argued with [75] and claimed that the MMSE SC-DFE with decision feedback can achieve full diversity for SEP, careful investigation shows that the analysis in [77] is the outage diversity order with infinite data block length, so the conclusion of [77] is in correspondence with Theorem 3 in this dissertation and does not contradict with [75].

5.5 Simulation

Diversity order is an asymptotic result, making verification by Monte Carlo simulation challenging. In other words, the SNR in the simulations must be high enough to see the slopes approach their limiting values, and because this implies low error rates, the simulations can be very time consuming. Choosing a higher modulation order can cause the slopes to reach their limiting values at lower SNRs. The channel memory length, ν, and the data block length, n, also play a role in how low the SNRs can be to see limit behavior. Not considering high enough modulation order and high enough SNRs can lead to a wrong conclusion, as we will show in this section.

Monte Carlo simulations are found in many previous works; in most cases, the limiting slopes are obvious [69, 73]. So for the sake of brevity, we show the one case, [69], in Table I that had a wrong conclusion, and in this case, the Monte Carlo simulations were not done at high enough SNR.

Figures 17 and 18 show the SEP for the MMSE SC-FDE versus Es/No, or $\bar{\gamma}$, for two different channel lengths, respectively. The legend in each figure tells the data block length, n. The QAM modulation orders for Fig. 19 and 20 are 16 and 64, respectively. The channel taps were i.i.d. complex Gaussian with a total average power of 1. The number of trials for each point was sufficient to generate at least 1000 symbol detection errors.

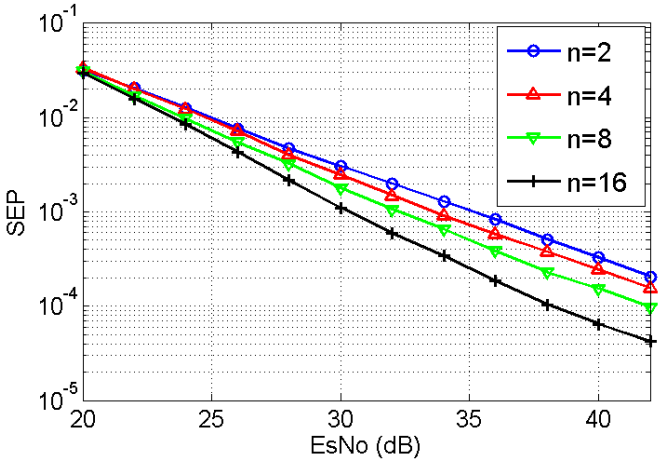

Figure 19 Average symbol error probability of MMSE SC-FDE, $\nu+1=2$.

We observe in the figures that the slopes are different for different values of n, and for different ν, for the lower SNRs. If the SNR is less than about 35dB, the slopes appear to be consistent with $\min\left(\lfloor \delta \rfloor+1, \nu+1\right)$, which is the conclusion of [69]. However, for higher SNRs, all slopes are observed to converge to one, which is the conclusion of this dissertation.

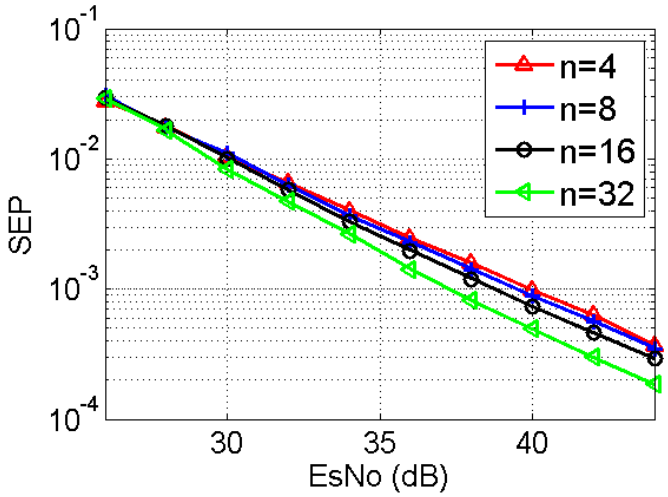

Figure 20 Average symbol error probability of MMSE SC-FDE, $\nu+1=3$.

5.6 Conclusion

The diversity order, which is an asymptotic result of linear SC-FDE is analyzed rigorously in a novel way with sets and bounding techniques, for both the ZF and MMSE equalizers, and for both outage and SEP. compared to previous works, the analysis treats a broader and more practical class of channels, specifically those with independent taps. The results resolve two previous contradictions and confirm the results of two problematic proofs.

CHAPTER 6. THE DISTRIBUTION OF NON-ZERO EIGENVALUES OF THE EQUIVALENT MIMO CHANNEL MATRIX FOR MULTI-HOP A&F RELAY NETWORK

Cooperative MIMO schemes are proposed in [11, 12], where cooperative transmission and/or cooperative reception for single-antenna nodes are used, to obtain the performance gains of the point-to-point MIMO system [9]. Similar ideas are proposed for multi-hop distributed networks as Virtual MIMO [13, 14] or distributed spatial multiplexing (DSM) in [15] (cooperative spatial multiplexing in [16]) to achieve high throughput and spectral efficiency in a distributed multi-hop network with single-antenna nodes.

Within these different proposals for virtual MIMO [11, 12, 13, 14] and DSM [15, 16], the DSM scheme with AF mode relaying [15] is of particular interesting for its simplicity and low coordination overhead. However, closed form analysis for this scheme is generally unavailable, and the performance evaluation generally depends on Monte-Carlo simulation. This is because we have little knowledge about the statistical characteristics of the equivalent cascaded MIMO channel of this scheme. To the author's knowledge, there are few exact closed form expressions and they exist only for the 2-hop case, including the SER analysis in [59] and the marginal probability density function (PDF) of the eigenvalues for ergodic capacity analysis in [61, 62]. As in the performance analysis for conventional MIMO [79, 80], where the distribution of the eigenvalues of the channel matrix [81] plays an important role, a closed form expression of the distribution of the

eigenvalues of the equivalent channel matrix for the multi-hop virtual MIMO or DSM is needed.

6.1 Introduction

In this section, we introduce the system model of multi-hop amplify and forward (A&F) relay network and its equivalent cascaded MIMO channel.

The network consists of L clusters of relay antennas (or single-antenna relay nodes), a source, and a destination. The source and destination can each consist of a cluster of single-antenna nodes or one multi-antenna node. So the network has $L+1$ hops. The relays within each relay cluster do not communicate (cooperate) with each other. We denote the cluster of source antennas as the 0th cluster, and the cluster of destination antennas as the $(L+1)$th cluster. The intermediate clusters are indexed from 1 to L. The transmission operates in a time slotted manner. All the antennas of the source transmit simultaneously in the first time slot, then the relays in the first cluster do A&F relaying and transmit simultaneously in the second time slot, then the relays in the second cluster do A&F relaying in the same manner in the third time slot to forward the signal to the third cluster. In this way the destination antennas finally receive the signal from the Lth cluster.

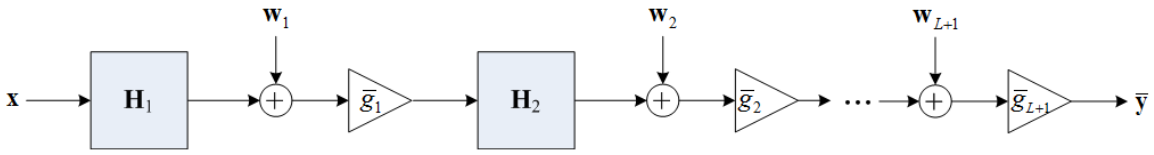

Figure 21 System Model for DSM with A&F

Suppose we have R_k antennas in the kth cluster. Assume each cluster transmits simultaneously. Let $\bar{\mathbf{y}}$ be the vector signal outputted by the destination node, $\mathbf{x}$ be the vector signal transmitted by the source node, $\mathbf{w}^{(l)}$ be the white noise vector added by the lth relay cluster to its received signal, $\mathbf{w}^{(L+1)}$ be the white noise vector added by the destination to its received signal, and $\bar{g}_l$ be the gain of the lth relay cluster. We assume $\bar{g}_l$ is a positive real, and the same for all the relays in the cluster. We assume the noise vector $\mathbf{w}^{(l)} \sim \mathcal{CN}(0, \sigma_l^2 \mathbf{I})$ is spatially white, i.e., its elements are i.i.d.. Let $\mathbf{H}_k$ be the $R_k \times R_{k-1}$ channel matrix of the channel between the $(k-1)th$ relay cluster and the kth relay cluster, i.e. the kth hop. We assume $\mathbf{H}_l$ has i.i.d. circularly symmetric complex Gaussian entries $h_{ij}^{(l)} = [\mathbf{H}_l]_{ij} \sim \mathcal{CN}(0, 1)$ for $l = 1, \ldots, L+1$. Let R_0 be the number of the source antennas, and let R_{L+1} be the number of the destination antennas. The channel is assumed to be frequency flat, time invariant, and have AWGN. The system model is shown in Fig. 21. Let $\prod_{l=L}^{1} \mathbf{H}_l = \mathbf{H}_L \mathbf{H}_{L-1} \cdots \mathbf{H}_1$. The input output relationship of the entire series of clusters, is

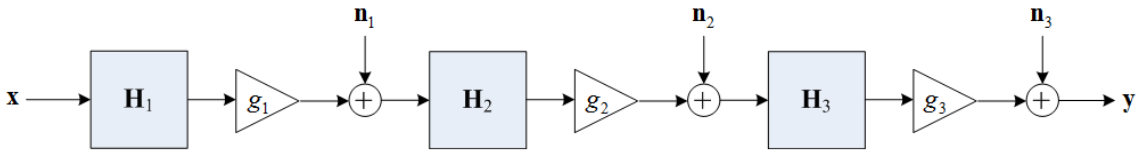

Figure 22 Equivalent System Model for a 3-hop DSM with A&F

$$\bar{\mathbf{y}} = \left(\prod_{l=L+1}^{1} \bar{g}_l \mathbf{H}_l \right) \mathbf{x} + \sum_{m=L+1}^{2} \left(\prod_{n=L+1}^{m} \bar{g}_n \mathbf{H}_n \right) \bar{g}_{m-1} \mathbf{w}^{(m-1)} + \bar{g}_{L+1} \mathbf{w}^{(L+1)} . \qquad (21)$$

To facilitate the derivation, we further get an equivalent system model, which is given in detail as the following. The equivalent system model for a 3-hop DSM with AF is shown in Fig. 22. From (21), we get

$$\frac{\bar{\mathbf{y}}}{\sigma_{L+1}\bar{g}_{L+1}} = \left(\prod_{l=L+1}^{2} \frac{\sigma_{l-1}}{\sigma_l} \bar{g}_{l-1} \mathbf{H}_l \right) \frac{1}{\sigma_1} \mathbf{H}_1 \mathbf{x} + \sum_{m=L+1}^{2} \left(\prod_{n=L+1}^{m} \frac{\sigma_{n-1}}{\sigma_n} \bar{g}_{n-1} \mathbf{H}_n \right) \frac{\mathbf{w}^{(m-1)}}{\sigma_{m-1}} + \frac{\mathbf{w}^{(L+1)}}{\sigma_{L+1}} .$$

Let $\mathbf{y} = \dfrac{\bar{\mathbf{y}}}{\sigma_{L+1}\bar{g}_{L+1}}$, $\mathbf{n}^{(k)} = \dfrac{\mathbf{w}^{(k)}}{\sigma_k}$ and $g_k = \begin{cases} 1 & \text{if } k = 1 \\ \bar{g}_{k-1}\sigma_{k-1}/\sigma_k & \text{if } 1 < k \le L+1 \end{cases}$. Then we get

$$\mathbf{y} = \underbrace{\left(\prod_{l=L+1}^{1} g_l \mathbf{H}_l \right)}_{\mathbf{H}} \mathbf{x} + \underbrace{\sum_{m=L+1}^{2} \left(\prod_{n=L+1}^{m} g_n \mathbf{H}_n \right) \mathbf{n}^{(m-1)} + \mathbf{n}^{(L+1)}}_{\mathbf{n}} , \qquad (22)$$

i.e., $\mathbf{y} = \mathbf{H}\mathbf{x} + \mathbf{n}$, where $\mathbf{H} = \prod_{l=L+1}^{1} g_l \mathbf{H}_l$ and $\mathbf{n} = \sum_{m=L+1}^{2} \left(\prod_{n=L+1}^{m} g_n \mathbf{H}_n \right) \mathbf{n}^{(m-1)}$. Note that in Equation (22) the variances of the noise and the channel coefficients are normalized, and the integrated effect of these parameters is represented by g_l a positive real constant as the gain of the *lth* hop.

Let $\mathbf{R} = E[\mathbf{n}\mathbf{n}^H]$, $\mathbf{H}_e = \mathbf{R}^{-1/2}\mathbf{H}$ and $\tilde{\mathbf{n}} = \mathbf{R}^{-1/2}\mathbf{n}$, where $\tilde{\mathbf{n}}$ is white. Then we have

$$\mathbf{R}^{-1/2}\mathbf{y} = \mathbf{H}_e\mathbf{x} + \tilde{\mathbf{n}}.$$

The Wishart of the equivalent cascaded MIMO channel $\mathbf{H}_e$ is $\mathcal{W} = \mathbf{H}_e\mathbf{H}_e^H$, but $\mathbf{B} = \mathbf{H}_e^H\mathbf{H}_e$ has the same nonzero eigenvalues as $\mathcal{W}$.

Our objective is to derive the joint PDF for the nonzero eigenvalues of $\mathbf{B}$. Although the joint distribution of nonzero eigenvalues of the Wishart matrix [81] is well developed in previous works [82] and has its application, the analytical approach for such a Wishart matrix of the equivalent MIMO channel in multi-hop AF is still absent, and for similar problems such as cascaded MIMO channel. In this dissertation, we will first derive a recursive algorithm to find the distribution of nonzero eigenvalues, and then the form of the PDF is found as a multiplication of matrix determinants. [83, 84] are good tutorials for Wishart matrix.

As an illustration of the recursive algorithm, we consider the simplest case. We assume a 3 hop case ($L+1=3$) with the same of number of antennas in each cluster, $\mathbf{H}_1$, $\mathbf{H}_2$, $\mathbf{H}_3$ are square matrices of the same size, and $g_1 = g_2 = g_3 = 1$ in Eq. (22). According to Eq. (26), we have

$$\mathbf{B} = \mathbf{H}_1^H\mathbf{H}_2^H\mathbf{H}_3^H(\mathbf{H}_3\mathbf{H}_2\mathbf{H}_2^H\mathbf{H}_3^H + \mathbf{H}_3\mathbf{H}_3^H + \mathbf{I})^{-1}\mathbf{H}_3\mathbf{H}_2\mathbf{H}_1.$$

Let "$\cong$" stands for "equivalence in distribution". Let $\bar{\mathbf{H}}_k = \begin{cases} \mathbf{H}_k & \text{for } k = 3 \\ \bar{\mathbf{D}}_{k+1}\mathbf{H}_k & \text{for } k = 1, 2 \end{cases}$ with singular value decomposition (SVD) $\bar{\mathbf{H}}_k = \mathbf{U}_k \mathbf{\Lambda}_k \mathbf{V}_k^H$ and $\bar{\mathbf{D}}_k = (\mathbf{I} + \mathbf{\Lambda}_k \mathbf{\Lambda}_k^H)^{-1/2} \mathbf{\Lambda}_k$, we can prove $\mathbf{B} \cong \bar{\mathbf{H}}_1 \bar{\mathbf{H}}_1^H$, which is given in detail in next section.

If we define $\mathbf{\Sigma}_k = \mathbf{\Lambda}_k \mathbf{\Lambda}_k^H = diag(\boldsymbol{\sigma}^{(k)})$ and $\mathbf{D}_k = \bar{\mathbf{D}}_k^H \bar{\mathbf{D}}_k = diag(\mathbf{d}^{(k)})$ for $k = 1, 2, 3$, then $\mathbf{D}_k = (g_k^{-2}\mathbf{I} + \mathbf{\Sigma}_k)^{-1}\mathbf{\Sigma}_k$. Note that $\bar{\mathbf{H}}_k \bar{\mathbf{H}}_k^H$ has the same eigenvalues as $\bar{\mathbf{H}}_k^H \bar{\mathbf{H}}_k$, let $\boldsymbol{\sigma}^{(k)}$ be the vector of the eigenvalues of $\bar{\mathbf{H}}_k \bar{\mathbf{H}}_k^H$. From previous works on Wishart matrix [89, 90] and the equality $\bar{\mathbf{H}}_k^H \bar{\mathbf{H}}_k = \mathbf{H}_k^H \mathbf{D}_{k+1} \mathbf{H}_k$ for $k = 1, 2$, we know the PDF of $\boldsymbol{\sigma}^{(k)}$ given $\mathbf{d}^{(k+1)}$ (or $\mathbf{D}_{k+1}$), i.e., the conditional PDF $f_{\boldsymbol{\sigma}^{(k)}|\mathbf{d}^{(k+1)}}(\boldsymbol{\sigma}^{(k)} \mid \mathbf{d}^{(k+1)})$; we also know the PDF of $\boldsymbol{\sigma}^{(3)}$ as $f_{\boldsymbol{\sigma}^{(3)}}(\boldsymbol{\sigma}^{(3)})$. We can get the pdf of $\boldsymbol{\sigma}^{(1)}$ by multi-dimensional integration in a recursive manner with the following steps:

1. With known $f_{\boldsymbol{\sigma}^{(3)}}(\boldsymbol{\sigma}^{(3)})$, from $\mathbf{D}_3 = (\mathbf{I} + \mathbf{\Sigma}_3)^{-1}\mathbf{\Sigma}_3$, we get $f_{\mathbf{d}^{(3)}}(\mathbf{d}^{(3)})$ by variable transformation.
2. From $\bar{\mathbf{H}}_2^H \bar{\mathbf{H}}_2 = \mathbf{H}_2^H \mathbf{D}_3 \mathbf{H}_2$, get $f_{\boldsymbol{\sigma}^{(2)}}(\boldsymbol{\sigma}^{(2)}) = \int_{\mathcal{D}_3} f_{\boldsymbol{\sigma}^{(2)}|\mathbf{d}^{(3)}}(\boldsymbol{\sigma}^{(2)} \mid \mathbf{d}^{(3)}) f_{\mathbf{d}^{(3)}}(\mathbf{d}^{(3)}) d\mathbf{d}^{(3)}$, and then $f_{\mathbf{d}^{(2)}}(\mathbf{d}^{(2)})$ by variable transformation from $\mathbf{D}_2 = (\mathbf{I} + \mathbf{\Sigma}_2)^{-1}\mathbf{\Sigma}_2$.
3. From $\bar{\mathbf{H}}_1^H \bar{\mathbf{H}}_1 = \mathbf{H}_1^H \mathbf{D}_2 \mathbf{H}_1$, get $f_{\boldsymbol{\sigma}^{(1)}}(\boldsymbol{\sigma}^{(1)}) = \int_{\mathcal{D}_2} f_{\boldsymbol{\sigma}^{(1)}|\mathbf{d}^{(2)}}(\boldsymbol{\sigma}^{(1)} \mid \mathbf{d}^{(2)}) f_{\mathbf{d}^{(2)}}(\mathbf{d}^{(2)}) d\mathbf{d}^{(2)}$, i.e., the joint PDF for the nonzero eigenvalues of $\mathbf{B}$.

The above example for the simplest case illustrated how the joint PDF $f_{\boldsymbol{\sigma}^{(1)}}(\boldsymbol{\sigma}^{(1)})$ can be obtained in a recursive manner. However, in this dissertation we will consider a general case with arbitrary number of hops and arbitrary number of antennas within each cluster, and take the gain of each hop into account. The details are given in the remaining of this chapter.

Let

$$\mathbf{T}_k = \prod_{l=k}^{1} g_l \mathbf{H}_l = g_k \mathbf{H}_k g_{k-1} \mathbf{H}_{k-1} \cdots g_1 \mathbf{H}_1 \text{ for } k \le L+1. \tag{23}$$

Observe that

$$\mathbf{T}_k = g_k \mathbf{H}_k \mathbf{T}_{k-1} \text{ if } k > 1. \tag{24}$$

Also let $\mathbf{M}_k = \sum_{m=2}^{k} \left(\prod_{n=k}^{m} g_n \mathbf{H}_n \right) \left(\prod_{n=k}^{m} g_n \mathbf{H}_n \right)^H$ for $k > 1$, and $\mathbf{M}_1 = \mathbf{0}$. Then we have

$$\mathbf{M}_k = g_k \mathbf{H}_k \left(\mathbf{I} + \sum_{m=2}^{k-1} \left(\prod_{n=k-1}^{m} g_n \mathbf{H}_n \right) \left(\prod_{n=k-1}^{m} g_n \mathbf{H}_n \right)^H \right) g_k \mathbf{H}_k^H \text{ , and}$$

$$\mathbf{M}_k = g_k^2 \left(\mathbf{H}_k \mathbf{M}_{k-1} \mathbf{H}_k^H + \mathbf{H}_k \mathbf{H}_k^H \right). \tag{25}$$

Note $\mathbf{H} = \prod_{l=L+1}^{1} g_l \mathbf{H}_l = \mathbf{T}_{L+1}$ and $\mathbf{R} = E[\mathbf{n}\mathbf{n}^H] = \sum_{m=2}^{L+1} \left(\prod_{n=L+1}^{m} g_n \mathbf{H}_n \right) \left(\prod_{n=L+1}^{m} g_n \mathbf{H}_n \right)^H + \mathbf{I} = \mathbf{M}_{L+1} + \mathbf{I}$,

where $\mathbf{I}$ is the identity matrix.

From Equations (23)-(25), and the definitions of $\mathbf{H}_e$, $\mathbf{R}$, $\mathbf{H}$ and $\mathbf{T}_{L+1}$, we get

$$\begin{aligned}\mathbf{B} &= \mathbf{H}_e^H \mathbf{H}_e = \mathbf{H}^H \mathbf{R}^{-1} \mathbf{H} = \mathbf{T}_{L+1}^H \left(\mathbf{M}_{L+1} + \mathbf{I}\right)^{-1} \mathbf{T}_{L+1} \\ &= \mathbf{T}_L^H \mathbf{H}_{L+1}^H \left(\mathbf{H}_{L+1}(\mathbf{M}_L + \mathbf{I})\mathbf{H}_{L+1}^H + g_{L+1}^{-2}\mathbf{I}\right)^{-1} \mathbf{H}_{L+1} \mathbf{T}_L\end{aligned} . \quad (26)$$

With Eq. 26, we will develop Preposition 4 and Theorem 4 in the next section, which are the basis for the recursive approach.

We use the following notation throughout the next. Let $\mathbf{X}$ be a matrix. We denote a submatrix of $\mathbf{X}$ as $\{\mathbf{X}\}_{\substack{a \le i \le b \\ c \le j \le d}}$ if it is composed of the elements $[\mathbf{X}]_{i,j}$, where $a \le i \le b$, $c \le j \le d$, and a, b, c and d are some positive integers. $\det(\mathbf{X})$ or $|\mathbf{X}|$ is the determinant of $\mathbf{X}$, $rank(\mathbf{X})$ is the rank of $\mathbf{X}$, and $\mathbf{X}^t$ is the transpose. Let $\boldsymbol{\sigma} = [\sigma_1, \sigma_2, \ldots, \sigma_R]$, denote $\boldsymbol{\Sigma} = diag(\sigma_1, \sigma_2, \ldots, \sigma_R)$ or $\boldsymbol{\Sigma} = diag(\boldsymbol{\sigma})$ the diagonal matrix with diagonal entry $[\boldsymbol{\Sigma}]_{i,i} = \sigma_i$.

6.2 Recursive Approach to Find the Distribution of the Non-zero Eigenvalues

In this section, we derive a recursive approach to the derivation of the PDF of the non-zero eigenvalues of $\mathbf{B}$. The work in this section will build the basis for the next section for further simplification. Suppose we have eigenvalue decompose (EVD) $\mathbf{B} = \mathbf{U}\boldsymbol{\Sigma}\mathbf{U}^H$, where $\boldsymbol{\Sigma} = diag(\sigma_1, \sigma_2, \ldots, \sigma_R, 0, \ldots, 0)$, $R = \min(R_0, R_1, \ldots, R_{L+1})$, and $\boldsymbol{\sigma} = [\sigma_1, \sigma_2, \ldots, \sigma_R]$ the vector of the non-zero eigenvalues of $\mathbf{B}$.

Define $r_k = \begin{cases} R_{L+1} & \text{if } k = L+2 \\ rank(\mathbf{H}_k) = \min(R_{k-1}, r_{k+1}) & \text{if } k \le L+1 \end{cases}$ and

$$\bar{\mathbf{H}}_k = \begin{cases} \mathbf{H}_k & \text{if } k = L+1 \\ \tilde{\mathbf{D}}_{k+1}\tilde{\mathbf{H}}_k & \text{if } k < L+1 \end{cases}, \tag{27}$$

where $\tilde{\mathbf{D}}_k$ and $\tilde{\mathbf{H}}_k$ will be defined as follows. Let $\bar{\mathbf{H}}_k = \mathbf{U}_k \mathbf{\Lambda}_k \mathbf{V}_k^H$ be the SVD, where $[\mathbf{\Lambda}_k]_{i,i} \neq 0$ for $1 \le i \le r_k$, and let

$$\bar{\mathbf{D}}_k = (g_k^{-2}\mathbf{I} + \mathbf{\Lambda}_k \mathbf{\Lambda}_k^H)^{-1/2} \mathbf{\Lambda}_k, \tag{28}$$

$$\tilde{\mathbf{\Lambda}}_k = \{\mathbf{\Lambda}_k\}_{1 \le i,j \le r_k}, \ \tilde{\mathbf{D}}_k = \{\bar{\mathbf{D}}_k\}_{1 \le i,j \le r_k}, \ \tilde{\mathbf{H}}_{k-1} = \{\mathbf{H}_{k-1}\}_{\substack{1 \le i \le r_k \\ 1 \le j \le R_{k-2}}}. \tag{29}$$

Note that $\tilde{\mathbf{\Lambda}}_k$ and $\tilde{\mathbf{D}}_k$ are diagonal matrices with full rank. We can get $\tilde{\mathbf{\Lambda}}_k$ (and $\tilde{\mathbf{D}}_k$) in a reverse recursive manner, i.e., with $\bar{\mathbf{H}}_k$, we can find $\tilde{\mathbf{\Lambda}}_k$, and then $\bar{\mathbf{H}}_{k-1}$ and $\tilde{\mathbf{\Lambda}}_{k-1}$. We illustrate this recursive manner with a simple example: suppose we have a 3-hop network, i.e., $L+1=3$; then start from $\bar{\mathbf{H}}_3$ (or $\mathbf{H}_3$), we find $\tilde{\mathbf{\Lambda}}_3$ and $\tilde{\mathbf{D}}_3$ from Eq. (28) and (29); then $\bar{\mathbf{H}}_2$ from Eq. (27) and then $\tilde{\mathbf{\Lambda}}_2$, $\tilde{\mathbf{D}}_2$ from Eq. (28) and (29); then $\bar{\mathbf{H}}_1$ from Eq. (27) and finally $\tilde{\mathbf{\Lambda}}_1$, $\tilde{\mathbf{D}}_1$ from Eq. (28) and (29).

We start from $k = L+1$ and Eq. (26) to get Preposition 4 at first.

Preposition 4: $\mathbf{B} \cong \mathbf{T}_L^H \bar{\mathbf{D}}_{L+1}^H (\bar{\mathbf{D}}_{L+1} \mathbf{M}_L \bar{\mathbf{D}}_{L+1}^H + \mathbf{I})^{-1} \bar{\mathbf{D}}_{L+1} \mathbf{T}_L$

Proof: With SVD $\mathbf{H}_{L+1} = \mathbf{U}_{L+1}\mathbf{\Lambda}_{L+1}\mathbf{V}_{L+1}{}^{H}$ and definition $\bar{\mathbf{D}}_{L+1} = (g_{L+1}^{-2}\mathbf{I} + \mathbf{\Lambda}_{L+1}\mathbf{\Lambda}_{L+1}^{H})^{-½}\mathbf{\Lambda}_{L+1}$, we will prove from (26) that

$$\mathbf{B} \cong \mathbf{T}_L^H \bar{\mathbf{D}}_{L+1}^H (\bar{\mathbf{D}}_{L+1}\mathbf{M}_L\bar{\mathbf{D}}_{L+1}^H + \mathbf{I})^{-1}\bar{\mathbf{D}}_{L+1}\mathbf{T}_L . \tag{30}$$

From (26), we have

$$\begin{aligned}
&\mathbf{B} = \mathbf{T}_L^H \mathbf{H}_{L+1}^H \left(\mathbf{H}_{L+1}(\mathbf{M}_L + \mathbf{I})\mathbf{H}_{L+1}^H + g_{L+1}^{-2}\mathbf{I}\right)^{-1}\mathbf{H}_{L+1}\mathbf{T}_L \\
&= \mathbf{T}_L^H \mathbf{V}_{L+1}\mathbf{\Lambda}_{L+1}^H\mathbf{U}_{L+1}^H(\mathbf{U}_{L+1}\mathbf{\Lambda}_{L+1}\mathbf{V}_{L+1}^H(\mathbf{M}_L + \mathbf{I})\mathbf{V}_{L+1}\mathbf{\Lambda}_{L+1}^H\mathbf{U}_{L+1}^H + g_{L+1}^{-2}\mathbf{I})^{-1}\mathbf{U}_{L+1}\mathbf{\Lambda}_{L+1}\mathbf{V}_{L+1}^H\mathbf{T}_L \\
&= \mathbf{T}_L^H \mathbf{V}_{L+1}\mathbf{\Lambda}_{L+1}^H(\mathbf{\Lambda}_{L+1}\mathbf{V}_{L+1}^H(\mathbf{M}_L + \mathbf{I})\mathbf{V}_{L+1}\mathbf{\Lambda}_{L+1}^H + g_{L+1}^{-2}\mathbf{I})^{-1}\mathbf{\Lambda}_{L+1}\mathbf{V}_{L+1}^H\mathbf{T}_L \\
&\cong \mathbf{T}_L^H \mathbf{\Lambda}_{L+1}^H(\mathbf{\Lambda}_{L+1}(\mathbf{M}_L + \mathbf{I})\mathbf{\Lambda}_{L+1}^H + g_{L+1}^{-2}\mathbf{I})^{-1}\mathbf{\Lambda}_{L+1}\mathbf{T}_L
\end{aligned} \tag{31}$$

Note we use the fact that $\mathbf{V}_{L+1}^H\mathbf{H}_L \cong \mathbf{H}_L$, because $\mathbf{H}_L$ is Gaussian matrix, and $\mathbf{V}_{L+1}^H$ is orthogonal matrix. From these we have $\mathbf{V}_{L+1}^H\mathbf{T}_L \cong \mathbf{T}_L$ and $\mathbf{V}_{L+1}^H(\mathbf{M}_L + \mathbf{I})\mathbf{V}_{L+1} \cong \mathbf{M}_L + \mathbf{I}$ which assure the last equivalence in Eq. (31).

From Eq. (30) and the definition in Eq. (28), we have

$$\begin{aligned}
&\mathbf{B} \cong \mathbf{T}_L^H \bar{\mathbf{D}}_{L+1}^H (\bar{\mathbf{D}}_{L+1}\mathbf{M}_L\bar{\mathbf{D}}_{L+1}^H + \mathbf{I})^{-1}\bar{\mathbf{D}}_{L+1}\mathbf{T}_L \\
&= \mathbf{T}_L^H \mathbf{\Lambda}_{L+1}^H(g_{L+1}^{-2}\mathbf{I} + \mathbf{\Lambda}_{L+1}\mathbf{\Lambda}_{L+1}^H)^{-½} \\
&((g_{L+1}^{-2}\mathbf{I} + \mathbf{\Lambda}_{L+1}\mathbf{\Lambda}_{L+1}^H)^{-½}\mathbf{\Lambda}_{L+1}\mathbf{M}_L\mathbf{\Lambda}_{L+1}^H(g_{L+1}^{-2}\mathbf{I} + \mathbf{\Lambda}_{L+1}\mathbf{\Lambda}_{L+1}^H)^{-½} + \mathbf{I})^{-1} . \\
&(g_{L+1}^{-2}\mathbf{I} + \mathbf{\Lambda}_{L+1}\mathbf{\Lambda}_{L+1}^H)^{-½}\mathbf{\Lambda}_{L+1}\mathbf{T}_L \\
&= \mathbf{T}_L^H \mathbf{\Lambda}_{L+1}^H(\mathbf{\Lambda}_{L+1}\mathbf{M}_L\mathbf{\Lambda}_{L+1}^H + \mathbf{\Lambda}_{L+1}\mathbf{\Lambda}_{L+1}^H + g_{L+1}^{-2}\mathbf{I})^{-1}\mathbf{\Lambda}_{L+1}\mathbf{T}_L
\end{aligned} \tag{32}$$

Eq. (32) is same to Eq. (31), so it is proved that Eq. (26) and Eq. (30) are the same, i.e., it is proved that $\mathbf{B} \cong \mathbf{T}_L^H \bar{\mathbf{D}}_{L+1}^H (\bar{\mathbf{D}}_{L+1}\mathbf{M}_L\bar{\mathbf{D}}_{L+1}^H + \mathbf{I})^{-1}\bar{\mathbf{D}}_{L+1}\mathbf{T}_L$. □

Based on Preposition 4 and Equations (23)-(29), we can further develop a recursive algorithm in Theorem 4 for $1 \le k \le L+1$. Note the recursive manner in Eq. (25) and (27).

Theorem 4: $\mathbf{B} \cong \mathbf{T}_k^{\ H} \bar{\mathbf{D}}_{k+1}^H (\bar{\mathbf{D}}_{k+1} \mathbf{M}_k \bar{\mathbf{D}}_{k+1}^H + \mathbf{I})^{-1} \bar{\mathbf{D}}_{k+1} \mathbf{T}_k$ for $1 \le k \le L+1$.

Proof: First, for $k = L+1$, Theorem 4 is proved to hold as in the proof of Preposition 4.

From the definitionin Eq. (27), $\bar{\mathbf{H}}_{L+1} = \mathbf{H}_{L+1}$, Eq. (26) turns into

$$\mathbf{B} = \mathbf{T}_L^H \bar{\mathbf{H}}_{L+1}^H \left(\bar{\mathbf{H}}_{L+1} (\mathbf{M}_L + \mathbf{I}) \bar{\mathbf{H}}_{L+1}^H + g_{L+1}^{-2} \mathbf{I} \right)^{-1} \bar{\mathbf{H}}_{L+1} \mathbf{T}_L . \tag{33}$$

Second step, we can prove from Preposition 4 that

$$\begin{aligned} \mathbf{B} &\cong \mathbf{T}_L^{\ H} \bar{\mathbf{D}}_{L+1}^H (\bar{\mathbf{D}}_{L+1} \mathbf{M}_L \bar{\mathbf{D}}_{L+1}^H + \mathbf{I})^{-1} \bar{\mathbf{D}}_{L+1} \mathbf{T}_L \\ &= \mathbf{T}_{L-1}^H \mathbf{H}_L^H \bar{\mathbf{D}}_{L+1}^H (\bar{\mathbf{D}}_{L+1} \mathbf{H}_L (\mathbf{M}_{L-1} + \mathbf{I}) \mathbf{H}_L^H \bar{\mathbf{D}}_{L+1}^H + g_L^{-2} \mathbf{I})^{-1} \bar{\mathbf{D}}_{L+1} \mathbf{H}_L \mathbf{T}_{L-1} . \\ &= \mathbf{T}_{L-1}^H \bar{\mathbf{H}}_L^H (\bar{\mathbf{H}}_L (\mathbf{M}_{L-1} + \mathbf{I}) \bar{\mathbf{H}}_L^H + g_L^{-2} \mathbf{I})^{-1} \bar{\mathbf{H}}_L \mathbf{T}_{L-1} \end{aligned} \tag{34}$$

Note that the last equality can be easily proved. We can find the similarity between (26), (33) and (34), except the index is changed. Sequentially, we can prove $\mathbf{B} \cong \mathbf{T}_{L-1}^H \bar{\mathbf{D}}_L^H (\bar{\mathbf{D}}_L \mathbf{M}_{L-1} \bar{\mathbf{D}}_L^H + \mathbf{I})^{-1} \bar{\mathbf{D}}_L \mathbf{T}_{L-1}$ as the proof in Preposition 4. So a reverse recursive algorithm can be developed, and we have $\mathbf{B} \cong \mathbf{T}_k^{\ H} \bar{\mathbf{D}}_{k+1}^H (\bar{\mathbf{D}}_{k+1} \mathbf{M}_k \bar{\mathbf{D}}_{k+1}^H + \mathbf{I})^{-1} \bar{\mathbf{D}}_{k+1} \mathbf{T}_k$ for $1 \le k \le L+1$. □

Next we will go further to develop the recursive algorithm to find the PDF of the non-zero eigenvalues of $\mathbf{B}$, which is similar to what we have explained in the example of the simplest 3-hop case. From Theorem 4 and Equations (23)-(29), we finally get

$$\mathbf{B} \cong \mathbf{T}_1^H \bar{\mathbf{D}}_2^H (\bar{\mathbf{D}}_2 \mathbf{M}_1 \bar{\mathbf{D}}_2^H + \mathbf{I})^{-1} \bar{\mathbf{D}}_2 \mathbf{T}_1 = g_1^2 \mathbf{H}_1^H \bar{\mathbf{D}}_2^H \bar{\mathbf{D}}_2 \mathbf{H}_1 \cong g_1^2 \bar{\mathbf{H}}_1^H \bar{\mathbf{H}}_1,$$

and if we find the distribution of $\mathbf{\Lambda}_1$, and consequently by variable transformation, the distribution of the non-zero eigenvalues of $\mathbf{B}$. We now make the following definitions:

$$\mathbf{\Sigma}_k = \tilde{\mathbf{\Lambda}}_k \tilde{\mathbf{\Lambda}}_k^H = diag(\sigma_1^{(k)}, \sigma_2^{(k)}, \cdots, \sigma_{r_k}^{(k)}) , \tag{35}$$

$$\mathbf{D}_k = \tilde{\mathbf{D}}_k^H \tilde{\mathbf{D}}_k = diag(d_1^{(k)}, d_2^{(k)}, \cdots, d_{r_k}^{(k)}) . \tag{36}$$

Then $\bar{\mathbf{H}}_k^H \bar{\mathbf{H}}_k = \tilde{\mathbf{H}}_k^H \tilde{\mathbf{D}}_{k+1}^H \tilde{\mathbf{D}}_{k+1} \tilde{\mathbf{H}}_k = \tilde{\mathbf{H}}_k^H \mathbf{D}_{k+1} \tilde{\mathbf{H}}_k$ could be Wishart or pseudo-Wishart matrix [89, 90], and we will offer a recursive algorithm. Let $\boldsymbol{\sigma}^{(k)} = \left[\sigma_1^{(k)}, \sigma_2^{(k)}, \cdots, \sigma_{r_k}^{(k)} \right]^t$ be the non-zero eigenvalue vector of $\bar{\mathbf{H}}_k^H \bar{\mathbf{H}}_k$, let $\mathbf{d}^{(k)} = \left[d_1^{(k)}, d_2^{(k)}, \cdots, d_{r_k}^{(k)} \right]^t$.

From definitions in Equations (28), (29), (35) and (36) we get

$$\mathbf{D}_k = (g_k^{-2} \mathbf{I} + \mathbf{\Sigma}_k)^{-1} \mathbf{\Sigma}_k , \tag{37}$$

and $d_i^{(k)} = \sigma_i^{(k)} / (g_k^{-2} + \sigma_i^{(k)})$ for $2 \le k \le L+1$ and $1 \le i \le r_k$.

For $k \le L$, if $r_{k+1} = \min(R_k, R_{k+1}, \cdots, R_{L+1}) \le R_{k-1}$, then $\bar{\mathbf{H}}_k^H \bar{\mathbf{H}}_k$ is correlated central Wishart [85]; else it is correlated central pseudo Wishart [87, 88]. For $k = L+1$, $\bar{\mathbf{H}}_k^H \bar{\mathbf{H}}_k = \bar{\mathbf{H}}_{L+1}^H \bar{\mathbf{H}}_{L+1}$ is always correlated central Wishart matrix. Note that $\bar{\mathbf{H}}_{L+1} \bar{\mathbf{H}}_{L+1}^H \cong \bar{\mathbf{H}}_{L+1}^H \bar{\mathbf{H}}_{L+1}$.

$f_{\boldsymbol{\sigma}^{(L+1)}}(\boldsymbol{\sigma}^{(L+1)})$ is known

$k \leftarrow L+1$

While $k > 1$ **do**

$f_{\boldsymbol{\sigma}^{(k-1)}|\mathbf{d}^{(k)}}(\boldsymbol{\sigma}^{(k-1)} \mid \mathbf{d}^{(k)})$ is known

get $f_{\boldsymbol{\sigma}^{(k-1)}|\boldsymbol{\sigma}^{(k)}}(\boldsymbol{\sigma}^{(k-1)} \mid \boldsymbol{\sigma}^{(k)})$ from $f_{\boldsymbol{\sigma}^{(k-1)}|\mathbf{d}^{(k)}}(\boldsymbol{\sigma}^{(k-1)} \mid \mathbf{d}^{(k)})$ with

variable transform $\mathbf{D}_k = (g_k^{-2}\mathbf{I} + \boldsymbol{\Sigma}_k)^{-1}\boldsymbol{\Sigma}_k$

find $f_{\boldsymbol{\sigma}^{(k-1)}}(\boldsymbol{\sigma}^{(k-1)}) \leftarrow \int_{\mathcal{D}_k} f_{\boldsymbol{\sigma}^{(k-1)}|\boldsymbol{\sigma}^{(k)}}(\boldsymbol{\sigma}^{(k-1)} \mid \boldsymbol{\sigma}^{(k)}) f_{\boldsymbol{\sigma}^{(k)}}(\boldsymbol{\sigma}^{(k)}) d\boldsymbol{\sigma}^{(k)}$

$k \leftarrow k-1$

End while

Figure 23 Recursive algorithm to find joint PDF

With Equations (28), (29), (35)-(37), we can get $\tilde{\boldsymbol{\Lambda}}_k$ (and $\tilde{\mathbf{D}}_k$) in a reverse recursive manner, i.e., with $\bar{\mathbf{H}}_k$, we find $\tilde{\boldsymbol{\Lambda}}_k$, and then $\bar{\mathbf{H}}_{k-1}$ and $\tilde{\boldsymbol{\Lambda}}_{k-1}$; We start from $k = L+1$, and with the results on distribution of the non-zero eigenvalues of Wishart and pseudo-Wishart matrix as in [85, 86, 87, 88], given $\mathbf{d}^{(k)}$, we can find the conditional pdf of $\boldsymbol{\sigma}^{(k-1)}$

as $f_{\boldsymbol{\sigma}^{(k-1)}|\mathbf{d}^{(k)}}(\boldsymbol{\sigma}^{(k-1)}|\mathbf{d}^{(k)})$. After variable transformation from $\mathbf{d}^{(k)}$ to $\boldsymbol{\sigma}^{(k)}$, we get $f_{\boldsymbol{\sigma}^{(k-1)}|\boldsymbol{\sigma}^{(k)}}(\boldsymbol{\sigma}^{(k-1)}|\boldsymbol{\sigma}^{(k)})$, and then the pdf of $\boldsymbol{\sigma}^{(k-1)}$ by multi-dimensional integration as:

$$f_{\boldsymbol{\sigma}^{(k-1)}}(\boldsymbol{\sigma}^{(k-1)}) = \int_{\mathcal{D}_k} f_{\boldsymbol{\sigma}^{(k-1)}|\boldsymbol{\sigma}^{(k)}}(\boldsymbol{\sigma}^{(k-1)}|\boldsymbol{\sigma}^{(k)}) f_{\boldsymbol{\sigma}^{(k)}}(\boldsymbol{\sigma}^{(k)}) d\boldsymbol{\sigma}^{(k)} . \quad (38)$$

So with $f_{\boldsymbol{\sigma}^{(L+1)}}(\boldsymbol{\sigma}^{(L+1)})$, the pdf of $\boldsymbol{\sigma}^{(L+1)}$, is known [85, 86], we can finally find $f_{\boldsymbol{\sigma}^{(1)}}(\boldsymbol{\sigma}^{(1)})$ with a reverse recursive algorithm by employing Eq. (38) and Equations (28), (29), (35)-(37). This recursive algorithm is summarized in Fig. 23.

This recursive approach plays a central role for this work. However, there are two problems when we do this integration as in Eq. (38):

1. The dimension of integration is $\sum_{k=2}^{L+1} r_k$ and could be a big number even for a small number of hops, which means very high computational load for numerical evaluation.
2. The explicit expression will be extremely complicated even if not impossible to get, even for a small number of hops.

Further steps to simplify the expression are developed in the next section.

6.3 The Form of Products of Matrix Determinants

In this section, we will go a further step which is based on the recursive approach of last section, and find that the joint PDF which can be expressed in the form of the products of determinants of matrices. The entries of these matrices are expressed as multi-

dimensional integration, where the maximum dimension is just the number of relay clusters (the number of hops minus one). The complete set of equations needed to find this joint PDF is given at the end of this section as shown in Theorem 6.

We denote the joint distribution of the ordered non-zero eigenvalue vector as $f^{o}_{\boldsymbol{\sigma}^{(k)}}(\boldsymbol{\sigma}^{(k)})$, where $\sigma_1^{(k)} \geq \sigma_2^{(k)} \geq \cdots \geq \sigma_{r_k}^{(k)}$.

To facilitate our discussion, we first make an extension to [86, Corollary 1] or Cauchy-Binet formula [91] in Theorem 5; and then presents Prepositions 5, 6 and 7.

Theorem 5: Given $\mathbf{A(x)} = \left[\mathbf{C} \quad \tilde{\mathbf{A}}\mathbf{(x)}\right]$, where $\mathbf{x} = \left[x_1, x_2, \cdots, x_M\right]^t$ is a $M \times 1$ vector, $\mathbf{A(x)}$ is a $N \times N$ matrix, $\tilde{\mathbf{A}}\mathbf{(x)}$ is a $N \times M$ matrix, $\mathbf{C}$ is a $N \times K$ matrix, $N \geq M$ and $K = N - M$. The elements of $\mathbf{C}$ are some constants (not a function of $\mathbf{x}$). The entries of $\tilde{\mathbf{A}}\mathbf{(x)}$ have the form $\left[\tilde{\mathbf{A}}\mathbf{(x)}\right]_{ij} = \tilde{\alpha}_i(x_j)$. Given **B(x)** which is a $M \times M$ matrix with the entry $\left[\mathbf{B(x)}\right]_{ij} = \beta_i(x_j)$, and arbitrary functions $\xi(\cdot)$, then the following identity holds:

$\int \cdots \int_{\mathcal{D}} |\mathbf{A(x)}||\mathbf{B(x)}| \prod_{l=1}^{M} \xi(x_l) d\mathbf{x} = M! |\boldsymbol{\Theta}|$, where the multiple integration is over the domain $\mathcal{D} = \{a \leq x_1 \leq b, a \leq x_2 \leq b, \cdots, a \leq x_M \leq b\}$, $d\mathbf{x} = dx_1 dx_2 \cdots dx_M$, $\boldsymbol{\Theta} = \left[\mathbf{C} \quad \tilde{\boldsymbol{\Theta}}\right]$ and $\left[\tilde{\boldsymbol{\Theta}}\right]_{ij} = \int_a^b \tilde{\alpha}_i(x) \beta_j(x) \xi(x) dx$.

Proof: see Appendix B.1. □

We make the following definitions in the remainder of this section.

Suppose $\mathbf{x} = \left[x_1, x_2, \cdots, x_q \right]^t$ is a $q \times 1$ vector, we define:

$\mathbf{V(x)}$ is a $q \times q$ Vandermonde matrix with the $(i, j)th$ element $\left[\mathbf{V(x)}\right]_{ij} = -x_j^{1-i}$,

$\mathbf{\Phi(x)}$ is a $q \times q$ Vandermonde matrix with the $(i, j)th$ element $\left[\mathbf{\Phi(x)}\right]_{ij} = \varphi_i(x_j) = x_j^{i-1}$,

Let $\mathbf{y} = \left[y_1, y_2, \cdots, y_p \right]^t$ be a $p \times 1$ vector, $p \geq q$, we define

$$\left[\mathbf{\Psi(x,y)}\right]_{ij} = \psi_i(y_j) = \begin{cases} \bar{\psi}(i,\ y_j) & 1 \leq i \leq p - q \\ \tilde{\psi}(x_{i-p+q}, y_j) & p - q < i \leq p \end{cases} \quad for \quad 1 \leq j \leq p$$ where

$\bar{\psi}(i,\ y) = y^{i-1}$ and $\tilde{\psi}(x, y) = y^{p-q-1} e^{-x/y}$.

Preposition 5: Let $\bar{\mathbf{H}} = \bar{\mathbf{D}}\mathbf{H}$, where $\mathbf{H}$ is a $M \times N$ matrix with i.i.d. complex Gaussian entries with variance 1, $\bar{\mathbf{D}}$ is a $M \times M$ diagonal matrix, and $\mathbf{D} = \bar{\mathbf{D}}\bar{\mathbf{D}}^H = diag(d_1, d_2, \ldots, d_M)$. $N \geq M$ so $\bar{\mathbf{H}}^H\bar{\mathbf{H}}$ is Wishart. Let $\boldsymbol{\sigma}$ be the vector of the non-zero eigenvalues of $\bar{\mathbf{H}}^H\bar{\mathbf{H}}$. Given $\mathbf{d} = (d_1, d_2, \ldots, d_M)^t$, the joint conditional pdf of ordered non-zero eigenvalues of $\bar{\mathbf{H}}^H\bar{\mathbf{H}}$ is

$f^o_{\boldsymbol{\sigma}|\mathbf{d}}(\boldsymbol{\sigma} \mid \mathbf{d}) = K^o \dfrac{|\mathbf{D}|^{1-P}}{|\mathbf{V(d)}|} |\mathbf{\Phi}(\boldsymbol{\sigma})| |\mathbf{\Psi}(\boldsymbol{\sigma}, \mathbf{d})| \prod_{l=1}^{M} \xi(\sigma_l)$, where $\xi(x) = x^{N-M}$, $K^o = \left(\prod_{i=1}^{M} (N-i)! \right)^{-1}$.

Proof: For the case that $\bar{\mathbf{H}}^H\bar{\mathbf{H}}$ is Wishart, $\boldsymbol{\sigma}$ and $\mathbf{d}$ are all $M\times 1$ vectors. From [85, 86], we get $f^o_{\boldsymbol{\sigma}|\mathbf{d}}(\boldsymbol{\sigma}\,|\,\mathbf{d}) = K^o \dfrac{|\mathbf{D}|^{-P}}{|\mathbf{V}(\mathbf{d})|}\left|\boldsymbol{\Phi}(\boldsymbol{\sigma})\right|\left|\hat{\boldsymbol{\Psi}}(\boldsymbol{\sigma},\mathbf{d})\right|\prod_{l=1}^{M}\xi(\sigma_l)$, where $\left[\hat{\boldsymbol{\Psi}}(\mathbf{x},\mathbf{y})\right]_{ij} = e^{-x_j/y_i}$ and $K^o = \left(\prod_{i=1}^{M}(N-i)!\right)^{-1}$, and when a constraint on $\mathbf{d}$ holds as $d_1 > d_2 > \cdots > d_M$. It is easy to prove that $\left|\hat{\boldsymbol{\Psi}}(\boldsymbol{\sigma},\mathbf{d})\right| = |\mathbf{D}|\left|\boldsymbol{\Psi}(\boldsymbol{\sigma},\mathbf{d})\right|$. And if we get a vector $\hat{\mathbf{d}}$ from $\mathbf{d}$ by swapping any two elements in $\mathbf{d}$, and let $\hat{\mathbf{D}} = diag(\hat{d}_1, \hat{d}_2, \ldots, \hat{d}_M)$, we find that $\left|\hat{\mathbf{D}}\right| = |\mathbf{D}|$ and $\dfrac{\left|\boldsymbol{\Psi}(\boldsymbol{\sigma},\hat{\mathbf{d}})\right|}{\left|\mathbf{V}(\hat{\mathbf{d}})\right|} = \dfrac{|\boldsymbol{\Psi}(\boldsymbol{\sigma},\mathbf{d})|}{|\mathbf{V}(\mathbf{d})|}$; and further, we find that the constraint on $\mathbf{d}$ actually does not matter for the expression of $f^o_{\boldsymbol{\sigma}|\mathbf{d}}(\boldsymbol{\sigma}\,|\,\mathbf{d})$; thus Preposition 5 holds. □

Preposition 6: Let $\bar{\mathbf{H}} = \bar{\mathbf{D}}\mathbf{H}$, $\mathbf{H}$ is a $M\times N$ matrix with i.i.d. complex Gaussian entries with variance 1, $\bar{\mathbf{D}}$ is a $M\times M$ diagonal matrix, and $\mathbf{D} = \bar{\mathbf{D}}\bar{\mathbf{D}}^H = diag(d_1, d_2, \ldots, d_M)$. Let $Q = \min(M, N)$ and $P = \max(M, N)$. Let $\boldsymbol{\sigma}$ be the vector of the unordered non-zero eigenvalues of $\bar{\mathbf{H}}^H\bar{\mathbf{H}}$. Given $\mathbf{d} = (d_1, d_2, \ldots, d_M)^t$, the joint conditional pdf of $\boldsymbol{\sigma}$ is $f_{\boldsymbol{\sigma}|\mathbf{d}}(\boldsymbol{\sigma}\,|\,\mathbf{d}) = \tilde{K}\dfrac{|\mathbf{D}|^{1-P}}{|\mathbf{V}(\mathbf{d})|}\left|\boldsymbol{\Phi}(\boldsymbol{\sigma})\right|\left|\boldsymbol{\Psi}(\boldsymbol{\sigma},\mathbf{d})\right|\prod_{l=1}^{M}\xi(\sigma_l)$, where $\xi(x) = x^{P-M}$, $\tilde{K} = \left(Q!\prod_{i=1}^{Q}(N-i)!\right)^{-1}$.

Proof: For the case that $\bar{\mathbf{H}}^H\bar{\mathbf{H}}$ is pseudo Wishart, $P = M$, $Q = N$ and $\xi(x) = x^{P-M} = 1$, from [87, Appendix A] or [88, eq. (14)], and with $\left|\boldsymbol{\Psi}^t(\boldsymbol{\sigma},\mathbf{d})\right| = \left|\boldsymbol{\Psi}(\boldsymbol{\sigma},\mathbf{d})\right|$, we have

$f_{\boldsymbol{\sigma}|\mathbf{d}}(\boldsymbol{\sigma}\,|\,\mathbf{d}) = \tilde{K}\dfrac{1}{|\boldsymbol{\Phi}(\mathbf{d})|}|\boldsymbol{\Phi}(\boldsymbol{\sigma})||\boldsymbol{\Psi}(\boldsymbol{\sigma},\mathbf{d})|$, where $\tilde{K} = \left(\prod_{k=1}^{Q} k!\right)^{-1} = \left(Q!\prod_{i=1}^{Q}(N-i)!\right)^{-1}$. Note that $|\boldsymbol{\Phi}(\mathbf{d})| = \prod_{1\le i<j\le M}(d_j - d_i)$ for a Vandermonde matrix $\boldsymbol{\Phi}(\mathbf{d})$, and

$$|\mathbf{D}|^{M-1} = \left(\prod_{1\le k\le M} d_M\right)^{M-1} = \prod_{1\le i<j\le M}(d_j d_i)\ .$$

Because $|\mathbf{V}(\mathbf{d})| = \prod_{1\le i<j\le M}((-\frac{1}{d_j})-(-\frac{1}{d_i})) = \prod_{1\le i<j\le M}(d_j - d_i) / \prod_{1\le i<j\le M}(d_j d_i) = |\boldsymbol{\Phi}(\mathbf{d})| / |\mathbf{D}|^{M-1}$,

it is proved that Preposition 6 holds for the pseudo Wishart case.

For the case that $\bar{\mathbf{H}}^H\bar{\mathbf{H}}$ is Wishart, $Q = M$, $P = N$, $\boldsymbol{\sigma}$ and $\mathbf{d}$ are all $M\times 1$ vectors. From Preposition 5, we have $f^o_{\boldsymbol{\sigma}|\mathbf{d}}(\boldsymbol{\sigma}\,|\,\mathbf{d}) = K^o\dfrac{|\mathbf{D}|^{1-P}}{|\mathbf{V}(\mathbf{d})|}|\boldsymbol{\Phi}(\boldsymbol{\sigma})||\boldsymbol{\Psi}(\boldsymbol{\sigma},\mathbf{d})|\prod_{l=1}^{M}\xi(\sigma_l)$, where $K^o = \left(\prod_{i=1}^{Q}(N-i)!\right)^{-1}$; and from [84, Theorem 2.6], the joint pdf for the unordered eigenvalues is $f_{\boldsymbol{\sigma}|\mathbf{d}}(\boldsymbol{\sigma}\,|\,\mathbf{d}) = (Q!)^{-1} f^o_{\boldsymbol{\sigma}|\mathbf{d}}(\boldsymbol{\sigma}\,|\,\mathbf{d})$. We find that Preposition 6 holds for the Wishart case. □

Before we proceed to the final result, we make the following definition for brevity:

Let $r_{L+2} = R_{L+1}$, we define for $k \le L+1$ that:

$q_k = r_k = \min(R_{k-1}, r_{k+1})$,

$$p_k = \max(R_{k-1}, r_{k+1}),$$

$$\tilde{K}_{k-1}^{o} = \left(\prod_{i=1}^{r_{k-1}} (R_{k-2} - i)! \right)^{-1} g_k^{-r_k(r_k-1)},$$

$$\tilde{K}_{k-1} = \left(q_{k-1}! \prod_{i=1}^{q_{k-1}} (R_{k-2} - i)! \right)^{-1} g_k^{-r_k(r_k-1)} = \left(r_{k-1}!\right)^{-1} \tilde{K}_{k-1}^{o}$$

$$\xi'_k(x) = x^{r_k - 1} \left(1 + \frac{g_k^{-2}}{x} \right)^{p_{k-1}-1},$$

$$\xi_k(x) = \begin{cases} x^{p_k - r_k} e^{-x} & \text{if } k = L+1 \\ x^{p_k - r_{k+1}} & \text{if } k < L+1 \end{cases}, \text{ and}$$

$$\left[\boldsymbol{\Psi}(\boldsymbol{\sigma}^{(k-1)}, \mathbf{d}^{(k)}) \right]_{ij} = \hat{\psi}_i^{(k-1)}(\sigma_j^{(k)}) = \begin{cases} \bar{\psi}^{(k-1)}(i,\ \sigma_j^{(k)}) & \text{if } 1 \le i \le r_k - r_{k-1} \\ \tilde{\psi}^{(k-1)}(\sigma_{i-r_k+r_{k-1}}^{(k-1)}, \sigma_j^{(k)}) & \text{if } r_k - r_{k-1} < i \le r_k \end{cases} \text{ for } 1 \le j \le r_k,$$

where $\bar{\psi}^{(k-1)}(i,\ z) = \left(\frac{z}{g_k^{-2} + z}\right)^{i-1}$ and $\tilde{\psi}^{(k-1)}(y, z) = \left(\frac{z}{g_k^{-2} + z}\right)^{r_k - r_{k-1} - 1} e^{-y(1+g_k^{-2}/z)}$.

Proposition 7: $\bar{\mathbf{H}}_{k-1}$ is a $r_k \times R_{k-2}$ matrix. Given $\boldsymbol{\sigma}^{(k)}$, the joint conditional pdf of $\boldsymbol{\sigma}^{(k-1)}$ is

$$f_{\boldsymbol{\sigma}^{(k-1)}|\boldsymbol{\sigma}^{(k)}}(\boldsymbol{\sigma}^{(k-1)} \mid \boldsymbol{\sigma}^{(k)}) = \tilde{K}_{k-1} \frac{1}{\left|\boldsymbol{\Phi}(\boldsymbol{\sigma}^{(k)})\right|} \left|\boldsymbol{\Phi}(\boldsymbol{\sigma}^{(k-1)})\right| \left|\boldsymbol{\Psi}(\boldsymbol{\sigma}^{(k-1)}, \mathbf{d}^{(k)})\right| \prod_{l=1}^{r_k} \xi'_k(\sigma_l^{(k)}) \prod_{l=1}^{r_{k-1}} \xi_{k-1}(\sigma_l^{(k-1)})$$

for $k \le L+1$,

Proof: with $d_j^{(k)} = \sigma_j^{(k)} / (g_k^{-2} + \sigma_j^{(k)})$, we find that $\left|\mathbf{D}_k\right| = \prod_{j=1}^{r_k} d_j^{(k)} = \prod_{j=1}^{r_k} \frac{\sigma_j^{(k)}}{g_k^{-2} + \sigma_j^{(k)}}$, and

$$\left|\mathbf{V}(\mathbf{d}_k)\right| = \prod_{1\le i<j\le r_k}((-\frac{1}{d_j^{(k)}})-(-\frac{1}{d_i^{(k)}})) = \prod_{1\le i<j\le r_k}(1+\frac{g_k^{-2}}{\sigma_i^{(k)}}-1-\frac{g_k^{-2}}{\sigma_j^{(k)}})$$
$$= \prod_{1\le i<j\le r_k} g_k^{-2}(\sigma_j^{(k)}-\sigma_i^{(k)}) / \prod_{1\le i<j\le r_k}(\sigma_j^{(k)}\sigma_i^{(k)}) = g_k^{-r_k(r_k-1)}\left|\mathbf{\Phi}(\boldsymbol{\sigma}^{(k)})\right| / \left|\mathbf{\Sigma}_k\right|^{r_k-1},$$

with $\left|\mathbf{D}_k\right|^{1-p_{k-1}}\left|\mathbf{\Sigma}_k\right|^{r_{k-1}} = \prod_{l=1}^{r_k}\xi'_k(\sigma_l^{(k)})$, from Preposition 6 we get

$$f_{\boldsymbol{\sigma}^{(k-1)}|\boldsymbol{\sigma}^{(k)}}(\boldsymbol{\sigma}^{(k-1)} \mid \boldsymbol{\sigma}^{(k)}) = \tilde{K}_{k-1}\frac{\left|\mathbf{\Sigma}_k\right|^{r_k-1}\left|\mathbf{D}_k\right|^{1-p_{k-1}}}{\left|\mathbf{\Phi}(\boldsymbol{\sigma}^{(k)})\right|}\left|\mathbf{\Phi}(\boldsymbol{\sigma}^{(k-1)})\right|\left|\mathbf{\Psi}(\boldsymbol{\sigma}^{(k-1)},\mathbf{d}^{(k)})\right|\prod_{l=1}^{q_{k-1}}\xi_{k-1}(\sigma_l^{(k-1)}) . \square$$

With all these preparations, we get our main result next.

Theorem 6: the pdf of the unordered non-zero eigenvalues has the form

$$f_{\boldsymbol{\sigma}^{(k)}}(\boldsymbol{\sigma}^{(k)}) = K_k\left|\mathbf{\Phi}(\boldsymbol{\sigma}^{(k)})\right|\left|\bar{\mathbf{\Phi}}_k(\boldsymbol{\sigma}^{(k)})\right|\prod_{l=1}^{r_k}\xi_k(\sigma_l^{(k)}),$$

where $\bar{\mathbf{\Phi}}_k(\boldsymbol{\sigma}^{(k)}) = \left[\mathbf{C}_L \quad \cdots \quad \mathbf{C}_{k+1} \quad \mathbf{C}_k \quad \tilde{\mathbf{\Phi}}_k(\boldsymbol{\sigma}^{(k)})\right]$ for $k \le L+1$, and the entries of $\mathbf{C}_L$, $\cdots$, $\mathbf{C}_k$ are not a function of $\boldsymbol{\sigma}^{(k)}$ but some constants. Also the entries of $\tilde{\mathbf{\Phi}}_k(\boldsymbol{\sigma}^{(k)})$ have the form $\left[\tilde{\mathbf{\Phi}}_k(\boldsymbol{\sigma}^{(k)})\right]_{ij} = \tilde{\phi}_i^{(k)}(\sigma_j^{(k)})$ and its value for a specific $\sigma_j^{(k)}$ can be evaluated by $L+1-k$ dimensional integration. $\bar{\mathbf{\Phi}}_k(\boldsymbol{\sigma}^{(k)})$ is a $r_{L+1}\times r_{L+1}$ matrix, $\mathbf{C}_k$ is a $r_{L+1}\times(r_{k+1}-r_k)$ matrix and its entries are obtained by $L+1-k$ dimensional integration, $\tilde{\mathbf{\Phi}}_k(\boldsymbol{\sigma}^{(k)})$ is a $r_{L+1}\times r_k$ matrix,

Proof: First, we will prove that Theorem 6 holds for $k = L+1$.

For the last hop, $q_{L+1} = r_{L+1} = \min(R_L, r_{L+2})$ and $p_{L+1} = \max(R_L, r_{L+2})$ where $r_{L+2} = R_{L+1}$. Note that $\bar{\mathbf{H}}_{L+1}\bar{\mathbf{H}}_{L+1}^H \cong \bar{\mathbf{H}}_{L+1}^H\bar{\mathbf{H}}_{L+1}$, so for the last hop, whatever the sizes of the last two clusters are, it is always a Wishart case. The joint distribution of the ordered non-zero eigenvalue vector of $\bar{\mathbf{H}}_{L+1}\bar{\mathbf{H}}_{L+1}^H$ is [85, 86]:

$$f^{o}_{\boldsymbol{\sigma}^{(L+1)}}(\boldsymbol{\sigma}^{(L+1)}) = K^{uc}_{L+1}\left|\boldsymbol{\Phi}(\boldsymbol{\sigma}^{(L+1)})\right|\left|\bar{\boldsymbol{\Phi}}_{L+1}(\boldsymbol{\sigma}^{(L+1)})\right|\prod_{l=1}^{q_{L+1}}\xi_{L+1}(\sigma_l^{(L+1)}), \text{ where } \bar{\boldsymbol{\Phi}}_{L+1}(\boldsymbol{\sigma}^{(L+1)}) = \boldsymbol{\Phi}(\boldsymbol{\sigma}^{(L+1)}),$$

$$\xi_{L+1}(x) = x^{p_{L+1}-q_{L+1}}e^{-x},\ K^{uc}_{L+1} = \left[\prod_{i=1}^{q_{L+1}}(p_{L+1}-i)!\prod_{j=1}^{q_{L+1}}(q_{L+1}-j)!\right]^{-1}.$$

From [84, Theorm 2.6], the joint pdf for the unordered eigenvalues is $f_{\boldsymbol{\sigma}^{(k)}}(\boldsymbol{\sigma}^{(k)}) = (q_k!)^{-1} f^{o}_{\boldsymbol{\sigma}^{(k)}}(\boldsymbol{\sigma}^{(k)})$.

So Theorem 6 holds for $k = L+1$, where $\tilde{\boldsymbol{\Phi}}_{L+1}(\boldsymbol{\sigma}^{(L+1)}) = \bar{\boldsymbol{\Phi}}_{L+1}(\boldsymbol{\sigma}^{(L+1)}) = \boldsymbol{\Phi}(\boldsymbol{\sigma}^{(L+1)})$,

$\tilde{\phi}_i^{(L+1)}(x) = \varphi_i(x) = x^{i-1}$, and $K_{L+1} = (q_{L+1}!)^{-1}K^{uc}_{L+1} = \left[q_{L+1}!\prod_{i=1}^{q_{L+1}}(p_{L+1}-i)!\prod_{j=1}^{q_{L+1}}(q_{L+1}-j)!\right]^{-1}$.

Note $q_{L+1} = r_{L+1}$, and $\xi_k(x) = \xi_{L+1}(x) = x^{p_{L+1}-q_{L+1}}e^{-x}$.

Next we will prove that Theorem 6 holds for $k = \kappa - 1$ if it holds for $k = \kappa$.

From Proposition 7, and multi-dimensional integration Eq. (38), we get

$$f_{\boldsymbol{\sigma}^{(\kappa-1)}}(\boldsymbol{\sigma}^{(\kappa-1)}) = \int_{\mathcal{D}_\kappa} f_{\boldsymbol{\sigma}^{(\kappa-1)}|\boldsymbol{\sigma}^{(\kappa)}}(\boldsymbol{\sigma}^{(\kappa-1)} \mid \boldsymbol{\sigma}^{(\kappa)})\, f_{\boldsymbol{\sigma}^{(\kappa)}}(\boldsymbol{\sigma}^{(\kappa)}) d\boldsymbol{\sigma}^{(\kappa)}$$

$$= \tilde{K}_{\kappa-1} K_\kappa \left|\boldsymbol{\Phi}(\boldsymbol{\sigma}^{(\kappa-1)})\right| \prod_{l=1}^{r_{\kappa-1}} \xi_{\kappa-1}(\sigma_l^{(\kappa-1)}) \bullet \int_{\mathcal{D}_\kappa} \left|\bar{\boldsymbol{\Phi}}_\kappa(\boldsymbol{\sigma}^{(\kappa)})\right| \left|\boldsymbol{\Psi}(\boldsymbol{\sigma}^{(\kappa-1)}, \mathbf{d}^{(\kappa)})\right| \prod_{l=1}^{r_\kappa} \xi_\kappa(\sigma_l^{(\kappa)}) \prod_{l=1}^{r_\kappa} \xi'_\kappa(\sigma_l^{(\kappa)}) d\boldsymbol{\sigma}^{(\kappa)}$$

$$= K_{\kappa-1} \left|\boldsymbol{\Phi}(\boldsymbol{\sigma}^{(\kappa-1)})\right| \left|\bar{\boldsymbol{\Phi}}_{\kappa-1}(\boldsymbol{\sigma}^{(\kappa-1)})\right| \prod_{l=1}^{r_{\kappa-1}} \xi_{\kappa-1}(\sigma_l^{(\kappa-1)})$$

where $K_{\kappa-1} = r_\kappa ! \tilde{K}_{\kappa-1} K_\kappa$, the domain $\mathcal{D}_\kappa = \left\{\sigma_1^{(\kappa)} \geq 0,\ \sigma_2^{(\kappa)} \geq 0,\ \cdots,\ \sigma_{r_\kappa}^{(\kappa)} \geq 0\right\}$,

$d\boldsymbol{\sigma}^{(\kappa)} = d\sigma_1^{(\kappa)} d\sigma_2^{(\kappa)} \cdots d\sigma_{r_\kappa}^{(\kappa)}$, and

$$r_\kappa ! \left|\bar{\boldsymbol{\Phi}}_{\kappa-1}(\boldsymbol{\sigma}^{(\kappa-1)})\right| = \int_{\mathcal{D}_k} \left|\bar{\boldsymbol{\Phi}}_k(\boldsymbol{\sigma}^{(\kappa)})\right| \left|\boldsymbol{\Psi}(\boldsymbol{\sigma}^{(\kappa-1)}, \mathbf{d}^{(\kappa)})\right| \prod_{l=1}^{r_\kappa} \xi_\kappa(\sigma_l^{(\kappa)}) \prod_{l=1}^{r_\kappa} \xi'_\kappa(\sigma_l^{(\kappa)}) d\boldsymbol{\sigma}^{(\kappa)} .$$

if Theorem 6 holds for $k = \kappa$, then we have

$$\bar{\boldsymbol{\Phi}}_\kappa(\boldsymbol{\sigma}^{(\kappa)}) = \left[\mathbf{C}_L \quad \cdots \quad \mathbf{C}_\kappa \quad \tilde{\boldsymbol{\Phi}}_\kappa(\boldsymbol{\sigma}^{(\kappa)})\right]. \tag{39}$$

From Theorem 5, we have

$$\bar{\boldsymbol{\Phi}}_{\kappa-1}(\boldsymbol{\sigma}^{(\kappa-1)}) = \left[\mathbf{C}_L \quad \cdots \quad \mathbf{C}_\kappa \quad \hat{\boldsymbol{\Phi}}_{\kappa-1}(\boldsymbol{\sigma}^{(\kappa-1)})\right],$$

where $\left[\hat{\boldsymbol{\Phi}}_{\kappa-1}(\boldsymbol{\sigma}^{(\kappa-1)})\right]_{ij} = \int_0^\infty \tilde{\phi}_i^{(\kappa)}(x) \hat{\psi}_j^{(\kappa-1)}(x) \xi_\kappa(x) \xi'_\kappa(x) dx$,

$$\left[\hat{\boldsymbol{\Phi}}_{\kappa-1}(\boldsymbol{\sigma}^{(\kappa-1)})\right]_{ij} = \begin{cases} \int_0^\infty \tilde{\phi}_i^{(\kappa)}(x) \bar{\psi}^{(\kappa-1)}(j,\ x) \xi_\kappa(x) \xi'_\kappa(x) dx & \text{if } 1 \leq j \leq r_\kappa - r_{\kappa-1} \\ \int_0^\infty \tilde{\phi}_i^{(\kappa)}(x) \tilde{\psi}^{(\kappa-1)}(\sigma_{j-r_\kappa+r_{\kappa-1}}^{(\kappa-1)}, x) \xi_\kappa(x) \xi'_\kappa(x) dx & \text{if } r_\kappa - r_{\kappa-1} < j \leq r_\kappa \end{cases}.$$

Apparently, an entry $\left[\hat{\boldsymbol{\Phi}}_{\kappa-1}(\boldsymbol{\sigma}^{(\kappa-1)})\right]_{ij}$ will be some constant if $1 \leq j \leq r_\kappa - r_{\kappa-1}$, so

$\hat{\boldsymbol{\Phi}}_{\kappa-1}(\boldsymbol{\sigma}^{(\kappa-1)}) = \left[\mathbf{C}_{\kappa-1} \quad \tilde{\boldsymbol{\Phi}}_{\kappa-1}(\boldsymbol{\sigma}^{(\kappa-1)})\right]$, and we get

$$\bar{\mathbf{\Phi}}_{\kappa-1}(\boldsymbol{\sigma}^{(\kappa-1)}) = \left[\mathbf{C}_L \quad \cdots \quad \mathbf{C}_\kappa \quad \mathbf{C}_{\kappa-1} \quad \tilde{\mathbf{\Phi}}_{\kappa-1}(\boldsymbol{\sigma}^{(\kappa-1)})\right], \tag{40}$$

where $\mathbf{C}_{\kappa-1}$ is a $r_{L+1} \times \left(r_\kappa - r_{\kappa-1}\right)$ matrix with its entries are some constants, $\tilde{\mathbf{\Phi}}_{k-1}(\boldsymbol{\sigma}^{(k-1)})$ is a $r_{L+1} \times r_{\kappa-1}$ matrix. We have

$$\left[\mathbf{C}_{\kappa-1}\right]_{ij} = \int_0^\infty \tilde{\phi}_i^{(\kappa)}(x)\bar{\psi}^{(\kappa-1)}(j,\ x)\xi_\kappa(x)\xi'_\kappa(x)dx \text{ for } 1 \le j \le r_\kappa - r_{\kappa-1}, \tag{41}$$

$$\left[\tilde{\mathbf{\Phi}}_{k-1}(\boldsymbol{\sigma}^{(k-1)})\right]_{ij} = \int_0^\infty \tilde{\phi}_i^{(\kappa)}(x)\tilde{\psi}^{(\kappa-1)}(\sigma_j^{(\kappa-1)}, x)\xi_\kappa(x)\xi'_\kappa(x)dx \text{ for } 1 \le j \le r_{\kappa-1}. \tag{42}$$

So if (39) exists, then (40) can be deduced, and it is proved that Theorem 6 holds for $k = \kappa - 1$ if it holds for $k = \kappa$.

By applying above procedure recursively, i.e., with $\bar{\mathbf{\Phi}}_{L+1}(\boldsymbol{\sigma}^{(L+1)})$, find $\bar{\mathbf{\Phi}}_L(\boldsymbol{\sigma}^{(L)})$ next, then $\bar{\mathbf{\Phi}}_{L-1}(\boldsymbol{\sigma}^{(L-1)})$ next, and keep on going, we develop an algorithm to find the entries of $\bar{\mathbf{\Phi}}_k(\boldsymbol{\sigma}^{(k)})$ as described next.

Let $\tilde{\psi}^{(L+1)}(\cdot,\cdot) = 1$, $\bar{\xi}_k(z_k) = \xi_k(z_k)\xi_k^{'}(z_k)$, and $h_k(\mathbf{z}) = \bar{\xi}_k(z_k)\prod_{m=L+1}^{k+1}\tilde{\psi}^{(m-1)}(z_{m-1}, z_m)\bar{\xi}_m(z_m)$, then for $k \le L-1$ the explicit expression is

$$\left[\tilde{\mathbf{\Phi}}_k(\boldsymbol{\sigma}^{(k)})\right]_{ij} = \tilde{\phi}_i^{(k)}(\sigma_j^{(k)}) = \int_0^\infty \cdots \int_0^\infty \varphi_i(z_{L+1})\tilde{\psi}^{(k)}(\sigma_j^{(k)}, z_{k+1})h_{k+1}(\mathbf{z})dz_{L+1}\cdots dz_{k+1}\ , \tag{41}$$

$$\left[\mathbf{C}_k\right]_{ij} = \int_0^\infty \cdots \int_0^\infty \varphi_i(z_{L+1})\bar{\psi}^{(k)}(j,\ z_{k+1})h_{k+1}(\mathbf{z})dz_{L+1}\cdots dz_{k+1}\ , \tag{42}$$

for $k = L$, the explicit expression is as in (39) and (40) where $\kappa = L + 1$. □

Briefly, we use the conclusion of Theorem 6 and Equations (39)-(42) to get the closed form expression for the joint PDF. We summarize in Fig. 26 how to get $f_{\boldsymbol{\sigma}^{(k)}}(\boldsymbol{\sigma}^{(k)})$.

6.4 Simulation Results

For simplicity, we analyze the eigenvalue distribution of a 2 hop with 2x2 configuration for each hop, while we employ the multiple DSM with AF scheme. Let $g_1 = g_2 = 1$ in Eq. (22), and we have $\mathbf{B} = \mathbf{H}_1^H \mathbf{H}_2^H (\mathbf{H}_2 \mathbf{H}_2^H + \mathbf{I})^{-1} \mathbf{H}_2 \mathbf{H}_1$ according to Eq. (26). We show in Fig. 24 and 25 the eigenvalue distribution of analytical approach and Monte-Carlo simulation, respectively. Gauss–Laguerre quadrature method is used in numerical analysis.

The analytical approach and Monte-Carlo simulation coincides perfectly, which proves the validity of our approach.

6.5 Conclusion

A closed form expression for the joint distribution of the eigenvalues of the equivalent channel matrix the DSM scheme with AF mode relaying is developed in this dissertation, the main conclusion is presented in Theorem 6 and validated through comparison with simulation. This work could be further employed for the analysis for multi-hop DSM networks as the SER analysis in [59, 80] and capacity analysis in [61, 62, 79].

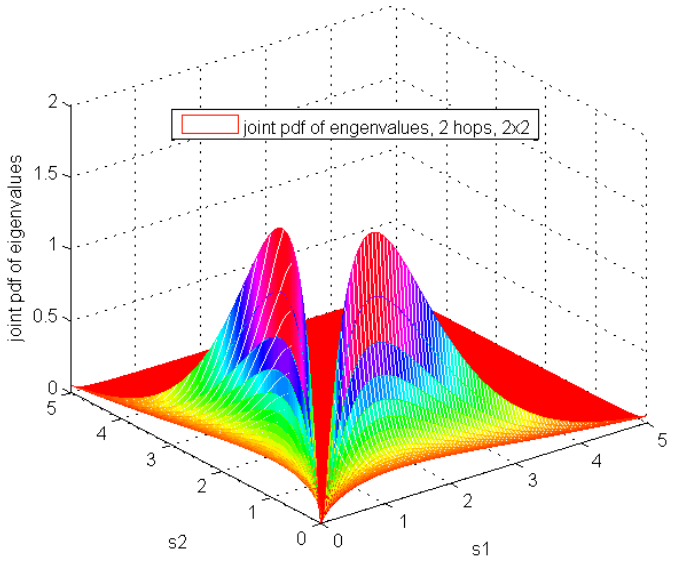

Figure 24 Analytical Result for joint PDF

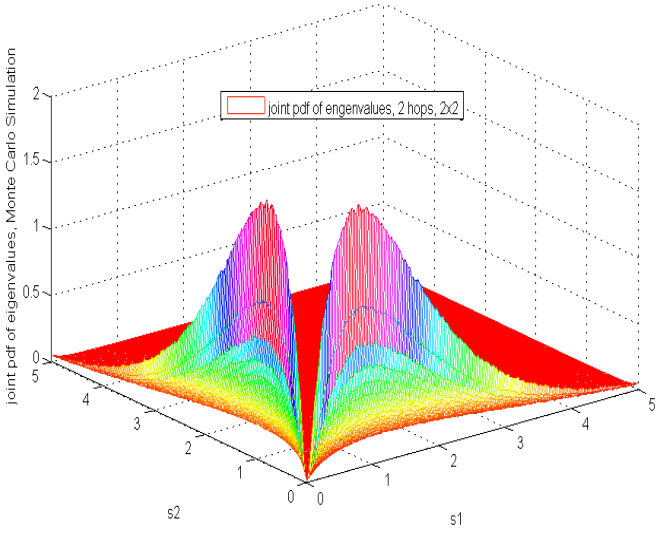

Figure 25 Monte Carlo Simulation for joint PDF

$$\bar{\xi}_{k+1}(z_{k+1}) = \xi_{k+1}(z_{k+1})\xi'_{k+1}(z_{k+1})$$

$$h_{k+1}(\mathbf{z}) = \bar{\xi}_{k+1}(z_{k+1}) \prod_{m=L+1}^{k+2} \tilde{\psi}^{(m-1)}(z_{m-1}, z_m)\bar{\xi}_m(z_m)$$

For $i = 1 \text{ to } r_{L+1},\ j = 1 \text{ to } r_k$ **do**

$$\left[\tilde{\mathbf{\Phi}}_k(\boldsymbol{\sigma}^{(k)})\right]_{i\,j} = \tilde{\phi}_i^{(k)}(\sigma_j^{(k)}) = \int_0^\infty \cdots \int_0^\infty \varphi_i(z_{L+1})\tilde{\psi}^{(k)}(\sigma_j^{(k)}, z_{k+1})h_{k+1}(\mathbf{z})\,dz_{L+1}\cdots dz_{k+1}$$

End for

For $l = L \text{ to } k$ **do**

$$\bar{\xi}_{l+1}(z_{l+1}) = \xi_{l+1}(z_{l+1})\xi'_{l+1}(z_{l+1})$$

$$h_{l+1}(\mathbf{z}) = \bar{\xi}_{l+1}(z_{l+1}) \prod_{m=L+1}^{l+2} \tilde{\psi}^{(m-1)}(z_{m-1}, z_m)\bar{\xi}_m(z_m)$$

For $i = 1 \text{ to } r_{L+1},\ j = 1 \text{ to } (r_{l+1} - r_l)$ **do**

$$[\mathbf{C}_l]_{i\,j} = \int_0^\infty \cdots \int_0^\infty \varphi_i(z_{L+1})\bar{\psi}^{(l)}(j,\ z_{l+1})h_{l+1}(\mathbf{z})\,dz_{L+1}\cdots dz_{l+1}$$

End for

End for

$$\bar{\mathbf{\Phi}}_k(\boldsymbol{\sigma}^{(k)}) = \left[\mathbf{C}_L \quad \cdots \quad \mathbf{C}_{k+1} \quad \mathbf{C}_k \quad \tilde{\mathbf{\Phi}}_k(\boldsymbol{\sigma}^{(k)})\right]$$

$$f_{\boldsymbol{\sigma}^{(k)}}(\boldsymbol{\sigma}^{(k)}) = K_k \left|\mathbf{\Phi}(\boldsymbol{\sigma}^{(k)})\right| \left|\bar{\mathbf{\Phi}}_k(\boldsymbol{\sigma}^{(k)})\right| \prod_{l=1}^{r_k} \xi_k(\sigma_l^{(k)})$$

Figure 26 the closed form expression for the joint PDF $f_{\boldsymbol{\sigma}^{(k)}}(\boldsymbol{\sigma}^{(k)})$

CHAPTER 7. CONCLUSIONS AND SUGGESTED FUTURE WORKS

This dissertation is focused on the design and analysis of novel approaches and issues in physical layer for cooperative communication in wireless multi-hop networks. In Chapter 3, we design a novel randomization based approach to reduce the coordination overhead in cooperative communication; In Chapter 4, we design a novel equalization algorithm in frequency domain for multiple CFOs problem; In Chapter 5, the first rigorous analysis for the diversity orders of linear SC-FDE equalizers is presented; In Chapter 6, for the first time, the closed form expression of the joint PDF of the nonzero eigenvalues of the equivalent matrix of the multi-hop DSM with AF is presented. In the subsections below, we expand on each of these contributions and give some ideas for future work.

7.1 Coordination overhead reduction for Cooperative Diversity

To reduce the coordination overhead in CT or CD, we have designed a novel randomization based approach In Chapter 3. The approach combines random delay and phase dithering. Simulation results, under different channel models, are compared with the results of the state-of-the-art practical phase dithering approach. The results show significant SNR gain, or equivalently, that higher data rates can be achieved. The approach is also robust to different channel models and can lower the overhead in channel estimation significantly, while the constant envelope characteristic of the transmitted signal is kept.

In our simulation, perfect channel estimation is assumed, which is impossible in practice. The design of the channel estimation and the training sequences, and the effect of channel estimation error to a real system, could be studied under different channel models.

7.2 Equalization for multiple CFOs

We have designed a novel equalization algorithm in frequency domain in Chapter 4 for multiple CFOs problem of cooperation communication. Using a permutation-based approach that employs the pseudo-banded matrix characterization, a recursive and computationally efficient equalization algorithm is proposed. Simulation results show that large frequency offsets can be compensated with high computational efficiency. This linear MMSE equalization algorithm is ready to be extended for both the virtual MIMO or DSM MIMO scheme and the STBC scheme, for both OFDM and SC-FDE.

In our simulation, perfect CFOs estimation and channel estimation is assumed, which is impossible in practice. The design of the training sequences for CFOs estimation, and the effect of estimation error could be studied. A tracking mechanism similar to [100] could be developed.

7.3 Diversity of linear SC-FDE

A new set-based bounding approach is presented in Chapter 5 to analyze diversity for SC-FDE over ISI channels, including linear equalizers such as ZF and MMSE. The diversity order of both the error probability and the outage diversity gain are analyzed. We have relaxed the constraint on the channel to be a more practical channel with just

independent paths. This is the first time a rigorous analysis about the diversity of linear SC-FDE is presented. The result is ready to be used for further analysis about the diversity of MIMO SC-FDE or STBC SC-FDE system.

7.4 The joint PDF of the nonzero eigenvalues of DSM with AF

We present a novel approach the first time to get the closed form expression for the joint PDF of the non-zero eigenvalues of the equivalent cascaded MIMO channel of the multi-hop AF relay network. The closed form expression has the form of a product of determinants of matrices, while the entries of these matrices are expressed as multi-dimensional integrals, where the maximum integration dimension is the number of relay clusters (the number of hops minus one). With this closed form expression, the joint PDF can be evaluated by computationally efficient numerical methods. The contribution can be further employed to analyze the performance of the multi-hop virtue MIMO network as the SER analysis and capacity analysis as in [59, 61, 62, 79, 80] for point-to-point MIMO system.

APPENDIX A. DIVERSITY ORDER ANALYSIS OF SC-FDE

A.1 Counter-example

We first describe our counterexample and then show how it applies to [69]. Then we show how these results might be confused with the relationship between convergence almost surely and convergence in distribution.

Let $f(\boldsymbol{\beta}, \rho) = 1/(\beta_1 \rho)$ and $g(\boldsymbol{\beta}, \rho) = 1/[(\beta_1 + \beta_2)\rho]$, where β_1 and β_2 are i.i.d. exponential random variables with pdf $p(x) = e^{-x}$ for $x > 0$. Observe that $\lim_{\rho\to\infty} f(\boldsymbol{\alpha}, \rho) = \lim_{\rho\to\infty} g(\boldsymbol{\alpha}, \rho) = 0$ almost surely. We now show that $f(\boldsymbol{\beta}, \rho) \doteq g(\boldsymbol{\beta}, \rho)$. Here the definition *exponential equality* [69, 78], denoted $f(\rho) \doteq g(\rho)$, is defined by $\lim_{\rho\to\infty} \frac{\log f(\rho)}{\log \rho} = \lim_{\rho\to\infty} \frac{\log g(\rho)}{\log \rho}$; if the expression involves random variables, the limits will be taken almost surely (with probability 1). We have

$$\lim_{\rho\to\infty} \frac{\log f(\boldsymbol{\beta}, \rho)}{\log \rho} = \lim_{\rho\to\infty} \frac{-[\log \beta_1 + \log \rho]}{\log \rho} = -1,$$

$$\lim_{\rho\to\infty} \frac{\log g(\boldsymbol{\beta}, \rho)}{\log \rho} = \lim_{\rho\to\infty} \frac{-[\log(\beta_1 + \beta_2) + \log \rho]}{\log \rho} = -1.$$

Therefore, by the definition of *exponential equality*, because

$$\lim_{\rho\to\infty}\frac{\log f(\boldsymbol{\beta},\rho)}{\log\rho}=\lim_{\rho\to\infty}\frac{\log g(\boldsymbol{\beta},\rho)}{\log\rho},\tag{20}$$

we may write $f(\boldsymbol{\beta},\rho)\doteq g(\boldsymbol{\beta},\rho)$.

Next we show that $f(\boldsymbol{\beta},\rho)\doteq g(\boldsymbol{\beta},\rho)$ does not imply $P(f(\boldsymbol{\beta},\rho)>c)\doteq P(g(\boldsymbol{\beta},\rho)>c)$ for any positive constant c. First consider a probability involving $f(\boldsymbol{\beta},\rho)$:

$$P(f(\boldsymbol{\beta},\rho)>c)=P(\frac{1}{\beta_1\rho}>c)=P(\beta_1<\frac{c}{\rho})=1-e^{-c/\rho}.$$

And we get

$$\lim_{\rho\to\infty}\frac{\log P(f(\boldsymbol{\beta},\rho)>c)}{\log\rho}=\lim_{\rho\to\infty}\frac{\log(1-e^{-c/\rho})}{\log\rho}=\lim_{\rho\to\infty}\frac{\log\left[1-\left(1-\frac{c}{\rho}+\frac{c^2}{2!\rho^2}+\cdots\right)\right]}{\log\rho}=-1.$$

We get the second equality by expansion of Taylor series. Next, consider the similar probability involving $g(\boldsymbol{\beta},\rho)$:

$$P(g(\boldsymbol{\beta},\rho)>c)=P(\frac{1}{(\beta_1+\beta_2)\rho}>c)=P(\beta_1+\beta_2<\frac{c}{\rho})=1-e^{-c/\rho}\left(1+\frac{c}{\rho}\right).$$

Note that $\beta_1+\beta_2$ is a χ^2 random variable with 4 degrees of freedom, and we get the last equality from [7, eq. (2.3-24)]. Again, using the Taylor expansion, we have

$$\lim_{\rho\to\infty}\frac{\log P\left(g(\boldsymbol{\beta},\rho)>c\right)}{\log\rho}=\lim_{\rho\to\infty}\frac{\log\left[1-e^{-c/\rho}\left(1+\frac{c}{\rho}\right)\right]}{\log\rho}$$
$$=\lim_{\rho\to\infty}\frac{\log\left[1-\left(1-\frac{c}{\rho}+\frac{c^2}{2!\rho^2}+\cdots\right)\left(1+\frac{c}{\rho}\right)\right]}{\log\rho}=-2 .$$

So $P(f(\boldsymbol{\beta},\rho)>c)\doteq P(g(\boldsymbol{\beta},\rho)>c)$ doesn't hold, and we see by this example that $f(\boldsymbol{\beta},\rho)\doteq g(\boldsymbol{\beta},\rho)$ does not necessarily imply $P(f(\boldsymbol{\beta},\rho)>c)\doteq P(g(\boldsymbol{\beta},\rho)>c)$.

Next, we show how the above example relates to the proof in [69, Lemma 1]. We note that the conclusion in [69, Lemma 1] is correct, but the method of proof is flawed. In [69], the functions $f(\boldsymbol{\beta},\rho)$ and $g(\boldsymbol{\beta},\rho)$ are different than our example. In [69, eq. (17)], their random variable λ_k is complex Gaussian, so we can write $f(\boldsymbol{\beta},\rho)=\sum_{k=1}^{n}\frac{1}{1+\rho\beta_k}$, where $\beta_k=|\lambda_k|^2$; and $g(\boldsymbol{\beta},\rho)=M(\boldsymbol{\alpha})+\max_{\{\alpha_k:\alpha_k<1\}}\rho^{\alpha_k-1}$, where $\boldsymbol{\alpha}$ is a function of $\boldsymbol{\beta}$. In going from [69, eq. (17)] to "$P\left[\sum_{k=1}^{n}\frac{1}{1+\rho|\lambda_k|^2}>m\right]\doteq P\left[M(\boldsymbol{\alpha})+\max_{\{\alpha_k:\alpha_k<1\}}\rho^{\alpha_k-1}>m\right]\doteq\cdots$", i.e., the expression following [69, eq. (18)], the authors simply assume $f(\boldsymbol{\beta},\rho)\doteq g(\boldsymbol{\beta},\rho)$ implies $P(f(\boldsymbol{\beta},\rho)>m)\doteq P(g(\boldsymbol{\beta},\rho)>m)$ for a positive real constant m, and explained this as "the first (asymptotic) equality follows from exchange of limit and probability due to continuity of functions…" in [69, p. 1025]. However, as we have shown, that implication is not true in general and requires proof for their particular f and g. In fact, the method of this dissertation can be used to prove their conclusion is correct.

Now we show how these results might be confused with the relationship between convergence almost surely and convergence in distribution.

First recall that almost sure convergence for a random sequence $\{X_n\}$, $P\left(\lim_{n\to\infty} X_n = X\right) = 1$, implies convergence in distribution [96], $\lim_{n\to\infty} P(X_n < c) = P(X < c)$. We may restate this in a slightly modified version for our functions $f(\boldsymbol{\beta}, \rho)$ and $g(\boldsymbol{\beta}, \rho)$, and after a discretization procedure, we will get $f(\boldsymbol{\beta}, \rho) \doteq g(\boldsymbol{\beta}, \rho)$ or eq. (20) implies $\lim_{\rho\to\infty} P\left(\frac{\log f(\boldsymbol{\beta}, \rho)}{\log \rho} > c\right) = \lim_{\rho\to\infty} P\left(\frac{\log g(\boldsymbol{\beta}, \rho)}{\log \rho} > c\right)$. We observe that the last equality is not the same as $P(f(\boldsymbol{\beta}, \rho) > c) \doteq P(g(\boldsymbol{\beta}, \rho) > c)$, which is denoted as $\lim_{\rho\to\infty} \frac{\log P(f(\boldsymbol{\beta}, \rho) > c)}{\log \rho} = \lim_{\rho\to\infty} \frac{\log P(g(\boldsymbol{\beta}, \rho) > c)}{\log \rho}$. In other words, there is a difference in the relative position of probability and log functions.

We can also show with a counter example that $\lim_{\rho\to\infty} \frac{f(\boldsymbol{\beta}, \rho)}{g(\boldsymbol{\beta}, \rho)} = 1$ does not imply $P(f(\boldsymbol{\beta}, \rho) > c) \doteq P(g(\boldsymbol{\beta}, \rho) > c)$, but ignore the details here for brevity.

A.2 Proof of Lemma 9

First we consider the case where $m \geq \nu + 1$. We choose $\boldsymbol{\lambda}'$ to be a $(\nu+1)\times 1$ sub-vector of $\tilde{\boldsymbol{\lambda}}$, and we also define $\gamma_i' = \overline{\gamma}\left|\lambda_i'\right|^2$. So $\boldsymbol{\lambda}'$ is also a sub-vector of $\boldsymbol{\lambda}$, and $\boldsymbol{\lambda}' = \mathbf{F}'\mathbf{h}$, where $\mathbf{F}'$ is a $(\nu+1)\times(\nu+1)$ submatrix of $\mathbf{F}$. With the result from [97, Lemma 2], $\mathbf{F}$ is full spark,

i.e., every $(\nu+1)\times(\nu+1)$ submatrix of $\mathbf{F}$ is invertible, the existence of the inverse of $\mathbf{F}^{'}$ is guaranteed. So $\mathbf{h}=(\mathbf{F}^{'})^{-1}\boldsymbol{\lambda}^{'}$; note that the $h_i{}'s$ are independent. If for $\nu+1\geq i\geq 1$, $\gamma_i^{'}\leq t$, then we have $\left|\lambda_i^{'}\right|\leq\sqrt{t/\bar{\gamma}}$ and $|h_i|^2\leq\tilde{t}/\bar{\gamma}$ for some positive real $\tilde{t}$, and

$$P\left(\tilde{\gamma}_i\leq t \text{ for } m\geq i\geq 1\right)\leq P\left(\gamma_i^{'}\leq t \text{ for } \nu+1\geq i\geq 1\right)\leq P\left(|h_i|^2\leq\tilde{t}/\bar{\gamma} \text{ for } \nu+1\geq i\geq 1\right)\doteq\bar{\gamma}^{-(\nu+1)}$$

,

where the last exponential equality follows from Prop. 4. It is also easy to find that if all $|h_i|^2\leq\hat{t}/\bar{\gamma}$ for some positive real $\hat{t}$, then $\tilde{\gamma}_i\leq t$ for $m\geq i\geq 1$, so

$$P\left(\tilde{\gamma}_i\leq t \text{ for } m\geq i\geq 1\right)\geq P\left(|h_i|^2\leq\hat{t}/\bar{\gamma} \text{ for } \nu+1\geq i\geq 1\right)\doteq\bar{\gamma}^{-(\nu+1)}.$$

We conclude $P\left(\tilde{\gamma}_i\leq t \text{ for } m\geq i\geq 1\right)\doteq\bar{\gamma}^{-(\nu+1)}$ if $m\geq\nu+1$.

Next we consider the case where $m<(\nu+1)$. Let $\mathbf{h}=\mathbf{D}^{-1/2}\bar{\mathbf{h}}$ where $\mathbf{D}^{-1/2}\mathbf{D}^{-1/2}=\mathbf{D}$, so $\mathbf{D}^{-1/2}$ is a diagonal matrix with non-zero diagonal elements, and $\bar{\mathbf{h}}$ is a vector with its elements i.i.d. complex Gaussian. We have $\tilde{\boldsymbol{\lambda}}=\tilde{\mathbf{F}}\mathbf{h}=\tilde{\mathbf{F}}\mathbf{D}^{-1/2}\bar{\mathbf{h}}$, where $\tilde{\mathbf{F}}$ is a submatrix of $\mathbf{F}$, and $\tilde{\mathbf{F}}$ can be proved to be full rank as following: we choose $\boldsymbol{\lambda}^{'}$ which is a $(\nu+1)\times 1$ sub-vector of $\boldsymbol{\lambda}$ such that $\tilde{\boldsymbol{\lambda}}$ is a sub-vector of $\boldsymbol{\lambda}^{'}$, and $\boldsymbol{\lambda}^{'}=\mathbf{F}^{'}\mathbf{h}$. As proved in last case, $\mathbf{F}^{'}$ is invertible, note that $\tilde{\mathbf{F}}$ is made from some rows of $\mathbf{F}^{'}$, so $\tilde{\mathbf{F}}$ is full rank. Next, it is easy to prove that $\bar{\mathbf{F}}=\tilde{\mathbf{F}}\mathbf{D}^{-1/2}$ is full rank, and we have $\bar{\mathbf{F}}=\mathbf{U}\boldsymbol{\Sigma}\mathbf{V}$ by singular value decomposition (SVD). Then $\tilde{\boldsymbol{\lambda}}=\bar{\mathbf{F}}\bar{\mathbf{h}}=\mathbf{U}\boldsymbol{\Sigma}\mathbf{V}\bar{\mathbf{h}}=\mathbf{U}\tilde{\boldsymbol{\Sigma}}\tilde{\mathbf{h}}$, where $\tilde{\boldsymbol{\Sigma}}$ is the submatrix of $\boldsymbol{\Sigma}$ in

the left corner, $\tilde{\mathbf{\Sigma}}$ is $m \times m$ diagonal matrix with nonzero diagonal elements, $\mathbf{U}$ and $\mathbf{V}$ are unitary matrix, $\mathbf{\Sigma} = \left[\tilde{\mathbf{\Sigma}}\ \mathbf{0}\right]$ and $\mathbf{V}\bar{\mathbf{h}} = \left[\tilde{\mathbf{h}}^t, \hat{\mathbf{h}}^t\right]^T$, where $\tilde{\mathbf{h}}$ is a $m \times 1$ vector. Note that the $\tilde{h}_i$'s are i.i.d. complex Gaussian because $\mathbf{V}$ is unitary and $\bar{h}_i$'s are i.i.d. complex Gaussian. From the above we have $\tilde{\mathbf{h}} = (\tilde{\mathbf{\Sigma}})^{-1}\mathbf{U}^H\tilde{\boldsymbol{\lambda}} = \mathbf{A}\tilde{\boldsymbol{\lambda}}$ and $\tilde{\boldsymbol{\lambda}} = \mathbf{A}^{-1}\tilde{\mathbf{h}}$, where $\mathbf{A} = (\tilde{\mathbf{\Sigma}})^{-1}\mathbf{U}^H$. From $\tilde{\gamma}_i \le t$ for $m \ge i \ge 1$, we get $\left|\tilde{h}_i\right|^2 \le t_3/\bar{\gamma}$ for a positive real t_3 for $m \ge i \ge 1$, so

$$P\left(\tilde{\gamma}_i \le t \text{ for } m \ge i \ge 1\right) \le P\left(\left|\tilde{h}_i\right|^2 \le t_3/\bar{\gamma} \text{ for } m \ge i \ge 1\right) \doteq \bar{\gamma}^{-m}.$$

It is also easy to find that if all $\left|\tilde{h}_i\right|^2 \le t_4/\bar{\gamma}$ for some positive real t_4, then $\tilde{\gamma}_i \le t$ for $m \ge i \ge 1$, so

$$P\left(\tilde{\gamma}_i \le t \text{ for } m \ge i \ge 1\right) \ge P\left(\left|\tilde{h}_i\right|^2 \le t_4/\bar{\gamma} \text{ for } m \ge i \ge 1\right) \doteq \bar{\gamma}^{-m}.$$

We have $P\left(\tilde{\gamma}_i \le t \text{ for } m \ge i \ge 1\right) \doteq \bar{\gamma}^{-m}$ if $m < \nu + 1$.

Finally, we conclude $P\left(\tilde{\gamma}_i \le t \text{ for } m \ge i \ge 1\right) \doteq \bar{\gamma}^{-m}$. □

A.3 Proof of Lemma 16

For the non-outage event, we have $\sum_{\substack{i=1 \\ i\neq j}}^{n}\frac{1}{1+\gamma_i} < \delta - \frac{1}{1+\gamma_j} = \delta - 1 + \frac{\gamma_j}{1+\gamma_j}$. Let $S=\{1,2,\cdots,n\}$, $K=\left\{1,2,\cdots,\binom{n-1}{n-\delta}\right\}$, and the set $S_{j,k}\subset S_j = S\setminus\{j\}$ with cardinality $|S_{j,k}| = n-\delta$, where $j\in S$ and $k\in K$. Let $a=n-\delta-1$, $b=n-\delta$ and $\tau_j = a+b/\gamma_j$. If $\gamma_i > \tau_j$ for every $i\in S_{j,k}$, we have

$$\sum_{\substack{i=1 \\ i\neq j}}^{n}\frac{1}{1+\gamma_i} < \delta - \frac{1}{1+\gamma_j} \text{ or } \sum_{i=1}^{n}\frac{1}{1+\gamma_i} < \delta .$$

Non-outage probability is $\mathrm{P}(\sum_{i=1}^{n}\frac{1}{1+\gamma_i} < \delta) \geq \mathrm{P}(\bigcup_{j=1}^{n}(\bigcup_{k=1}^{|K|}U_{j,k}^{'}))$, so we get the outage probability as

$$\mathrm{P}(\sum_{i=1}^{n}\frac{1}{1+\gamma_i} > \delta) \leq 1-\Pr(\bigcup_{j\in S,\,k\in K}U_{j,k}^{'}) = \Pr(\overline{\bigcup_{j\in S,\,k\in K}U_{j,k}^{'}}) = \Pr(\bigcap_{j\in S,\,k\in K}\bar{U}_{j,k}^{'}),$$

where $U_{j,k}^{'} = \{U : \gamma_i > \tau_j \text{ for every } i\in S_{j,k}\}$, and we have $U_{j,k}^{'} = \bigcap_{i_{j,k}\in S_{j,k}} U_{j,i_{j,k}}$ and $\bar{U}_{j,k}^{'} = \bigcup_{i_{j,k}\in S_{j,k}} \bar{U}_{j,i_{j,k}}$, where $U_{j,i_{j,k}} = \{U : \gamma_{i_{j,k}} > \tau_j,\, i_{j,k}\in S_{j,k}\}$. So we get

$$\bigcap_{j\in S,\,k\in K}\bar{U}_{j,k}^{'} = \bigcap_{j\in S,\,k\in K}(\bigcup_{i_{j,k}\in S_{j,k}}\bar{U}_{j,i_{j,k}}) = \bigcup_{\mathbf{i}\in\mathfrak{I}}(\bigcap_{j\in S,\,k\in K}\bar{U}_{j,i_{j,k}}),$$

$$\mathrm{P}(\sum_{i=1}^{n}1/(1+\gamma_i) > \delta) \leq \Pr(\bigcap_{j\in S,\,k\in K}\bar{U}_{j,k}^{'}) \leq \sum_{\mathbf{i}\in\mathfrak{I}}\Pr(\bigcap_{j\in S,\,k\in K}\bar{U}_{j,i_{j,k}}),$$

where $\mathbf{i}=(i_{1,1},i_{1,2},\cdots,i_{1,|K|},i_{2,1},i_{2,2},\cdots,i_{2,|K|},\cdots,i_{n,1},i_{n,2},\cdots,i_{n,|K|})$, $i_{j,k}\in S_{j,k}$, and $\Im$ is the set composed of all possible $\mathbf{i}$, its cardinality $|\Im|=(n-\delta)^{n|K|}$.

Note the fact that $\bar{U}_{j,i_{j,k}}=\{U:\gamma_{i_{j,k}}<\tau_j\}\subseteq\{U:\gamma_{i_{j,k}}<t_5\}\cup\{U:t_5<\gamma_{i_{j,k}}<\tau_j,\gamma_j<t_5\}$ for $i_{j,k}\in S_{j,k}$; here t_5 is a positive constant, such that if $\gamma_j>t_5$, then $\gamma_{i_{j,k}}<t_5$.

We call $\gamma_{i_{j,k}}<t_5$ the Type I constraint, and define $\bar{U}^{I}_{j,i_{j,k}}=\{U:\gamma_{i_{j,k}}<t_5\}$. We call $t_5<\gamma_{i_{j,k}}<\tau_j$ when $\gamma_j<t_5$ the Type II constraint, and define $\bar{U}^{II}_{j,i_{j,k}}=\{U:t_5<\gamma_{i_{j,k}}<\tau_j,\quad\gamma_j<t_5\}$. So $\bigcap_{j\in S,\,k\in K}\bar{U}'_{j,k}\subseteq\bigcup_{\substack{\mathbf{i}\in\Im\\ \mathbf{\iota}\in\mathfrak{L}}}(\bigcap_{j,k}\bar{U}^{l_{j,k}}_{j,i_{j,k}})$, where $l_{j,k}\in\{\text{I},\ \text{II}\}$, $\mathbf{\iota}$ is the vector whose elements are $l_{j,k}$ with all possible j and k, and $\mathfrak{L}$ is the set composed of all possible $\mathbf{\iota}$.

If $\mathbf{\iota}=\mathbf{I}$, i.e., the all I vector, then $U_E=\bigcup_{\mathbf{i}\in\Im,\,\mathbf{\iota}=\mathbf{I}}(\bigcap_{j\in S,\,k\in K}\bar{U}^{l_{j,k}}_{j,i_{j,k}})$ has the same form as the case where $\delta\notin\mathbb{Z}$, we have $\min_{\mathbf{i}\in\Im,\,\mathbf{\iota}=\mathbf{I}} order(\bigcap_{j\in S,\,k\in K}\bar{U}^{l_{j,k}}_{j,i_{j,k}})=\delta+1$ and $\Pr(U_E)\doteq\bar{\gamma}^{-(\delta+1)}$ with a discussion similar to *Lemmas 11* and *12*. With these facts, we only need to focus our study on the case where $\mathbf{\iota}\neq\mathbf{I}$, i.e., there is at least one Type II constraint involved in our analysis. W. l. o. g., we assume the specific term involved is $\bar{U}^{II}_{j,i_{j,k}}$ where $(j,k)=(n,|K|)$ and $i_{j,k}=i_{n,|K|}=1$, i.e., $\bar{U}^{II}_{n,1}$. Next, we will prove for this case the diversity order is lower bounded by $\delta+1$. We have

$$\bigcap_{j\in S,k\in K}\bar{U}'_{j,k}=\bigcap_{j\in S,k\in K}(\bigcup_{i_{j,k}\in S_{j,k}}\bar{U}_{j,i_{j,k}})=(\bigcap_{\substack{j\in S,k\in K\\(j,k)\neq(n,|K|)}}(\bigcup_{i_{j,k}\in S_{j,k}}\bar{U}_{j,i_{j,k}}))\cap(\bigcup_{\substack{(j,k)=(n,|K|)\\i_{j,k}\in S_{j,k}}}\bar{U}_{j,i_{j,k}})$$

$$=(\bigcap_{\substack{j\in S,k\in K\\(j,k)\neq(n,|K|)}}(\bigcup_{i_{j,k}\in S_{j,k}}\bar{U}_{j,i_{j,k}}))\cap((\bigcup_{i_{n,|K|}\in S_{n,|K|}\setminus\{1\}}\bar{U}_{n,i_{n,|K|}})\cup\bar{U}_{n,1})$$

$$\subseteq U_O\cap((\bigcup_{i_{n,|K|}\in S_{n,|K|}\setminus\{1\}}(\bar{U}^I_{i_n,|K|}\cup\bar{U}^{II}_{i_n,|K|}))\cup\bar{U}^I_{n,1}\cup\bar{U}^{II}_{n,1})$$

$$=\bigcup_{\substack{\mathbf{i}\in\mathfrak{I}\\\mathbf{l}\in\mathfrak{L}}}(\bigcap_{j\in S,k\in K}\bar{U}^{l_{j,k}}_{j,i_{j,k}})=U_A\cup U_B\cup U_C$$

,

where we define as

$$U_O=\bigcap_{\substack{j\in S,k\in K\\(j,k)\neq(n,|K|)}}(\bigcup_{i_{j,k}\in S_{j,k}}(\bar{U}^I_{j,i_{j,k}}\cup\bar{U}^{II}_{j,i_{j,k}})),$$

$$U_A=U_O\cap(\bigcup_{i_{n,|K|}\in S_{n,|K|}\setminus\{1\}}(\bar{U}^I_{i_n,|K|}\cup\bar{U}^{II}_{i_n,|K|})),$$

$U_B=U_O\cap\bar{U}^I_{n,1}$, and $U_C=U_O\cap\bar{U}^{II}_{n,1}$.

As already cited, we only need to analyze U_C, where the specific Type II constraint term $\bar{U}^{II}_{n,1}$ is involved. Note that $\bar{U}^I_{j,i_{j,k}}=\bar{U}_{i_{j,k}}$ and $\bar{U}^{II}_{j,i_{j,k}}\subset\{U:\gamma_j<t_5\}=\bar{U}_j$. Using the fact $\bar{U}_{j,i_{j,k}}\subseteq\bar{U}^I_{j,i_{j,k}}\cup\bar{U}^{II}_{j,i_{j,k}}\subseteq\bar{U}_{i_{j,k}}\cup\bar{U}_j$, it is easy to find that $U_O\subseteq U_D$, where

$$U_D=\bigcap_{\substack{j\in S,k\in K\\(j,k)\neq(n,|K|)}}(\bigcup_{i_{j,k}\in S_{j,k}}(\bar{U}_{i_{j,k}}\cup\bar{U}_j))=\bigcap_{k\in K'}(\bigcup_{i_k\in\tilde{S}_k}\bar{U}_{i_k})=\bigcup_{\mathbf{i}'\in\mathfrak{I}'}(\bigcap_{k\in K'}\bar{U}_{i_k}),$$

the set $K^{'}=\left\{1,2,\cdots,\binom{n}{n-\delta+1}\right\}$, $\tilde{S}_k \subset S$ with cardinality $\left|\tilde{S}_k\right|=n-\delta+1$, and $\mathbf{i}^{'}=(i_1,i_2,\cdots,i_{\left|K^{'}\right|})$ where $i_k \in \tilde{S}_k$ for every $k \in K^{'}$, and $\Im^{'}$ is the set composed of all possible $\mathbf{i}^{'}$. Note the second equality in the above equation can be easily found by enumeration. From $U_C = U_O \cap \bar{U}_{n,1}^{II}$, we get $U_C \subseteq U_D \cap \bar{U}_{n,1}^{II}$.

Next we prove $U_D \cap \bar{U}_{n,1}^{II}$ has diversity $\delta+1$. For a specific $\mathbf{i}^{'}$, let $U_E\left(\mathbf{i}^{'}\right)=(\bigcap_{k\in K^{'}}\bar{U}_{i_k})\cap\bar{U}_{n,1}^{II}$. Note $U_E\left(\mathbf{i}^{'}\right)=\varnothing$ if any $i_k=1$; we also note that for all possible$\bigcap_{k\in K^{'}}\bar{U}_{i_k}$, the minimum order is δ , which can be proved in the same manner as in the former case where $\delta \notin \mathbb{Z}$, i.e., Lemma 12. So for $U_E\left(\mathbf{i}^{'}\right)\neq\varnothing$, the $\bigcap_{k\in K^{'}}\bar{U}_{i_k}$ which has the minimum order δ should has the form $\bigcap_{k\in K^{'}}\bar{U}_{i_k}=\bigcap_{q=1}^{\delta}\bar{U}_{p_q}$, where $\{p_1, p_2, \cdots, p_\delta\} \subset \{1, 2, \cdots, \mathrm{n}\}/\{1\}$ and $p_i \neq p_j$ if $i \neq j$, we also have $\mathrm{n} \in \{p_1, p_2, \cdots, p_\delta\}$ for $P\left(U_E\left(\mathbf{i}^{'}\right)\right)$ to be of minimum diversity. For the specific $\mathbf{i}^{'}$ such that $\bigcap_{k\in K^{'}}\bar{U}_{i_k}$ is of minimum order δ , w.l.o.g., we can assume the specific set $U_E\left(\mathbf{i}^{'}\right)=\left\{U: t_5<\gamma_1<\tau_n,\quad \gamma_j<t_5 \text{ for } \mathrm{n}\geq j\geq n-\delta+1\right\}$. The diversity of this set's probability is lower bounded by $d_{out}^{LB}=\delta+1$ using Lemma 15. The probability of the set $U_D \cap \bar{U}_{n,1}^{II}$ also has diversity low bounded by $\delta+1$ because it is dominated by the sets $(\bigcap_{k\in K^{'}}\bar{U}_{i_k})\cap\bar{U}_{n,1}^{II}$ which are of the minimum order.

We conclude $d_{out}^{MMSE} \geq d_{out}^{LB} = \delta + 1$ if $\delta < \nu + 1$. □

APPENDIX B. JOINT PDF OF NONZERO EIGENVULUES

B.1 Proof of Theorem 5

Proof: let $\sigma = \sigma_1, \sigma_2, \cdots, \sigma_N$ be a permutation of the arrangement 1 2 $\cdots$ N, and sgn(σ) denotes the sign or signature of the permutation.

Let $\pi = \pi_1, \pi_2, \cdots, \pi_M$ be a permutation of the arrangement 1 2 $\cdots$ M, and sgn(π) denotes the sign of the permutation. Let $\mu = \mu_1, \mu_2, \cdots, \mu_N$ to be a partial permutation of the arrangement 1 2 $\cdots$ N, and sgn(μ) denotes the sign of the permutation. Let $\mu_k = k$ for $1 \le k \le K$ and $\mu_{k+K} = K + \pi_k$ for $1 \le k \le M$. Because the correspondence between π and μ, we denote μ as μ^π. Then $\text{sgn}(\mu^\pi) = \text{sgn}(\pi)$.

Define $\tilde{\beta}_{k+K}(\cdot) = \beta_k(\cdot)$ for $1 \le k \le M$. Then $\tilde{\beta}_{\mu_k^\pi}(\cdot) = \beta_{\pi_{k-K}}(\cdot)$ for $K+1 \le k \le N$.

From [86, Eq. 37], we have

$$\begin{aligned} |\mathbf{A}(\mathbf{x})| &= \sum_\sigma \text{sgn}(\sigma) \prod_{k=1}^{N} \alpha_{\sigma_k, k} = \sum_\sigma \text{sgn}(\sigma) \left(\prod_{k=1}^{K} C_{\sigma_k, k} \right) \left(\prod_{k=K+1}^{N} \alpha_{\sigma_k, k} \right) \\ &= \sum_\sigma \text{sgn}(\sigma) \left(\prod_{k=1}^{K} C_{\sigma_k, k} \right) \left(\prod_{k=K+1}^{N} \tilde{\alpha}_{\sigma_k}(x_{k-K}) \right) \end{aligned},$$

and

$$|\mathbf{B}(\mathbf{x})| = \sum_\pi \text{sgn}(\pi) \prod_{k=1}^{M} \beta_{\pi_k, k} = \sum_\pi \text{sgn}(\pi) \prod_{k=1}^{M} \beta_{\pi_k}(x_k) = \sum_\pi \text{sgn}(\mu^\pi) \prod_{k=K+1}^{N} \tilde{\beta}_{\mu_k^\pi}(x_{k-K}), \text{ then}$$

$$
\begin{aligned}
D &= \int\cdots\int_{\mathcal{D}} |\mathbf{A}(\mathbf{x})||\mathbf{B}(\mathbf{x})| \prod_{l=1}^{M} \xi(x_l) d\mathbf{x} \\
&= \int\cdots\int_{\mathcal{D}} \sum_{\sigma} \operatorname{sgn}(\sigma) \left(\prod_{k=1}^{K} C_{\sigma_k, k} \right) \left(\prod_{k=K+1}^{N} \tilde{\alpha}_{\sigma_k}(x_{k-K}) \right) \cdot \left(\sum_{\pi} \operatorname{sgn}(\mu^{\pi}) \prod_{k=K+1}^{N} \tilde{\beta}_{\mu_k^{\pi}}(x_{k-K}) \right) \prod_{l=1}^{M} \xi(x_l) d\mathbf{x} \\
&= \sum_{\pi} \operatorname{sgn}(\mu^{\pi}) \sum_{\sigma} \operatorname{sgn}(\sigma) \left(\prod_{k=1}^{K} C_{\sigma_k, \mu_k^{\pi}} \right) \left(\prod_{k=K+1}^{N} \int_a^b \tilde{\alpha}_{\sigma_k}(x_{k-K}) \tilde{\beta}_{\mu_k^{\pi}}(x_{k-K}) \xi(x_{k-K}) dx_{k-K} \right) \\
&= \sum_{\pi} \operatorname{sgn}(\mu^{\pi}) \sum_{\sigma} \operatorname{sgn}(\sigma) \left(\prod_{k=1}^{K} C_{\sigma_k, \mu_k^{\pi}} \right) \left(\prod_{k=K+1}^{N} \int_a^b \tilde{\alpha}_{\sigma_k}(x) \tilde{\beta}_{\mu_k^{\pi}}(x) \xi(x) dx \right) \\
&= M! |\boldsymbol{\Theta}| = M! \operatorname{sgn}(\mu^{\pi}) \sum_{\sigma} \operatorname{sgn}(\sigma) \prod_{k=1}^{N} \theta_{\sigma_k, \mu_k^{\pi}}
\end{aligned}
$$

We get the last equality from [86, Eq. 38], and $M!$ is the number of all possible permutation π.

Here we have $[\boldsymbol{\Theta}]_{ij} = \theta_{ij} = \begin{cases} C_{ij} & \text{for } 1 \le j \le K \\ \int_a^b \tilde{\phi}_i(x) \tilde{\psi}_j(x) \xi(x) dx & \text{for } K+1 \le j \le N \end{cases}$, so we have the form $\boldsymbol{\Theta} = \begin{bmatrix} \mathbf{C} & \tilde{\boldsymbol{\Theta}} \end{bmatrix}$ where $\left[\tilde{\boldsymbol{\Theta}}\right]_{ij} = \int_a^b \tilde{\alpha}_i(x) \beta_j(x) \xi(x) dx$.

It is obvious that [86, Corollary 1] is a special case of Theorem 1 when $N = M$. □

REFERENCES

[1] Van Der Meulen, Edward C. "Three-terminal communication channels." Advances in applied Probability (1971): 120-154.

[2] Cover, Thomas, and A. EL Gamal. "Capacity theorems for the relay channel." IEEE Transactions on Information Theory 25.5 (1979): 572-584.

[3] Ford, L. R., & Fulkerson, D. R. (1956). "Maximal flow through a network." Canadian journal of Mathematics, 8(3), 399-404.

[4] A. Sendonaris, E. Erkip, and B. Aazhang, "User cooperation diversity, Part I & II: System description," IEEE Trans. Commun., vol. 51, pp. 1927–1948, Nov. 2003.

[5] J. N. Laneman, D. N. C. Tse, and G. W. Wornell, "Cooperative Diversity in Wireless Networks: Efficient Protocols and Outage Behavior," *IEEE Trans.* Inform. Theory, vol. 50, no. 12, pp. 3062-3080, Dec. 2004.

[6] Hunter, Todd E., and Aria Nosratinia. "Cooperation diversity through coding." Information Theory, 2002. Proceedings. 2002 IEEE International Symposium on. IEEE, 2002.

[7] J. Proakis, M. Salehi, Digital Communications, 5th edition, McGraw Hill 2008.

[8] Kramer, Gerhard, Michael Gastpar, and Piyush Gupta. "Cooperative strategies and capacity theorems for relay networks." IEEE Transactions on Information Theory 51.9 (2005): 3037-3063.

[9] Laneman, J. N. &Wornell, G. W. "Distributed space-time-coded protocols for exploiting cooperative diversity in wireless networks," IEEETrans. On Information Theory, vol. 49, pp. 2415–2425, Feb. 2003

[10] Biglieri, Ezio, Robert Calderbank, Anthony Constantinides, Andrea Goldsmith, Arogyaswami Paulraj, and H. Vincent Poor. MIMO wireless communications. Cambridge university press, 2007.

[11] Mercado, Alejandra, and Babak Azimi-Sadjadi. "Power efficient link for multi-hop wireless networks." PROCEEDINGS OF THE ANNUAL ALLERTON CONFERENCE ON COMMUNICATION CONTROL AND COMPUTING. Vol. 41. No. 3. The University; 1998, 2003.

[12] Cui, Shuguang, Andrea J. Goldsmith, and Ahmad Bahai. "Energy-efficiency of MIMO and cooperative MIMO techniques in sensor networks." IEEE Journal on selected areas in communications 22.6 (2004): 1089-1098.

[13] Del Coso, Aitor, et al. "Virtual MIMO channels in cooperative multi-hop wireless sensor networks." 2006 40th Annual Conference on Information Sciences and Systems. IEEE, 2006.

[14] Jayaweera, Sudharman K. "Virtual MIMO-based cooperative communication for energy-constrained wireless sensor networks." IEEE Transactions on Wireless communications 5.5 (2006): 984-989.

[15] Rankov, Boris, and Armin Wittneben. "Distributed spatial multiplexing in a wireless network." Signals, Systems and Computers, 2004. Conference Record of the Thirty-Eighth Asilomar Conference on. Vol. 2. IEEE, 2004.

[16] Kim, Sang Wu. "Cooperative spatial multiplexing in mobile ad hoc networks." IEEE International Conference on Mobile Adhoc and Sensor Systems Conference, 2005.. IEEE, 2005.

[17] Telatar, Emre. "Capacity of Multi-antenna Gaussian Channels." European transactions on telecommunications 10.6 (1999): 585-595.

[18] Foschini, Gerard J., and Michael J. Gans. "On limits of wireless communications in a fading environment when using multiple antennas."Wireless personal communications 6.3 (1998): 311-335.

[19] Bernhardt, Richard. "Macroscopic diversity in frequency reuse radio systems." IEEE Journal on Selected Areas in Communications 5.5 (1987): 862-870.

[20] Turkmani, A. M. D. "Performance evaluation of a composite microscopic plus macroscopic diversity system." IEE Proceedings I-Communications, Speech and Vision 138.1 (1991): 15-20.

[21] D. Chen, J. N. Laneman, “Noncoherent Demodulation for Cooperative Diversity in Wireless Systems,” *IEEE Globecom* 2004.

[22] T.Himsoon, W.P. Siriwongpairat, W. Su, K.J.Ray Liu, “Differential Modulations for Multinode Cooperative Communications,” *IEEE Trans. Signal Processing*, Vol. 576, No. 7, July 2008.

[23] Giannakis, Georgios B., Zhiqiang Liu, Xiaoli Ma, and Shengli Zhou. Space-time coding for broadband wireless communications. John Wiley & Sons, 2006.

[24] Alamouti, Siavash M. "A simple transmit diversity technique for wireless communications." IEEE Journal on selected areas in communications 16.8 (1998): 1451-1458.

[25] B. Hochwald and T. L. Marzetta, “Unitary space-time modulation for multiple antenna communications in Rayleigh flat fading,” IEEE Trans. on Information Theory, vol. 46, No. 2, Mar., 2000

[26] V. Tarokh, H. Jafarkhani, and A. R. Calderbank, “A differential detection scheme for transmit diversity,” IEEE Journal on Selected Areas in Communications,, Vol. 18, No. 5, July 1999

[27] B. Hochwald and W. Sweldens, “Differential unitary space-time modulation,” IEEE Trans. on Communications, vol. 48, No. 12, Dec., 2000

[28] B. L. Hughes, “Differential space-time modulation,” IEEE Trans. on Information Theory, vol. 46, No. 7, Nov., 2000

[29] Falconer, David, et al. "Frequency domain equalization for single-carrier broadband wireless systems." IEEE Communications Magazine 40.4 (2002): 58-66.

[30] CIMINI JR, LEONARD J., and YE GEOFFREY LI. "Orthogonal frequency division multiplexing for wireless channels." IEEE Global Telecommunications Conference GLOBECOM. 1998.

[31] E. Lindskog, A. Paulraj, “A transmit diversity scheme for channels with intersymbol interference,” IEEE ICC, 2000.

[32] N. Al-Dhahir, “Single-carrier frequency-domain equalization for space-time block-coded transmissions over frequency-selective fading channels,” IEEE Commun. Lett., Vol. 5. No. 7, July 2001.

[33] J. H. Jang, H. C. Won, G. H. Im, “Cyclic prefixed single carrier transmission with SFBC over mobile wireless channels,” IEEE Signal Process. Lett., Vol. 13, No. 5, May 2006.

[34] Liu, Z., et al. "Block precoding and transmit-antenna diversity for decoding and equalization of unknown multipath channels." Proc 33rd Asilomar Conference Signals, Systems and Computers. 1999.

[35] H. Mheidat, M. Uysal, N. Al-Dhahir, “Equalization techniques for distributed space-time block codes with amplify-and-forward relaying, ” IEEE Trans. Signal Process., Vol. 55, No. 5, May 2007.

[36] Jing, Yindi, and Babak Hassibi. "Distributed space-time coding in wireless relay networks." IEEE Transactions on Wireless communications 5.12 (2006): 3524-3536.

[37] Y. Jing, H. Jafarkhani, “Distributed Differential Space-Time Coding for Wireless Relay Networks,” IEEE Trans. Commun., Vol. 56, No. 7, July 2008.

[38] F. Oggier, B. Hassibi, “A Coding Scheme for Wireless Networks with Multiple Antenna Nodes and No Channel Information,” ICASSP 2007.

[39] I. Chatzigeorgiou, W. S. Guo, I. J. Wasell, “Comparison of Cooperative Schemes using Joint Channel Coding and High-order Modulation,” ISCCSP 2008, Malta, 12-14 March 2008.

[40] T. E. Hunter, A. Nosratinia, “Diversity through coded cooperation,” IEEE Trans. Wireless Commun., Vol. 5, Feb. 2006.

[41] A. Scaglione, Y.W. Hong, “Opportunistic large arrays: Cooperative transmission in wireless multihop ad hoc networks to reach far distances,” IEEE Trans. Signal Processing, Vol. 51, No. 8, 2003.

[42] B. Sirkeci-Mergen, A. Scaglione, G. Mergen, “Asymptotic analysis of multistage cooperative broadcast in wireless networks,” IEEE Trans. Info. Theory, Vol. 52, No. 6, Jun. 2003.

[43] Hammerstrom, Ingmar, Marc Kuhn, and Armin Wittneben. "Cooperative diversity by relay phase rotations in block fading environments." Signal Processing Advances in Wireless Communications, 2004 IEEE 5th Workshop on. IEEE, 2004.

[44] D. K. Lee, K. M. Chugg, “Pragmatic cooperative diversity communications,” in Proc. IEEE Military Comm. Conf., Oct. 2006

[45] S. Wei, D. L. Goeckel, M. Valenti, “Asynchronous Cooperative Diversity,” IEEE Trans. Wireless Commun., Vol. 5, No. 6, June 2006.

[46] Mergen, A. Scaglione, “Randomized Space-Time Coding for Distributed Cooperative Communication,” IEEE Trans. Signal Processing, Volume 55, Issue 10, Oct. 2007.

[47] S. Jagannathan, H. Aghajan, A. Goldsmith, “The effect of time synchronization errors on the performance of cooperative MISO,” IEEE Communication Society, Globecom 2004 Workshops.

[48] Y. W. Hong, A. Scaglione, “A Scalable Synchronization Protocol for Large Scale Sensor Networks and Its Applications,” IEEE J. Sel. Areas Commun., May 2005.A.

[49] D. Veronesi, D.L. Goeckel, “Multiple Frequency Offset Compensation in Cooperative Wireless Systems,” IEEE Globecom 2006B.

[50] H. Wang, X.-G. Xia, Q. Yin, “Computationally Efficient Equalization for Asynchronous Cooperative Communications with Multiple Frequency Offsets,” IEEE Trans. Wireless Commun., Vol. 8, No. 2, Feb. 2009.

[51] Yilmaz, “Cooperative Diversity in Carrier Frequency Offset,” IEEE Commun. Letters, Vol. 11, No. 4, April 2007.

[52] X. Li, F. Ng, “Carrier Frequency Offset Mitigation in Asynchronous Cooperative OFDM Transmissions,” IEEE Trans. Signal Processing, Vol. 56, No., 2, Feb. 2008.

[53] Benvenuto, Nevio, Stefano Tomasin, and Daniele Veronesi. "Multiple frequency offsets estimation and compensation for cooperative networks."2007 IEEE Wireless Communications and Networking Conference. IEEE, 2007.

[54] Li, Zheng, Daiming Qu, and Guangxi Zhu. "An equalization technique for distributed STBC-OFDM system with multiple carrier frequency offsets."IEEE Wireless Communications and Networking Conference, 2006. WCNC 2006. Vol. 2. IEEE, 2006.

[55] Ng, Fan, and Xiaohua Li. "Cooperative STBC-OFDM transmissions with imperfect synchronization in time and frequency." Conference Record of the Thirty-Ninth Asilomar Conference on Signals, Systems and Computers, 2005.. IEEE, 2005.

[56] Nguyen, T-D., Olivier Berder, and Olivier Sentieys. "Impact of transmission synchronization error and cooperative reception techniques on the performance of cooperative MIMO systems." 2008 IEEE International Conference on Communications. IEEE, 2008.

[57] Ni, Hao, Guangliang Ren, and Yilin Chang. "Synchronization for cooperative spatial multiplexing MIMO-OFDM systems in multipath fading environments." Communication Systems, 2008. ICCS 2008. 11th IEEE Singapore International Conference on. IEEE, 2008.

[58] Deng, Kai. "Frequency offset compensation for spatial multiplexing MIMO-OFDM systems with distributed transmit antennas." 2012 IEEE International Conference on Information Science and Technology. IEEE, 2012.

[59] Duong, Trung Q., and Hans-Jürgen Zepernick. "Performance analysis of cooperative spatial multiplexing with amplify-and-forward relays." 2009 IEEE 20th International Symposium on Personal, Indoor and Mobile Radio Communications. IEEE, 2009.

[60] Duong, Trung Q., and Hans-Jurgen Zepernick. "On the ergodic capacity of cooperative spatial multiplexing systems in composite channels." 2009 IEEE Radio and Wireless Symposium. IEEE, 2009.

[61] Jin, Shi, et al. "Ergodic capacity analysis of amplify-and-forward MIMO dual-hop systems." IEEE Transactions on Information Theory 56.5 (2010): 2204-2224.

[62] Firag, Abdulla, J. P. Smith, and Matthew R. McKay. "Capacity analysis for MIMO two-hop amplify-and-forward relaying systems with the source to destination link." 2009 IEEE International Conference on Communications. IEEE, 2009.

[63] Tüchler, Michael, and Joachim Hagenauer. "" Turbo equalization" using frequency domain equalizers." (2000).

[64] Arnold, Dieter, and H-A. Loeliger. "On the information rate of binary-input channels with memory." Communications, 2001. ICC 2001. IEEE International Conference on. Vol. 9. IEEE, 2001.

[65] Kay, Steven M. "Fundamentals of statistical signal processing, volume I: estimation theory." (1993).

[66] Sari, Hikmet, Georges Karam, and Isabelle Jeanclaude. "Transmission techniques for digital terrestrial TV broadcasting." IEEE communications magazine 33, no. 2 (1995): 100-109.

[67] Fabrizio Pancaldi, Giorgio M. Vitetta, Reza Kalbasi, Al-Dhahir, Naofal, Murat Uysal, and Hakam Mheidat. "Single-carrier frequency domain equalization." IEEE SIGNAL PROCESSING MAGAZINE, Sept. 2008.

[68] 3rd Generation Partnership Project (3GPP); Technical Specification Group Radio Access Network; Physical Layer Aspects for Evolved UTRA, http://www.3gpp.org/ftp/Specs/html-info/25814.htm

[69] Tajer, Ali, and Aria Nosratinia. "Diversity order in ISI channels with single-carrier frequency-domain equalizers." Wireless Communications, IEEE Transactions on 9, no. 3 (2010): 1022-1032.

[70] Song, S. H., and Khaled Letaief. "Diversity analysis for linear equalizers over ISI channels." Communications, IEEE Transactions on 59, no. 9 (2011): 2414-2423.

[71] Saleh, Adel AM, and Reinaldo Valenzuela. "A statistical model for indoor multipath propagation." IEEE Journal on selected areas in communications 5.2 (1987): 128-137.

[72] Hedayat, Ahmadreza, Aria Nosratinia, and Naofal Al-Dhahir. "Outage probability and diversity order of linear equalizers in frequency-selective fading channels." Asilomar Conference on Signals, Systems & Computers. 2004.

[73] Tajer, Ali, and Aria Nosratinia. "Diversity order of MMSE single-carrier frequency domain linear equalization." IEEE GLOBECOM 2007-IEEE Global Telecommunications Conference. IEEE, 2007.

[74] Liu, Zhiqiang. "Maximum diversity in single-carrier frequency-domain equalization." IEEE transactions on information theory 51.8 (2005): 2937-2940.

[75] Zhang, Wei. "Comments on" Maximum diversity in single-carrier frequency-domain Equalization"." IEEE Transactions on Information Theory 52.3 (2006): 1275-1277.

[76] Zhou, Shengli, and Georgios B. Giannakis. "Single-carrier space-time block-coded transmissions over frequency-selective fading channels." IEEE Transactions on Information Theory 49.1 (2003): 164-179.

[77] Wang, Hui-Ming, and Qinye Yin. "Outage and diversity analysis of single carrier cyclic prefix systems with frequency domain decision feedback equalizers." Global Telecommunications Conference (GLOBECOM 2011), IEEE, 2011.

[78] Zheng, Lizhong, and David NC Tse. "Diversity and multiplexing: a fundamental tradeoff in multiple-antenna channels." Information Theory, IEEE Transactions on 49, no. 5 (2003): 1073-1096.

[79] Telatar, Emre. "Capacity of Multi- antenna Gaussian Channels." European transactions on telecommunications 10.6 (1999): 585-595.

[80] Zanella, Alberto, Marco Chiani, and Moe Z. Win. "MMSE reception and successive interference cancellation for MIMO systems with high spectral efficiency." IEEE Transactions on Wireless Communications 4.3 (2005): 1244-1253.

[81] Wishart, John. "The generalised product moment distribution in samples from a normal multivariate population." *Biometrika* (1928): 32-52.

[82] James, Alan T. "Distributions of matrix variates and latent roots derived from normal samples." The Annals of Mathematical Statistics (1964): 475-501.

[83] Tulino, Antonia M., and Sergio Verdú. *Random matrix theory and wireless communications*. Vol. 1. Now Publishers Inc, 2004.

[84] Couillet, Romain, and Merouane Debbah. *Random matrix methods for wireless communications*. Cambridge University Press, 2011.

[85] Zanella, Alberto, Marco Chiani, and Moe Z. Win. "A general framework for the distribution of the eigenvalues of Wishart matrices." *2008 IEEE International Conference on Communications*. IEEE, 2008.

[86] Chiani, Marco, Moe Z. Win, and Alberto Zanella. "On the capacity of spatially correlated MIMO Rayleigh-fading channels." *IEEE Transactions on Information Theory* 49.10 (2003): 2363-2371.

[87] Smith, Peter J., Sumit Roy, and Mansoor Shafi. "Capacity of MIMO systems with semicorrelated flat fading." *IEEE Transactions on Information Theory*49.10 (2003): 2781-2788.

[88] Alfano, Giuseppa, et al. "Capacity of MIMO channels with one-sided correlation." *Spread Spectrum Techniques and Applications, 2004 IEEE Eighth International Symposium on*. IEEE, 2004.

[89] Díaz-García, José A., Ramón Gutierrez Jáimez, and Kanti V. Mardia. "Wishart and pseudo-Wishart distributions and some applications to shape theory." *Journal of Multivariate Analysis* 63.1 (1997): 73-87.

[90] Mallik, Ranjan K. "The pseudo-Wishart distribution and its application to MIMO systems." *IEEE Transactions on Information Theory* 49.10 (2003): 2761-2769.

[91] A. M. Kshirsagar, *Multivariate Analysis*. New York: Marcel Dekker, 1972.

[92] George R., Cooper, and Clare D. McGillem. Probabilistic methods of signal and system analysis, 3rd edition, Oxford University Press, 1999.

[93] Wang, Zhengdao, and Georgios B. Giannakis. "A simple and general parameterization quantifying performance in fading channels." Communications, IEEE Transactions on 51, no. 8 (2003): 1389-1398.

[94] Tao Liu, Shihua Zhu, Feifei Gao, "A Simplified MMSE Equalizer for Distributed TR-STBC Systems with Multiple CFOs", IEEE Communications Letters, Volume: 16, Issue: 8, August 2012.

[95] Golub, Gene H., and Charles F. Van Loan. "Matrix computations. 1996." *Johns Hopkins University Press*, 1996.

[96] Stark, Henry, and John W. Woods. Probability, random processes, and estimation theory for engineers, 2nd edition, Prentice Hall, 1994.

[97] Alexeev, Boris, Jameson Cahill, and Dustin G. Mixon. "Full spark frames." Journal of Fourier Analysis and Applications 18, no. 6 (2012): 1167-1194.

[98] Yong Jun Chang, Haejoon Jung, and Mary Ann Ingram, "Demonstration of an OLA-based Cooperative Routing Protocol in an Indoor Environment", *European Wireless*, Vienna, Austria, April 2011.

[99] Haejoon Jung and Mary Ann Weitnauer, "Multi-packet Opportunistic Large Array Transmission on Strip-shaped Cooperative Routes or Networks," *IEEE Transactions on Wireless Communications*, Volume 13, Issue 1, pp. 144-158, January 2014.

[100] Wang, Feng, and Mary Ann Ingram. "A practical equalizer for cooperative delay diversity with multiple carrier frequency offsets." In *Communications (ICC), 2012 IEEE International Conference on*, pp. 4100-4104. IEEE, 2012.